STRUCTURE AND GAS TRANSMISSION PROPERTIES OF SURFACE MODIFIED FOOD PACKAGING MATERIALS BY LAYER-BY-LAYER ASSEMBLY

A Thesis Submitted to
the Graduate School of Engineering and Sciences of
İzmir Institute of Technology
in Partial Fulfillment of the Requirements
for the Degree of

MASTER OF SCIENCE

in Food Engineering

by
Nazan KOCA

April 2019
İZMİR

We approve the thesis of **Nazan KOCA**

Examining Committee Members:

Assist. Prof. Dr. Beste BAYRAMOĞLU
Department of Food Engineering, İzmir Institute of Technology

Prof. Dr. Figen KOREL
Department of Food Engineering, İzmir Institute of Technology

Assoc. Prof. Dr. Seda ERSUS BİLEK
Department of Food Engineering, Ege University

3 April 2019

Assist. Prof. Dr. Beste BAYRAMOĞLU
Supervisor,
Department of Food Engineering
İzmir Institute of Technology

Prof. Dr. Figen KOREL
Head of the Department of Food Engineering

Prof. Dr. Aysun SOFUOĞLU
Dean of the Graduate School of Engineering and Sciences

ACKNOWLEDGEMENTS

First and foremost, I would like to thank my thesis adviser, Assist. Prof. Dr Beste BAYRAMOĞLU for her valuable advice and guidance regarding the difference aspects of this thesis. I was able to learn much from her, and I am grateful for the opportunity to work on this thesis while growing to be a better researcher under her mentorship. I also sincerely thank my thesis committee Prof. Dr. Figen KOREL and Assoc. Prof. Dr. Seda ERSUS BİLEK for their helpful advice and guidance. A big thank goes to the researchers, experts and anyone who lightened my way of research at IZTECH.

I would like to appreciate deeply my friends Nagihan BAŞAK, Pınar ŞİRİN, Goncagül ARPAZ, Merve Betül ADALI and Nazlıcan YILMAZ for their support, encouragements and friendship. I'm so grateful for you to be there whenever I needed you. We may be apart in distance but never in heart.

Finally, I owe a debt of gratitude to my parents Ali KOCA, Emine KOCA, my sister Selin VAROL, my brother-in-law Mehmet VAROL and other family members for their unconditional support and cooperation throughout my time at IZTECH, without their support I would not have been able to finish this master.

ABSTRACT

STRUCTURE AND GAS TRANSMISSION PROPERTIES OF SURFACE MODIFIED FOOD PACKAGING MATERIALS BY LAYER-BY-LAYER ASSEMBLY

In this study, two different LbL coatings of chicken egg white lysozyme (LZ) (0.2 % w/v)-gum arabic (GA) (0.2 % w/v) and lysozyme (LZ) (0.2 % w/v)-iota carrageenan (IC) (0.2 % w/v) were investigated as a potential agent in the fabricaton of surface-modified food packaging materials with improved gas barrier properties. The effects of solution pH, adsorption time, number of layers, and inclusion of drying step in between deposition steps on multilayer formation were explored for both LbL coatings seperately. Film growth was monitored up to 10 layers by UV-Vis spectrometry and Surface Plasmon Resonance (SPR), which allows for *in situ* observation of the multilayer formation. The LbL coatings were characterized by AFM (Atomic Force Microscopy) and SEM (Scanning Electron Microscopy). The oxygen and water vapor transmission rates of the coatings (assembled on corona treated polypropylene (PP) films) were also measured. The most successful LbL assembly was obtained at pH 7-7 combination, with 20 minutes adsorption time and with intermediate drying steps for both (LZ-GA and LZ-IC) LbL coatings. For both LbL coating, both the UV-Vis and SPR measurements showed the similar zig-zag trend; i.e. desorption of some of the pre-adsorbed LZ from the interface with the deposition of GA (or IC) on it, probably due to formation of soluble complexes between them. The importance of intermediate drying steps was established by UV-Vis, AFM and gas transmission rate measurements. The absence of intermediate drying caused a reduction in total mass deposited and the gas barrier properties of the coatings.

ÖZET

KATMANLI DEPOZİSYON İLE YÜZEYİ MODİFİYE EDİLMİŞ GIDA PAKETLEME MALZEMELERİNİN YAPISAL VE GAZ GEÇİRGENLİĞİ ÖZELLİKLERİ

Bu çalışmada, lizozim (LZ) (0.2 % w/v) – arap zamkı (GA) (0.2 % w/v) ve lizozim (0.2 % w/v)-iota karragenan (IC) (0.2 % w/v) olmak üzere katmanlı depozisyon (LbL) yöntemi ile hazırlanan iki farklı kaplama, gaz bariyer özellikleri geliştirilmiş, yüzeyi modifiye edilmiş gıda paketleme malzemelerinin üretilmesinde potansiyel bir ajan olarak incelenmiştir. pH, adsorpsiyon süresi, katman sayısı ve kurutma adımının tüm katmanlara dahil edilmesinin film oluşumuna etkileri her iki LbL kaplama için ayrı ayrı incelenmiştir. Film oluşumu 10. katmana kadar, UV-Vis spektrometre ve yüzey plazmon rezonansı (YPR) ile '*yerinde*' takip edilmiştir. Çok katmanlı filmler atomik kuvvet mikroskobu (AKM) ve taramalı elektron mikroskobu (TEM) ile karakterize edilmiştir. Ayrıca koronalı polipropilen üzerinde oluşturulan LbL kaplamaların oksijen ve su buharı geçirgenliği ölçülmüştür. Her iki film için (LZ-GA, LZ-IC) de, en başarılı LbL kaplama, pH 7-7 kombinasyonunda, 20 dakika adsorpsiyon süresi ile ve kurutma adımının tüm katmanlarda uygulanması halinde elde edilmiştir. Her iki LbL kaplama için, hem UV-Vis hem de YPR sonuçları kaplama oluşumunda aynı eğilimi göstermiştir. Buna göre, önceki adımda adsorbe olan LZ'nin bir kısmının, sonraki GA (veya IC) depozisyon adımında, muhtemelen LZ ve GA (veya IC) arasında çözünebilen komplekslerin oluşması nedeniyle, arayüzeyden geri salındığı anlaşılmıştır. Katmanlar arası kurutma adımının önemi UV-Vis, AKM ve gaz iletim hızı ölçümleri ile belirlenmiştir. Katmanlar arası kurutma adımının olmaması, adsorbe olan toplam kütlede ve kaplamaların gaz bariyer özelliklerinde azalmaya neden olmuştur.

TABLE OF CONTENTS

LIST OF FIGURES ix
LIST OF TABLES xi

CHAPTER 1. INTRODUCTION 1
1.1. Preservation Methods for Fresh Fruits and Vegetables 1
1.2. Modified Atmosphere Packaging (MAP) on Fresh Produce 2
1.3. Motivation and Aims of the Study 4
1.4. Layer-by-Layer Assembly 5
1.4.1. History of Polyelectrolyte Multilayer Films/Coatings 5
1.4.2. Basic Principle of the Layer-by-Layer Deposition of Polyelectrolyte Multilayer Films 5
1.4.3. Layer-by-Layer assembly buildup techniques 7
1.4.4. Coating materials utilized in LbL assembly 8
1.4.4.1. Lysozyme 9
1.4.4.2. Gum Arabic 11
1.4.4.3. Iota Carrageenan 12
1.4.5. The factors influence layer-by-layer assembly 13
1.4.5.1. Solution pH 13
1.4.5.2. Adsorption time 14
1.4.5.3. Drying step 15
1.4.6. Layer-by-Layer Assembly Applications for Fresh Produce 17

CHAPTER 2. MATERIALS AND METHODS 20
2.1. Materials 20
2.1.1. Cleaning Procedure of Quartz and Glass Slides 20
2.2. Methods 21
2.2.1. Preparation of Lysozyme, Gum Arabic and Iota-carrageenan Solutions 21
2.2.2. Determination of the Electrical Properties of the Polyelectrolyte Solutions 21
2.2.3. The Layer-By-Layer (LbL) Assembly Procedure 22

2.2.4. Characterization of the LbL coatings UV-Visible Spectroscopy.... 23
2.2.5. Characterization of the LbL coatings in situ by Surface Plasmon Resonance (SPR) 24
2.2.6. Characterization of the LbL Coatings by Atomic Force Microscopy (AFM) 24
2.2.7. Characterization of the LbL Coatings by Scanning Electron Microscopy (SEM) 26
2.2.8. Oxygen Transmission Rate (OTR) Measurements 26
2.2.9. Water Vapor Transmission Rate (WVTR) Measurements 27
2.2.10. Statistical Analysis 28

CHAPTER 3. RESULTS AND DISCUSSION 29
3.1. Preliminary Results 29
3.1.1. Zeta Potential Measurements of Lysozyme, Gum Arabic and Iota Carrageenan 29
3.1.2. Determination of the Multilayer Growth Follow-Up Wavelength Used in UV-Vis Spectroscopy Experiments 32
3.2. LbL coatings Fabricated from Lysozyme and Gum Arabic 33
3.2.1. UV-Visible Spectroscopy Results 33
3.2.1.1. Effect of Solution pH 33
3.2.1.2. Effect of Adsorption Time 35
3.2.1.3. Effect of Number of Layers 37
3.2.1.4. Effect of Intermediate Drying Step 37
3.2.2. Surface Plasmon Resonance (SPR) Results 38
3.2.3. Atomic Force Microscopy (AFM) Results 40
3.2.4. Scanning Electron Microscopy Results 46
3.2.5. Oxygen Permeability and Water Vapor Permeability Results 46
3.3. LbL coatings Fabricated from Lysozyme and Iota Carrageenan 49
3.3.1. UV-Visible Spectroscopy Results 49
3.3.1.1. Effect of Solution pH 50
3.3.1.2. Effect of Adsorption (Dipping) Time 50
3.3.1.3. Effect of Intermediate Drying Step 52
3.3.2. Surface Plasmon Resonance (SPR) Results 53
3.3.3. Atomic Force Microscopy (AFM) Results 54

3.3.4. Scanning Electron Microscopy Results 61
3.3.5. Oxygen Permeability and Water Vapor Permeability Results 62

CHAPTER 4. CONCLUSIONS 65

REFERENCES 67

APPENDIX A. ANOVA TABLES 75

LIST OF FIGURES

Figure **Page**

Figure 1.1. The principle of polyelectrolyte multilayer film construction via LbL deposition by dipping 6
Figure 1.2. Structure of Lysozyme 10
Figure 1.3. Schematic representation of the molecular structure of gum arabic 11
Figure 1.4. Chemical structure of kappa, iota and lambda carrageenans 12
Figure 2.1. Schematic illustration of LbL assembly on a planar substrate using oppositely charged polymers (LZ-GA, LZ-IC) 23
Figure 3.1. Zeta Potential of a particle with negative surface charge 30
Figure 3.2. UV-Vis absorption spectra of 0.01%-0.3% (w/v) lysozyme, gum arabic and iota carrageenan solutions within the wavelength range of 190-400nm 32
Figure 3.3. Monitoring the effect of solution pH on Lysozyme-Gum Arabic multilayer formation by UV-Vis spectroscopy 34
Figure 3.4. Monitoring the effect of adsorption time on Lysozyme-Gum Arabic multilayer deposition at pH 7&7 combination by UV-Vis spectroscopy 35
Figure 3.5. Monitoring the effect of drying step on Lysozyme-Gum Arabic multilayer deposition at pH 7&7 combination by UV-Vis spectroscopy 38
Figure 3.6. Monitoring the change in SPR angle with the deposition of each layer (LZ-GA) 39
Figure 3.7. Shifts in SPR angle during the adsorption of each layer in LbL assembly of lysozyme and gum arabic 40
Figure 3.8. AFM images (in-air and in-fluid) of surface topography of layers obtained by LZ-GA LbL assembly at pH 7&7 combination with 20 min adsorption time 41
Figure 3.9. Determination of 5^{th} and 10^{th} layer thicknesses for both LZ-GA LbL coatings which are prepared with drying and without drying step using stratch method by scanning atomic force microscopy 45
Figure 3.10. AFM images (in-air) of surface topography of the (a)1^{st} layer LZ and (b)2^{nd} layer GA obtained by applying intermediate drying step at pH 7&7 combination with 20 min adsorption time 45

Figure 3.11. Scanning electron microscopy images of surface morphology of a) blank corona treated polypropylene (PP) film surface, b) 5 layers of LZ-GA LbL coating on corona treated PP c) 10 layers of LZ-GA LbL coating on corona treated PP 46
Figure 3.12. Monitoring the effect of solution pH on Lysozyme-Iota carrageenan multilayer formation by UV-Vis spectroscopy 51
Figure 3.13. Monitoring the effect of adsorption time on Lysozyme-Iota carrageenan multilayer deposition at pH 7&7 combination by UV-Vis spectroscopy 51
Figure 3.14. Monitoring the effect of drying step on Lysozyme-Iota carrageenan multilayer deposition at pH 7&7 combination and with 20 min adsorption time by UV-Vis spectroscopy 52
Figure 3.15. Monitoring the change in SPR angle with the deposition of each layer (LZ-IC) 53
Figure 3.16. Shifts in SPR angle during the adsorption of each layer in LbL assembly of lysozyme and iota carrageenan 54
Figure 3.17. AFM images (in-air) of surface topography of the layers obtained with intermediate drying step at pH 7&7 combination of LZ-IC LbL coating with 20 min adsorption time 56
Figure 3.18. AFM images (in-air and in-fluid) of surface topography of layers obtained by LZ-IC LbL assembly at pH 7&7 combination with 20 min adsorption time 57
Figure 3.19. AFM images (in-air) of surface topography of the (a)1st layer LZ and (b)2nd layer IC obtained by applying intermediate drying step at pH 7&7 combination with 20 min adsorption time 58
Figure 3.20. AFM tip image from LZ-IC LbL coating *in situ* analysis 58
Figure 3.21. Determination of 5th and 10th layer thicknesses for both LZ-IC LbL coatings which are prepared with drying and without drying step using stratch method by scanning atomic force microscopy 60
Figure 3.22. Scanning electron microscopy images of surface morphology of a) blank corona treated polypropylene (PP) film surface, b) 5 layers of LZ-IC LbL coating on corona treated PP c) 10 layers of LZ-IC LbL coating on corona treated PP 61

LIST OF TABLES

Table **Page**

Table 3.1 Zeta potential of Gum arabic, Lysozyme and Iota carrageenan solutions at different pH values 31
Table 3.2. The surface roughness values of LZ-GA LbL layers in air and fluid medium obtained from 10x10 μm^2 scan areas 43
Table 3.3. Changes in thickness of the LZ-GA LbL coatings with respect to number of layers and inclusion of intermediate drying step 44
Table 3.4. Oxygen and Water vapor transmission rate results for LbL films obtained by lysozyme and gum arabic at pH 7 48
Table 3.5. Comparison of LZ/GA LbL coatings with other coatings from literature in terms of OP(oxygen permeability) and WVP(water vapor permeability) 49
Table 3.6. The surface roughness values of LZ-IC LbL layers in air and fluid medium obtained from 10x10 μm^2 scan areas 59
Table 3.7. Changes in thickness of the LZ-IC LbL layers with respect to number of layers and inclusion of intermediate drying step 59
Table 3.8. Oxygen and water vapor transmission rate results for LbL films obtained by lysozyme and iota carrageenan at pH 7 63
Table 3.9. Comparison of LZ/IC LbL coatings with other coatings from literature in terms of OP (oxygen permeability) and WVP (water vapor permeability) ... 64

CHAPTER 1

INTRODUCTION

1.1. Preservation Methods for Fresh Fruits and Vegetables

Fresh fruits and vegetables play an important role in balanced and healthy diet since they are sources of key nutrients such as minerals, antioxidants, and vitamins. The market for freshly prepared fruit and vegetable products (fresh produce) has grown over the last decade. Increasing consumer demand for fresh, healthy, convenient and additive-free prepared product items is the main driving force behind this market growth (Koutsimanis et al., 2012). Fresh produces are living tissues and their metabolic processes proceed even after harvest which makes them highly perishable products, therefore there is a need for optimal postharvest technologies to maintain their storage stability and extend their shelf life. The products expose various biological processes, which also proceed after the products have been harvested. The processes provoke gradual changes in quality (Ščetar et al., 2010). Fresh produce is deprived of their source of nutrients, water and anti-senescence hormones, and normal factors such as transpiration and respiration finally lead to weight loss and senescence of the product. A decrease in the quality of fresh produce caused by the growth of pathogens or physical damage as evident through their appearance also stimulates senescence. The major component of weight loss in fresh produce is transpiration and their texture is unfavorably influenced by excessive water loss which is making the product unmarketable. Respiration is a metabolic process that produces the energy needed for several plant biochemical reactions. The respiration rate of fresh produce is inversely proportional to their shelf life; higher respiration rates are associated with shorter shelf lives (Kyriacou and Rouphael, 2018). Postharvest technologies do not actively improve the quality of fresh produce, but they may passively enhance the quality of fresh fruits and vegetables wherethrough the manipulation of the maturation process to assist optimal expression of potential quality except determined in the field up to the time of harvest.

Prolonging the shelf life of the fresh produce can be attained by minimizing the deterioration. Many preservation techniques like canning, freeze-drying, controlled

atmosphere and hypobaric, low temperature and modified atmosphere can be used to reduce the respiration of fresh fruits and vegetables (Sandhya, 2010). One way to enhance their storage is to use chilled temperature, and this is currently applied to fresh-cut produce (Vargas et al., 2006). However, most of the whole produce is distributed at ambient temperature because using chilled temperature is costly and difficult to manage. The other way is to change the atmosphere surrounding the produce in order to reach the optimal atmosphere of storage, specific to each produce (Kader et al., 1989; Charles et al., 2008; Sandhya 2010). Maintaining the safety and extending the shelf life of whole and minimally processed fruits and vegetables can be achieved by using modified atmosphere packaging (MAP) in combination with refrigeration.

1.2. Modified Atmosphere Packaging (MAP) on Fresh Produce

MAP is an indirect food preservation method, where the gaseous composition of the package is modified such that chemical deterioration reactions and microbial growth are kept at minimal levels. Modified atmosphere packaging of fresh products consists in altering the atmosphere inside the package by a reduction in O_2 and an increase in CO_2 concentrations, which is accomplished by the natural interaction between the respiration rate of the product and the transfer of gases through the packaging material. This slows down the respiration rate of many fresh produce items and inhibits the plant hormone ethylene, which are the factors responsible for aging and ripening process (Fonseca et al., 2002; Kader et al., 1989).

MAP can be defined as the preservation of food in a package in which the atmosphere inside the package is modified or altered which can be done by either actively or passively to ensure an optimum atmosphere for improving shelf life and maintaining food quality. Active modification contains displacing the air with a controlled, desired mixture of gases, a procedure generally attributed to as gas flushing. Absorbers (active packaging) of O_2, CO_2 or ethylene might be involved within the pack to inspect the concentration of these gases. In passive modification systems, the atmosphere is achieved through the respiration of produce inside the package, therefore the final equilibrium atmosphere relies on the natural processes of produce respiration and film permeability (Ščetar et al., 2010).

CO_2, O_2 and N_2 are the most commonly used gases in modified atmosphere packaging. During product storage, oxygen is consumed and carbon dioxide is created by produce respiration. Nitrogen, which is an inert gas, is used as 'filler' gas in MAP to compensate the volume decrease based on CO_2 absorption and to prevent package collapse (Sandhya, 2010). Applying high CO_2 and low O_2 MAP is effective to reduce quality deterioration of fresh products during storage, and these effects are related to a reduction in respiration rate, water loss, phenolic oxidation, ethylene biosynthesis and aerobic microbial count. Additionally, other gasses like argon, xenon, helium and nitrous oxide(N_2O) have been utilized in MAP applications to maintain the quality of the product and reduce microbial growth (Meng et al., 2012).

Successful MAP of fresh produce is achieved when using a packaging film of accurate intermediary permeability where a desirable equilibrium modified atmosphere (EMA) which is established when the rate of oxygen and carbon dioxide transmission through the package equals the produce respiration rate. Typically, in successful MAP of fresh produce, the equilibrium MA (EMA) contains 2/10 % O_2/CO_2 within the package. The EMA attained is affected by various factors, such as the temperature, packaging film, respiration rate, pack volume, light and fill weight. The utilization of polymeric films in MAP serves as mechanical barrier to the movement of water vapor which helps to maintain a high level of relative humidity within the package and decrease produce weight loss. Nevertheless, an immensely high level of relative humidity (RH) within the package can result in moisture condensation on produce, hence generating a favorable condition for the growth of pathogenic and spoilage microorganisms (Aharoni et al., 2007; Távora et al., 2004). Common petroleum-based plastics used for fresh produce packaging include polyethylene terephthalate (PET), low-density polyethylene (LDPE), high-density polyethylene (HDPE), polypropylene (PP), and polystyrene (PS), ethylene-vinyl alcohol (EVAL), poly (vinyl chloride) (PVC), ethylene-vinyl acetate (EVAC) (Ščetar et al., 2010).

Polypropylene (PP), which is linear addition polymer of propylene, is a versatile polymer that has applications in flexible, rigid, and semi-rigid packaging structures. PP offers excellent electrical and chemical resistance at higher temperatures and does not present stress-cracking problems. While the properties of PP are similar to those of polyethylene, there are specific differences which include a lower density, higher softening point, and higher rigidity and hardness (Allahvaisi, 2012). PP is a good water vapor barrier. In many applications, the biaxially oriented film (BOPP) is preferred.

1.3. Motivation and Aims of the Study

Even though it has advantages, the use of MAP alone for fresh produce is quite restricted for a number of reasons. Packages that supplies safe atmosphere at one temperature may result in anaerobic conditions at higher temperature. Therewithal, the plastic films used for modified atmosphere packaging must be flexible and easy to use, but strong enough to survive normal handling operations. Furthermore, there are also many concerns about the environmental issues related with the use of petroleum-based plastic films. These concerns, as well as the cost issues, force the manufacturers to downsize the films in thickness. However, minimizing the use of plastics while maintaining or prolonging the freshness of fruits and vegetables requires alternative strategies. Fabrication of packaging films surface-modified with ultra-thin coatings made of edible biomaterials, which would possess improved gas barrier properties might be a good alternative. In order to be applicable, edible coatings must combine a number of properties such as sufficient antimicrobial activity, good adhesion, well-balanced gas and water vapor permeabilities. It is hard to satisfy such variable requests with a single coating material. There is, therefore, recent attention in developing composite edible coatings that combine multiple advantages from their various components. In the field of nanotechnology, Layer-by-Layer Deposition / Assembly (LbL) method, which has been widely used for the last 20 years, is a promising technique for this goal.

The main aim of the study is to investigate the development of novel, ultra-thin multilayered coatings via LbL deposition method, primarily for the purpose of surface-modification of MAP materials to improve their gas barrier properties, but which also have the potential to be used as edible coatings with adequate gas barrier properties for fresh fruits and vegetables. The specific aims are to investigate the effects of solution pH, type of polyelectrolytes, number of layers, adsorption time and inclusion of drying step on LbL deposition and structural properties of the coatings.

In this study, three different biopolymers, lysozyme (an antimicrobial protein), gum arabic (a heteropolysaccharide) and iota carrageenan (a polysaccharide) were used to obtain two different LbL coatings as Lysozyme-Gum Arabic and Lysozyme-Iota Carrageenan.

1.4. Layer-by-Layer Assembly

LbL Assembly/Deposition is a bottom-up nanofabrication technique which is based on the successive adsorption of two or more materials onto each other due to the physicochemical interactions (mainly electrostatic) in between.

1.4.1. History of Polyelectrolyte Multilayer Films/Coatings

"Langmuir-Blodgett" or "Langmuir" thin films were the first nanostructured films to be designed at the beginning of the last century. Langmuir-Blodgett films were produced from the building of a monolayer of amphiphilic molecules at an air/water interface upon compression transfer to a solid substrate (Blodgett and Langmuir, 1937), and the adsorption is based on hydrophobic/hydrophilic type of interactions. Moreover, the thickness of such films may range from few Angstroms to several nanometers.

The concept of self-assembled monolayers was developed in the early 1980s. This technique contains the covalent adherence of an amphiphilic molecule to a solid surface, stating that the polar head of the amphiphilic molecule must have a group capable of forming covalent bonds with the chemical groups of the substrate (Maoz et al., 1988).

Iler introduced the principle of polyelectrolyte multilayer films based on mixing oppositely charged polyelectrolyte solutions to compose colloidal complexes for the first time in 1966 (Iler, 1966). Iler showed that multilayer films can be created by successive adsorption of cationic and anionic colloids.

1.4.2. Basic Principle of the Layer-by-Layer Deposition of Polyelectrolyte Multilayer Films

During the LbL process, the study of the deposition is crucial to understand the assembly mechanism and optimize the conditions for the use of nanofilms in practical applications. The surface modification is of great interest for controlling the adhesion between substrates. Layer-by-Layer (LbL) deposition method is one of the most promising and versatile methods for surface modification of substrates. The versatility, simplicity and nanoscale control that LbL assembly makes it one of the most widely used

technologies for coating both planar and particulate substrates in a various range of fields (Richardson et al., 2015).

The LBL technique is based on the sequential deposition of oppositely charged polyelectrolytes (a polycation and a polyanion) on a charged substrate. Even though the major driving force for the LbL assembly is usually electrostatic interactions, other interactions involving hydrogen bonding, van der Waals forces, covalent bonding, hydrophobic interactions etc., lead to the formation of such assemblies (Zhang et al., 2007; Kharlampieva et al., 2009). In electrostatically driven polyelectrolyte-polyelectrolyte assembly, LbL growth occurs based on charge overcompensation, i.e. the surface charge reverses by deposition of each film ingredient, making it ready to adsorb the next LbL layer (Mohammadi et al., 2017).

Generally, LbL self-assembly progresses as follows: (1) A charged substrate is immersed in a solution of an oppositely-charged colloid to adsorb the first layer. (2) A rinsing step takes place between each polyelectrolyte deposition layer. This helps in removing weakly bounded polyelectrolytes on the surface. It is also important to prevent the contamination of the subsequent oppositely-charged colloidal solution. (3) The coated substrate is submerged in the oppositely-charged colloidal solution to deposit a second layer, and thus the first bilayer is formed. (4) The procedure is repeated until a desired number of layers are deposited on the substrate. The deposition is usually ended with the final the rinsing step (Figure 1.1).

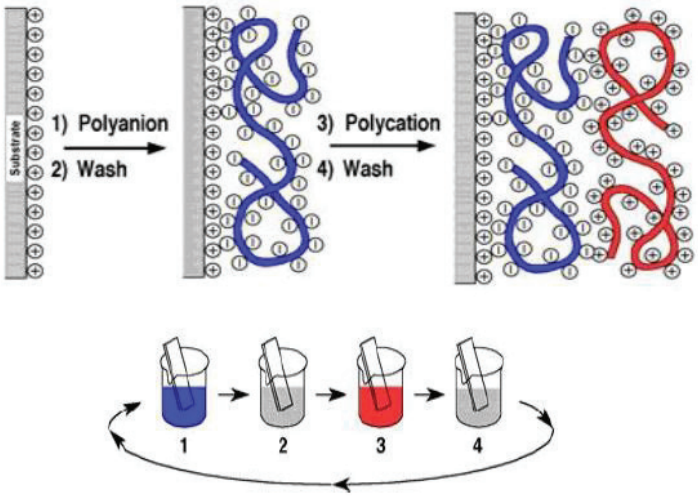

Figure 1.1. The principle of polyelectrolyte multilayer film construction via LbL deposition by dipping (Source: Decher, 1997). The molecular representation shows how the polyanion and polycation are adsorbed on the positively charged substrate. Blue is used for polyanion, while red is used for polycation.

The LbL assembly method offers advantages compared to more conventional coating methods. These include (1) the freedom to apply on flexible objects with irregular shapes and sizes, (2) the simplicity of the process and equipment, (3) the availability of an abundance of natural and synthetic colloids, (4) the capability to fabricate stable coatings and (5) a decent control over the thickness of the coatings.

1.4.3. Layer-by-Layer Assembly Buildup Techniques

The LbL deposition procedure can be performed following different approaches including spraying, spin-coating, and dipping (Li et al., 2012; Decher, 2012). Because of its convenience and low cost, the dipping mode has already been widely generalized, as the use of various beakers could help to finish experiments. Initially, the substrates are immersed into the charged (positively or negatively charged) solution for several minutes, followed by the rinsing step. After that, the substrates are exposed to the oppositely charged solution for another several minutes. Finally, the rinsing step is performed in a similar manner. Although the dipping method has many advantages, it is costly regarding time. In this method, each pair of oppositely charged monolayers takes about 5 to 20 minutes to be manufactured, since the total time depends on diffusion times and adsorption of polyelectrolyte molecules and colloidal particles within the substrate.

The construction of dip coating to make films concludes the following procedures, the adsorption, diffusion and rearrangement of polymer chains, and may engross plenty of time, which depends on the proportions of the macromolecule, the density of charge in the solution together with the mobility of chains. In order to expedite the LbL assembly process, a spin-assisted LbL assembly method was introduced by Char, Wang and co-workers at nearly the same time through the combination of both the spin-coating and LbL assembly techniques. In this technique, the suspensions or solutions are deposited on a substrate adhered to a spin coater, and the rotation speed produces a high centrifugal force and air flow at the surface that encourage a fast thinning and drying of the liquid and a high uniformity of the layers. The polymer chains are not capable to interpenetrate as in the dipping-LBL since the drying is very fast, and as a result, the internal multilayer structure is highly stratified (Chiarelli et al., 2002; Jiang et al., 2004). The shear forces included with film assembly can make the depositing multilayer films on non-flat surfaces or even flat but rough surfaces challenging. However, the film and process properties

arising from spin assembly, including smooth films assembled in a relatively short time, make it an attractive choice.

Following the progressions of the spin-assisted and the dip coating LbL assembly, spray-assisted LbL assembly has gradually caught attention after the year 2000 as Schlenoff and co-workers reported on the spray-assisted coating instead of dipping mode (Schlenoff et al., 2000). The spray-assisted LbL assembly contains certain steps (use polyelecrolyte as an example): In the first step, the substrates would be sprayed with the polyelectrolyte solution, after that draining of the polyelectrolyte solution, as well as surface adsorption of the polyelectrolyte molecules by the substrates, would take place. After the drainage, de-ionized water is sprayed onto the substrate to remove the physically adsorbed polyelectrolyte molecules. Then the other oppositely charged polyelectrolyte solution is sprayed onto the surface again. Eventually, another draining of de-ionized water is used. Alternate spraying of polyanion and polycation forms the polyelectrolyte multilayer films. For the spray-assisted assembly, advantages are various. On the contrary, the time-consuming dip coating process, it would be a popular application to be performed into the industrial fields as only several seconds applying in each step could reach the requirements (Liu et al., 2013). Moreover, the spray-assisted assembly could avoid cross-contamination, which could always happen during the process of the dip coating when the substrates transfer from one recipient to another. Limitations are also obvious for this method as large amounts of prepared solutions would be wasted, so more material-saving LbL assembly techniques are still under development.

1.4.4. Coating Materials Utilized in LbL Assembly

The LbL method is based on the attractive interaction of complementary charges. Thus, the compound must have a minimal number of charged groups. Several nanoparticles and polyelectrolytes can be used to create the ultrathin multilayer structures using the LbL self-assembly technique. Many natural polysaccharides are made of monomers having charged groups like carboxylic acids, amines or sulfates which makes them suitable candidates for electrostatic multilayer build-up. The materials can be small organic molecules or inorganic compound macromolecules including macromolecules, such as proteins or DNA or even colloids (metallic or oxidic colloids or latex particles). The material used for the construction of a nanolaminate coating for food should be

electrostatically charged and preferentially with functional properties of interest, such as antimicrobial, antioxidant and gas barrier properties (Decher, 2012).

Polyelectrolytes are macromolecules or polymers with high molecular weight whose repeating unit bears an electrolyte group that decomposes in a proper polar solvent (usually water) giving the polyelectrolyte its charge. Polyelectrolytes are classified pursuant to their origin. Standard synthetic polyelectrolytes include poly (dimethyldiallylammonium chloride) (PDDA), poly(styrene sulfonate) (PSS), poly(ethylenimine) (PEI), poly(acrylic acid) (PAA), poly(N-isopropyl acrylamide (PNIPAM), poly (methacrylic acid) (PMA), poly(vinyl sulfate) (PVS) and poly(allylamine) (PAH) (Bertrand et al., 2000). In addition to synthetic polymers and charged nanoobjects, natural polyelectrolytes have been used for LbL assembly such as proteins, nucleic acids, and polysaccharides. Many amino acids bear negatively or positively charged side chains, most proteins are amphoteric, and may behave as global polyanions or polycations at a pH below or above their isoelectric point, respectively.

Also, nanoparticles and positively-negatively charged platelets utilized for multilayer construction are derived from naturally-occurring clays such as hectorite, montmorillonite and saponite (Van Duffel et al., 1999).

1.4.4.1. Lysozyme

Lysozyme, also referred as muramidase or N-acetylmuramic hydrolase, is a small, monomeric protein stabilized by four disulfide linkages among the eight cysteine residues of its polypeptide chain. Lysozymes were divided into three families: chicken-type (c-type), invertebrate-type (i-type) and goose-type (g-type), based on different characteristics (e.g., structure, catalysis and immunization). The primary structure of c-type lysozymes consists of 129 amino acid residues with a molecular weight of 14.3 kDa, which contain four intact disulfide bonds (6Cys–127Cys, 30Cys–115Cys, 64Cys–80Cys, and 76Cys–94Cys) and three tyrosine (Tyr), six tryptophan (Trp), and three phenylalanine (Phe) residues (Cao et al., 2015). Lysozyme is an ellipsoidal protein with dimensions of 3 nm x 3 nm x 4.5 nm. The antimicrobial activity of lysozyme is limited to Gram-positive bacteria. The practical application of free lysozyme is limited because it is unstable and easily inactivated. Therefore, most researchers have paid attention to its immobilization (Hashemi et al., 2014). The protein has a very high isoelectric point (pI = 11.3) (Mine et

al., 2004; Luckarift et al., 2006), performing the surface overall positively charged, and therefore they are proper for assembly of multilayer films with negatively charged polymers or nanoparticles through electrostatic interactions. Due to its functional and physiological properties, lysozyme has been applied in medicine and in the food industry (Benkerroum, 2008).

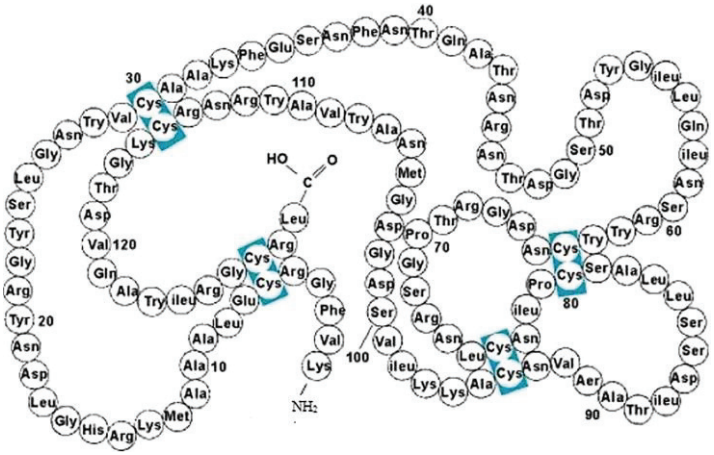

Figure 1.2. Structure of Lysozyme (Source: Wu et al., 2018).

Nepal et al. (2008) prepared multilayer films from carbon nanotube conjugates of Lysozyme and DNA by LbL assembly which showed strong antimicrobial activity against *Micrococcus lysodeikticus (M. lysodeikticus)*. The films were generated as a result of electrostatic interactions between positively charged lysozyme and negatively charged DNA. Multilayer films ceasing in a LSZ-based layer initiated strong antibacterial activity, while those with the DNA nanotube layer on top did not present any effect against *M. lysodeikticus*. The antimicrobial influence seen in this case was reported to be due to contact and not a result of enzyme leaching from the film.

Medeiros et al. (2014) prepared and examined five alternate layers of alginate (0.2% w/v, pH:7) and lysozyme (0.2% w/v, pH:3.8) that were assembled on an aminolysed polyethylene terephthalate (A/C PET) substrate. Alginate and lysozyme nanocoating assembly was confirmed by UV–vis spectroscopy and contact angle measurements. The characterization of the coatings was performed by scanning electron microscopy (SEM) analyses, and gas transmission rate measurements. The coating presented WVTR and OTR values of 1.03×10^{-3} and 1.28×10^{-4} g m^{-2} s^{-1}, respectively. On the 20th day, the mass loss of coated cheese was 1.52-fold lower than that was found for uncoated cheese. The psychrotropic and mesophilic microbial counts and the visual evaluation of fungal contamination were also determined to be lower on coated cheese than on uncoated cheese.

1.4.4.2. Gum Arabic

Acacia gum (AG, E414), also called gum arabic, is an edible dried gummy exudate obtained from the trunk and branches of Acacia senegal and Acacia seyal trees, which is rich in soluble fibers of low viscosity (Williams et al., 1990). It is widely used in the food, pharmaceutical and cosmetic industries because it's good emulsification, encapsulation, stabilization and adhesion properties. Gum arabic is a complex, branched heteropolysaccharide, either neutral or slightly acidic and composed of 1, 3-linked β-D-galactopyranosyl units. The side chains are composed of two to five 1,3 linked β-D-galactopyranosyl units, participated to the main chain by 1,6 linkages. L-arabinose, L-rhamnose, and D-glucuronic acid have also been detected as components of this polymer. Gum arabic is an anionic arabinogalactan polysaccharide-protein complex, composed of three main fractions which vary mainly in their protein contents and molecular size. The bulk of the gum (90%) is referred to as the arabinogalactan fraction (AG). It has a molecular mass of 2–3 × 10^5 g/mol and contains very little protein. The second major component is referred to as the arabinogalactan-protein fraction (AGP) which represents ~10% of the gum. The AGP has a molecular mass of ~1–2 × 10^6 g/mol and contains about 10% protein. The third minor fraction, referred to as the glycoprotein fraction (GP) represents ~1% of the total gum. It has a molecular mass of ~2 × 10^5 g/mol and contains 20–50% protein (Evans et al., 2013). The gum arabic also exists as a mixed salt of sodium, calcium, magnesium, and potassium ions.

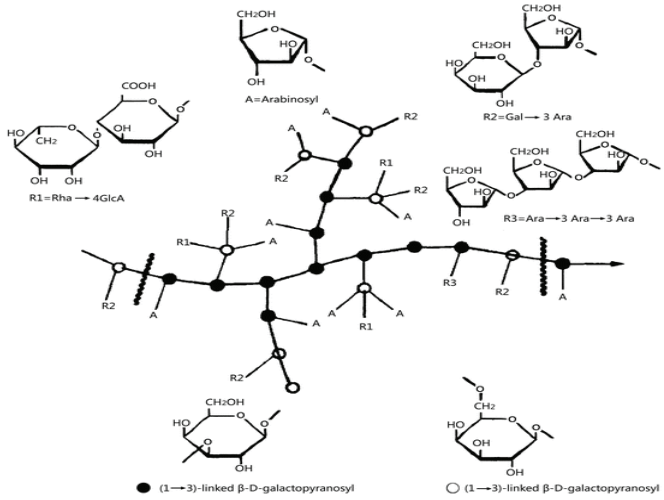

Figure 1.3. Schematic representation of the molecular structure of gum arabic. The mark at the end of the structure indicates the point of attachment of another molecule (Source: Zhao et al., 2015).

1.4.4.3. Iota Carragenaan

Carrageenan is a generic name for a family of viscosifying and gel-forming polysaccharides, and it is attained by extraction from certain species of red seaweeds of the class Rhodophyceae. Carrageenan has the EU additive E-number E407 or E407a, when it's used in food products. Carrageenan has no nutritional value and is used in food preparation for its thickening, emulsifying and gelling properties (van de Velde et al., 2002). Carrageenan is a sulfated polygalactan with 15 to 40 % of ester-sulfate content and an average relative molecular mass well above 100 kDa. It is formed by alternate units of D-galactose and 3,6-anhydro-galactose (3,6-AG) joined by α-1,3 and β-1,4-glycosidic linkage. The three most relevant commercial carrageenan types: kappa (κ), iota (ι) and lambda (λ) (van de Velde and de Ruiter, 2005). The primary differences which influence the properties of carrageenan type are the position and number of ester sulfate groups as well as the content of 3,6-AG. Kappa type carrageenan contains the lowest number of sulfate groups and the highest concentrations of the 3,6-anhydro-α-D-galactopyranosyl units, ι-Carrageenan differs from κ-Carrageenan with an additional sulfate group at the 2-position, while λ-Carrageenan differs from κ- and ι-Carrageenan by bearing variable amounts of sulfate groups and no 3,6-anhydro-α-D-galactopyranosyl residues (Barbeyron et al., 2000). They are commonly used as gelling agents, thickeners and stabilizers in the food and pharmaceutical industries (Bourgoin et al., 2008).

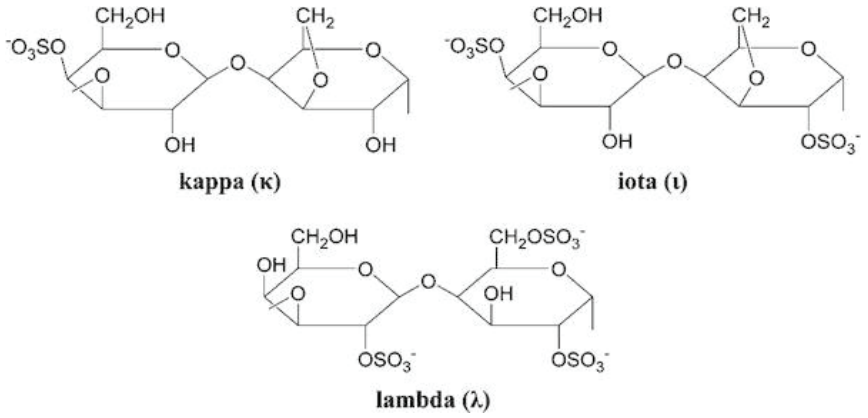

Figure 1.4. Chemical structure of kappa, iota and lambda carrageenans (Source: Chauhan and Saxena, 2016).

Gezgin et al. (2017) investigated the potential of commercially available food grade biopolymers such as chitosan, carrageenan and pectin to replace synthetic

polyelectrolytes when fabricating nanostructured multilayers. Chitosan molecular weight (1,10,44,130 and 330 kDa), carrageenan charge density (furcellaran, kappa, iota and lambda, in the respective order of low to high charge density), and pectin degree of esterification (DE:29-33%, 31-33% and 90%) and amidation (DA:20%) was varied to investigate their respective influences on the nanoscale morphology and wettability of these surfaces. Incremental bilayers of $(Chitosan/Carrageenan)_n$ and $(Chitosan/Pectin)_n$ (n from 1 to 6) were built on silicon wafers, to perform as the foundation for the attachment of extracellular ice nucleators (ECINs). It was found that iota-carrageenan performed better than others based on the high charge density and ideal positioning of charged groups. They recommended that iota carrageenan and amidated low methoxyl pectins as the negatively charged and high molecular weight chitosan (130 and 330 kDa both perform well) as the positively charged biopolymers to fabricate a robust food grade multilayer system.

1.4.5. The Factors Influencing LbL Assembly

Parameters assumed to be important with respect to the underlying surface are, for example, density and nature of charged groups, their local mobility (in the case of a polymeric surface), and the surface roughness. Other important parameters are solvent type, solution pH, concentration of adsorbing species, humidity of the surrounding air, temperature, adsorption time, nature and concentration of added salt, rinsing time, drying, dipping speed, agitation during adsorption or rinsing, and so forth. Processing parameters play an important role in determining the organization, layer thickness, and surface properties (roughness, wettability, adhesively, porosity) of multilayer films.

Some authors state that the effect of pH is much stronger than that of ionic strength and other factors on an electrostatic self-assembly process of a weak and strong polyelectrolyte (Choi and Rubner, 2005; Yoo et al., 1998).

1.4.5.1. Solution pH

The pH of the polyelectrolyte solutions plays a key role especially in cases where at least one of the two polymers used for constructing the polyelectrolyte multilayer is a weak polyelectrolyte. The polyelectrolyte ionization (the degree of charge dissociation)

is pH-sensitive in the case of weak polyelectrolytes. Therefore, the charge density can be adjusted by a simple change of pH of the polyelectrolyte solutions. Increasing amounts of base, acid, or buffer to establish a given pH will raise the ionic strength. This usually leads to thicker adsorbed layers. On the other hand, many of the charged groups used, such as protonated carboxylates or amines, are prone to protonation-deprotonation equilibria. Thus, the adjusted pH will alter the charge density of the polyelectrolytes. An increasing charge density on the adsorbing polymer will generally favor thinner adsorption layers, whereas an increasing charge density at the surface will favor thicker adsorbed layers (Yoo et al., 1998). The effect of pH on the overall film growth is therefore not clear a priori. In fact, most studies exploring pH effects report an optimum pH range for a successful film growth (Zacharia et al., 2007). In order to obtain a stable LbL film, it is ideal for the layered deposition process to be carried out under conditions where each polyelectrolyte exhibits a maximum degree of ionization in solution. However, extreme pH values may completely inhibit film growth by favoring desorption. These different results suggest that LbL deposition actualizes as a result of a balance of complex interactions involving the various driving forces (electrostatic, entropy recovery, hydrophobic-hydrophilic equilibrium interactions, hydrogen bonds, etc.). Thus, the morphology and the stability of the films/coatings are specific to the chemical structure of polyelectrolytes utilized in multilayer deposition.

Bieker and Schönhoff, (2010); investigated the effect of the pH of the depositing solutions on the growth of poly(allyl amine hydrochloride) (PAH)/poly(acrylic acid) (PAA) LbL assemblies. They disclosed several growth regimes with different growth behavior (exponential and linear) and film quality (rigid and soft) with simple variation of pH. They rationalized their investigations by noting that at different pH values, the degrees of ionization, electrostatic interactions, inter-diffusion and mobility of polyelectrolyte chains vary.

1.4.5.2. Adsorption Time

One of the factors that determine the success of LbL deposition and the properties of films/coatings is the adsorption (deposition) time of polyelectrolytes to the substrates. In general, the longer adsorption time results in a more successful deposition. For long deposition times, the polymer chains have enough time to relax and reconstruct on the

surface as well as inside the multilayers, leading to smoother surfaces; while for short deposition times, the polymer chains have limited time to settle down on the surface, leading to the formation of the small islets (Yu et al., 2017). Normally, it would be expected that the increase of deposition time would lead to a thicker film. However, in their study of the LbL assembly of PAH and a polyanion containing an azobenzene chromophore (PAzo), Barrett et al. (2003) found that in some PAH/P-Azo films, a significantly large thickness was achieved in less than 5s. Similar outcomes were obtained from poly (ethylene imine) (PEI)/PAA/PEI/montmorillonite (MMT) clay quad-layer system (Xiang et al., 2013). Tsukruk et al. (1997) has examined the LbL process for Poly(styrenesulfonate) (PSS) and Poly(allylamine) (PAA) molecular layers and they chose deposition time as their factor. They suggested that assembly of polyions on a charged surface occurs in two stage process (fast and slow). At the very first stage of film formation, within the first 1-2 min of self-assembly, charged PSS polymer chains are adsorbed nonuniformly, mainly on chosen sites of oppositely charged substrates with high concentrations of local charges (holes, scratches, foreign microparticles and edges). Obviously, at this stage of deposition, chains are linked to the surface by only a few segments, and therefore, preserve their coiled conformation. Then polymer chains are relaxed to a dense packing during the longer second stage of the self-assembly. Probably, a stable homogeneous polymer monolayer which envelops the original surface. The results showed that a stable homogenous assembled layer which envelops the original surface is created only after a complete "relaxation" of absorbed macromolecules. Polymer islands gradually expand over the surface: after 10-30 min adsorption time, their height decreases to 1-1.5 nm. Yu et al. (2017) observed that the thickness of $(PAH8.5/PAA3.5)_{20}$ films increased with the deposition time, which was varied from 10s to 15 min.

1.4.5.3. Drying Step

Another feature to consider during the assembly process of the polyelectrolyte multilayer formation is the inclusion of drying steps after the deposition of the successive layers. This is important since the LbL method is a wet assembly technology and drying can modify the properties and structure of the materials (Decher and Schlenoff, 2006). The modifications can alter the growth behavior, leading in some cases to complete

blocking of the adsorption, therefore stopping the propagation of the assembly process. Raposo et al., (1997) showed that multilayers formed by poly(vinylsulfonic acid) (PVS) and poly(o- methoxyaniline) (POMA) needed drying steps between the successive adsorption cycles to provide the propagation of the multilayer formation. In another study of Decher (2012), it was found that the final structure of the materials also depends on the type of drying process, e.g for $(PAH+ PSS)_n$ films the structure obtained is significantly different when the drying is applied under ambient air or under nitrogen stream. More disoredered materials were fabricated when use of the nitrogen stream in drying process.

Despite other parameters have been well researched, the effects of drying step after each deposition on the film structure and composition is not still clear. For example, some researches indicated that drying would cause increase in the thickness of PEMs assembled from poly(sodium 4-styrene sulfonate) (PSS) and poly(allylamine hydrochloride) (Lvov et al., 1999; Lourenço et al., 2007), whereas another study showed that the intermediate drying does not provoke any irreversible changes in the structure of polyelectrolyte multilayers made of poly(L-glutamic acid) and poly(L-lysine) (Halthur et al., 2004).

Exclusion of intermediate drying steps may dramatically influence the structure of LbL polymeric films composed of alternately deposited polymeric complexes (Zhang et al., 2012). For example, skipping the drying steps in the LbL assembly of negatively charged polyelectrolyte complexes of poly(acrylic acid) (PAA) and diazoresin (DAR) (noted as PAA-DAR) with positively charged polyelectrolyte complexes of DAR and PSS (noted as DAR-PSS) enabled a rapid fabrication of micrometer-thick PAA-DAR/DAR-PSS foam films. The 15-bilayer PAA-DAR/DAR-PSS film had a thickness of ~1.8 μm. The LbL assembled 15-bilayer PAADAR/ DAR-PSS film that was prepared including drying steps after each layer deposition was found to be compact and had a thickness of ~130 nm (Zhang &Sun, 2009). Also, they showed that the aggregated particles, which were the LbL assembled PAA/ DAR-PAA, were observable but had much lower height and were less aggregated compared with those in their corresponding films fabricated without drying steps (Zhang and Sun, 2010).

Chen et al. (2001) investigated LbL films of diphenylamine-4-diazoniumformaldehyde resin (DR) and 2-nitro-N-methyl-4-diazoniumformaldehyde resin (NDR) and other polyelectrolytes. They concluded that the samples prepared with intermediate drying steps had higher adsorbed amounts than samples prepared without

drying. They also showed that drying makes the films flatter and rather hydrophobic. De Souza et al. (2004) also remarked that drying affects the film build-up and morphology. They stated that LbL films fabricated with drying under room conditions exhibited a more homogeneous surface, thus lower roughness and higher adsorbed amounts when compared with films dried by nitrogen flow or under vacuum. The lower roughness was predicated to lower solvent evaporation rates for samples dried in air.

1.4.6. Layer-by-Layer Assembly Applications for Fresh Produce

Medeiros et al. (2012) has developed multilayer coatings based on pectin and chitosan. Five layers of alternating polyelectrolytes were applied to whole "Tommy Atkins" mangoes. The LbL coating performed by immersion of the fruit into pectin solution (0.2% w/v, pH 7) and chitosan solutions (0.2% w/v, pH 3) for 15 min. Rinsing step was applied by distilled water with pH of 7 after each deposition step. The control group was immersed in double distilled water with the same pH as of each polyelectrolyte solution. Fourier transform infrared spectroscopy (FTIR), zeta potential measurement, UV/Vis spectrometer, contact angle analysis, scanning electron microscopy (SEM), water vapor permeability (WVP), oxygen and carbon dioxide permeabilities were performed to characterize the nano-multilayer coating ob PET. The quality parameters of coated and uncoated mangoes were determined by measuring mass loss, total soluble solids (TSS) and titratable acidity (TA). The WVP results showed that LbL coatings caused a drastic reduce on WVP of the PET films ($(1.42 \pm 0.39)*10^{-11}$ g*m/Pa*s*m^2 for original A/C PET, and $(0.019 \pm 0.005)*10^{-11}$ g*m/Pa*s*m^2 for the A/C PET coated with five polysaccharide nanolayers). The LbL coating effect on the oxygen permeability ($(2.5 \pm 0.03)*10^{-14}$ g*m/ Pa*s*m^2 for original A/C PET film vs $(0.069 \pm 0.066)*10^{-14}$ g*m/ Pa*s*m^2 for the LbL coated film) and carbon dioxide permeability of the films ($(39.7 \pm 22.9)*10^{-14}$ g*m/Pa*s*m^2 for the original film vs $(44.8 \pm 32)*10^{-14}$ g*m/Pa*s*m^2 for the LbL coated film) was determined. Higher mass loss, higher total soluble solids (TSS) and a lower titratable acidity (TA) was onserved from the analyse of the uncoated mangoes in comparison to coated mangoes. In addition to this, coated mangoes maintained good quality, whereas uncoted fruits exposed a brownish color and had less appeal visual appearence which present evidence of microbial spoilage.

In another study of Medeiros et al. (2012), five layers of the polysaccharide kappa-carrageenan (0.2% (w/v), pH:7) and the protein lysozyme (0.2% (w/v), pH:3.8) were applied on whole and fresh-cut 'Rocha' pears. Characterization of nanolayers on PET support was performed using FTIR analysis, UV/Vis spectrometer, contact angle analysis, scanning electron microscopy, water vapor and oxygen permeability analyses. Shelf lives of coated and uncoated pears (whole and fresh-cut) were evaluated through mass loss, TSS, TA and color measurements. It was found that uncoated whole and fresh-cut pears showed higher mass losses (3.8 and 1.75 times, respectively) compared to the coated pears. As a result of oxidation processes, a darker color was appeared on the surface of uncoated fresh-cut pears. Oxygen permeability of A/C PET and five nanolayers were meausered as $(2.5\pm0.03)\times10^{-14}$ g m^{-1} s^{-1} Pa^{-1}, and $(0.1\pm0.01)\times 10^{-14}$ g m^{-1} s^{-1} Pa^{-1}, respectively. Uncoated fresh-cut pears showed a darker color, therefore this study showed the nanolayered coating had positive effect on the quality and shelf life of fresh fruits.

Souza et al. (2015) applied five alternated layers of alginate/chitosan on fresh-cut "Tommy Atkins" mangoes. The LbL assembly was performed with the deposition of alginate (0.2% w/v, pH:7, 15 min ads. time) and chitosan (0.2% w/v, pH:3, 15 min ads. time) on fresh-cut mangoes. Coated and uncoated fruits were stored at 8 °C for 14 days. Their mass loss, titratable acidity, pH, ascorbic acid content, total soluble solids, browning rate and microbial count was invastigated during the storage period. It was found that the nanomultilayered coatings showed improvement on the microbiological and physicochemical quality of the fruit. Mesophilic and psychotropic microorganism counts demonstrated a 5 log CFU/g and 2 log CFU/g reduction in coated fresh-cut mangoes, respectively.

Yan et al. (2019), applied and compared two different coatings on postharvest strawberries; an LbL coating fabricated from chitosan/carboxymethyl cellulose (CMC), and a conventional coating from 1% (w/v) chitosan solution. Control samples are immersed into distilled water. All samples were packaged and stored at 0° C for 8 days. Quality of the fruits was assessed through the analyses of firmness, total soluble solids, total acidity and volatile compounds. Both the conventional chitosan coating and LBL coating induced positive effects on strawberry firmness, but they had little effect on the total soluble solids and total acids after eight days storage at 0 °C. Results showed potential of LbL coatings for maintaining quality of posharvest strawberry.

Arnon et al. (2015) aimed at developing a coating that can serve as a natural alternative to synthetic waxes that are used to prolong the shelf life of citrus fruits. The

performances of methylcellulose (MC), hydroxypropyl methylcellulose (HPMC), carboxymethylcellulose (CMC) and chitosan (CH) were investigated separately on mandarins. CMC did not show any effect on the fruit natural flavor and respiration process, but it provided the fruits lowest weight loss and best firmness. CMC concentration of (1.5% (w/v)) was selected as an internal layer and three different chitosan concentrations (0.5%, 1% and 1.5% (w/v)) were used as second external layer. The LbL coatings showed better firmness than single layer-coated and uncoated mandarins. On the other hand, excessive chitosan concentration caused an increase in ethanol content in the fruit juice, which is not desired since it may cause off-flavor. In this study, the concentration of 1.5% (w/v) CMC and 1% (w/v) chitosan were chosen for the formation of LbL coating. This formulation was applied to various citrus fruits: two types of mandarins ('Or' and 'Mor'), 'Navel' oranges and 'Star Ruby' grapefruit. Quality parameters of the fruits were investigated after four weeks of cold storage and an additional five days at shelf- life conditions (20° C). Also, the LbL coatings were compared to commercial wax in terms of the quality of the fruits. The results showed that the LbL CMC/chitosan coating and commercial polyethylene-based wax revealed similar effect in terms of fruit gloss, firmness enhancement, and water loss inhibition. Eventually, they concluded that the LbL edible coating was found as an alternative to the currently used commercial synthetic waxes (Arnon et al. 2014).

CHAPTER 2

MATERIALS AND METHODS

2.1. Materials

Lysozyme (BCBP6286V) and gum arabic (from Acacia Tree, BCBP5087V) were obtained from Sigma-Aldrich (St. Louis, MO, USA), Iota-carrageenan was obtained from Alfa Aesar (T06B041- Karlsruhe, Germany). NaOH and HCl (Sigma-Aldrich, St. Louis, MO, ABD) solutions of appropriate molarity were used for the adjustment of pH values of the solutions. Ethanol and glass slide cleaning liquid (Hellmanex III, Fluka, Germany) were purchased from Sigma (St. Louis, MO, USA). Substrates on which the layer-by-layer deposition was carried out were quartz slides (50 x 25 x 1 mm, Lightpath Optical, UK) for UV-VIS spectrometer, Cr (2nm)+Au (50 nm) +SiO_2 (10 nm) coated glass sensors (Bionavis, Finland) for Surface Plasmon Resonance (SPR), microscope slides for Atomic Force Microscopy (AFM) analysis, and corona treated polypropylene (PP) films (kindly donated by Polinas, Manisa) for the O_2 and water vapor transmission (WVT) analysis.

2.1.1. Cleaning Procedure of Quartz and Glass Slides

The quartz slides (for UV experiments) and glass substrates (for AFM analysis) were cleaned throughly in order to avoid any contamination during the LbL assembly. Ultra pure water, 2% (v/v) Hellmanex III solution, and absolute ethanol were used for this purpose. Cleaning was performed following the method of Artyukhin and Stroeve (2003). Briefly, the substrates were exposed to ultrasonication at 55˚C for 15 minutes each in ultra pure water (18 mΩ, Milli-Q Ultrapure Water System, Millipore), 2% (v/v) Hellmanex III solution and absolute ethanol, respectively. After each step, the substrates were rinsed with plenty of ultra pure water and completely dried with pure nitrogen gas (Güneş Industrial Gases Manufacturing and Trading Co., Turkey) at the end of the final stage. Then they were stored in a clean container until being used. The quartz cuvettes,

which were used in the determination the follow-up absorption wavelength for each type of polyelectrolyte, were also cleaned following the same procedure.

Freshly prepared piranha solution (H_2O_2, H_2SO_4) was used to clean Cr+Au+SiO_2 coated glass sensors (for SPR analysis) and also quartz slides (for UV experiments) when necessary. Piranha solution is a 3:1 mixture of sulfuric acid (H_2SO_4) and 30% hydrogen peroxide (H_2O_2), and it is used to wash the persistent organic residues off the substrates. After the substrates were incubated for 15 minutes in the piranha solution, they were rinsed throughly with plenty amounts of ultra pure water followed by gentle drying using pure nitrogen.

2.2. Methods

2.2.1. Preparation of Lysozyme, Gum Arabic and Iota-carrageenan solutions

Lysozyme and gum arabic solutions were prepared dissolving 0.2 % (w/v) of material in ultra pure water under agitation, with a magnetic stirrer (250 rpm) for 24 hours at room temperature (25 °C). Iota-carrageenan solution was also prepared dissolving 0.2 % (w/v) in ultra pure water at 70 °C under agitation (250 rpm) for 2 h followed by further agitation for 22 h at 25 °C.

The pH values of lysozyme solutions were adjusted to 3, 5, 7, 8 using aproppriate amounts of 1M NaOH or 1 M HCl solutions. The pH values of iota-carrageenan and gum arabic solutions were adjusted to 6, 7, 8 and 3, 5, 7, respectively, using proper amounts of 0.5 M NaOH or 0.5 M HCl solutions.

2.2.2. Determination of the Electrical Properties of the Polyelectrolyte Solutions

Zeta potential of lysozyme, gum arabic and iota-carrageenan solutions at various pH values were performed in order to determine the appropriate LbL assembly conditions for each polyelectrolyte solution.

The choice of the pH range to work at for each polyelectrolyte solution was made according to the corresponding pKa and the isoelectric point (pI) values of the biopolymers. For lysozyme, a set of three different solutions with pH values of 3,5,7 was prepared at the given concentration. As the pI of lysozyme is ~11, the proteins in the solutions were expected to carry a net positive charge, the density of which depends on the pH value. The presence of glucuronic acids (pKa ~ 2) on gum arabic, and the sulfate groups (pKa ~ 2) on iota-carrageenan are responsible of the polyanionic character of the two polyelectrolytes, respectively. Therefore, in order to ensure that the polyelectrolytes carry a net negative charge in solutions, the pH values of the set of three solutions were adjusted to 3, 5, and 7 for gum arabic, and to 6, 7, and 8 for iota-carrageenan. The reason that smaller pH values were not considered for iota-carrageenan solutions is that the pKa value for Iota carrageenan is 4.9 according to some other studies.

Each solution was prepared at 0.2% (w/v) and passed through a syringe filter (pore size 0.45μm, CA, Isolab, Germany) before the measurements. After degassing the filtered solutions by ultrasonification (Elmasonic, S40, Germany) for 15 min, the measurements were carried out with DLS Nano Particle Size and Zeta Potential Analyzer (NanoPlus-3, Micromeritics Particulate Systems, Japan) at room temperature in at least two replications. 3 measurements were taken for each sample. The results were calculated as the average of 6 readings.

The zeta potential is calculated from the electrophoretic mobility (particle velocity) of the molecules via Henry equation (Equation 1). The measurement of the electrophoretic mobility is performed based on the Laser Doppler Velocimetry principle as a result of the electrophoresis process applied to the sample.

$$U_E = 2\varepsilon z f(Ka)/3\eta \quad (1)$$

where U_E is electrophoretic mobility; ε is dielectric coefficient; z is zeta potential; *f(Ka)* is Henry function and η is the dynamic viscosity.

2.2.3. The Layer-By-Layer (LbL) Assembly Procedure

The substrates for multilayer assembly were quartz slides for UV-Vis experiments, glass slides for AFM experiments, Cr+Au+SiO_2 coated glass sensors for SPR (Surface Plasmon Resonance) analysis and coronated PP films for O_2 and water vapor transmission rate experiments. Two types of multilayered coatings of different

chemistry were constructed; i.e., Lysozyme-gum arabic, and lysozyme-iota-carrageenan. The LbL deposition by dipping method was carried out as follows: Because the surfaces of all the substrates are negatively charged, the substrates were firstly incubated in the polycation solution (Lysozyme) of the desired pH for 10 (or 20) minutes, followed by rinsing in ultrapure water at the same pH with the polyelectrolyte for 1 minute. Rinsing step was performed to remove excess lysozyme molecules that were weakly bound on the surface. Afterwards, the substrates (onto which the lysozyme layer has been deposited) were dried with a gentle flow of nitrogen gas. Subsequently, theywere immersed into the polyanion solution (gum arabic or iota-carrageenan) for another 10 (or 20) minutes and washed with ultrapure water for 1 minute. All these steps resulted in the deposition of one bilayer on the substrate. The steps were repeated to form 5 bilayers (10 layers) in total. The substrates with LbL coatings were left to drying in a desiccator containing silica gel granules (BDH, VWR Chemicals, Belgium) under 0% relative humidity until being used in the AFM and gas transmission experiments.

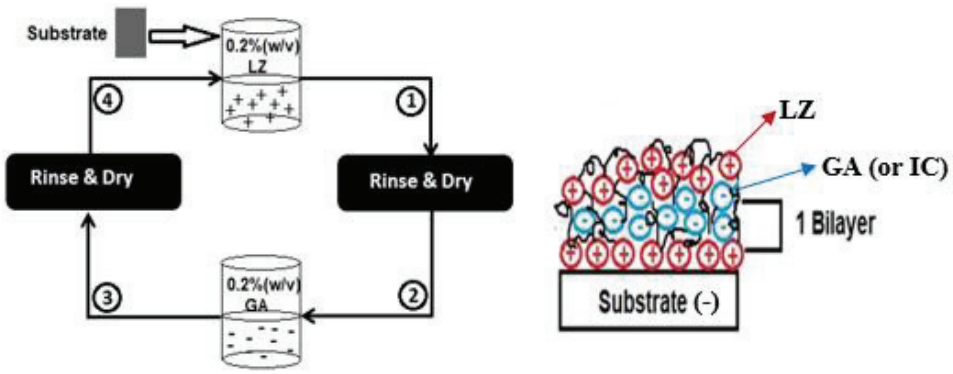

Figure 2.1. Schematic illustration of LbL assembly on a planar substrate using oppositely charged polymers (LZ-GA, LZ-IC).

2.2.4. Characterization of the LbL coatings by UV-Visible Spectroscopy

This method was used at each deposition step to monitor the multilayered coating formation. The measurements were performed using Perkin Elmer Lambda 25 UV-Vis Spectrometer (USA). In order to specify the follow-up wavelength(s), dilute solutions (0.01-0.3 % w/v) of lysozyme, gum arabic and iota-carrageenan were prepared separately and analyzed with UV-Vis sperctroscopy at 190-400 nm. Coatings were prepared separately for each layer on quartz slides as explained in Section 2.2.3. The follow-up wavelenghts were determined as 280 nm, which is the exitation wavelenght of proteins,

and 195 nm to monitor the total adsorption wavelength. All measurements were repeated at room temperature at least twice, and each measurement was corrected by reference (uncoated quartz slide).

2.2.5. Characterization of the LbL coatings in situ by Surface Plasmon Resonance (SPR)

SPR (BioNavis SPR-Navi 200, Finland) was used both in scan and fixed angle modes for the *in situ* characterization of LbL coatings at each deposition layer. The optic prisim was used in Kretschmann configuration. A special glass substrate coated with 2 nm Cr + 50 nm Au + 10 nm SiO_2 (Bionavis, Finland) was used as an SPR sensor. The purpose of the silicon dioxide layer was to imitate the quartz surface on which the LbL deposition process was carried out by dipping in UV-Vis experiments. Formation of the LbL coatings on the SPR sensor was actualized within the flow cell of the instrument to allow *in situ* characterization of the coatings. All of the solutions were filtered by a 0.45 μm cellulose acetate syringe filter (Isolab, Germany) followed by degassing with ultrasonification (Elmasonic, S40, Germany) for 15 min before being injected into the flow cell. For the deposition of the first layer, the lysozyme solution (% 0,2 w/v, pH 7) was injected into the flow cell with the aid of a syringe and allowed to stand for 10 min. At the end of this process, deionized water (pH 7) was injected into the flow cell for rinsing. Later, the SPR measurement was taken in angular scan mode. The same steps were repeated for the formation of the second layer with the gum arabic solution at the appropriate concentration and pH value. During the deposition of Lysozyme-iota-carrageenan coatings, iota-carrageenan solution at the desired concentration and pH was injected as the second layer. The characterization of each layer was performed in this manner up to 10 layers.

2.2.6. Characterization of the LbL Coatings by Atomic Force Microscopy (AFM)

AFM was used to determine the thickness, surface morphology and roughness of the LbL coatings. Scans were made both in air and liquid (*in situ*) environments using the Atomic Force Microscopy Digital Instruments – MMSPM Nanoscope IV (USA). The

data analyses were performed by NanoScopeAnalysis v1.4 (Bruker, Germany). The glass slides were prepared by cutting them into small pieces (1 cm x 1 cm) and used as substrate for AFM analysis. Prior to AFM imaging in air, each sample was dried completely in a desiccator containing silicon beads (0% relative humidity). AFM air scans were performed in peak force tapping mode with a silicon tip probe (Rtespa, 300 kHz resonance frequency, 40 N / m spring constant). AFM imaging in liquid medium was performed *'in situ'* (right after the formation of the layers within the flow cell of the instrument). The scans were conducted in static mode with a silicon nitrate Scanasyst-fluid (+) probe (resonance frequency 150 kHz, spring constant 0.7 N/m). All of the scans in air and liquid media were performed over areas of 10 x 10 μm^2. Additionally, 100 x 100 μm^2 areas were scanned in air imaging.

The images were taken for only the 1st, 2nd, 5th, 6th, 9th and 10th layers in both media. Post-imaging process involved the flattening of each image using a function of 1st or 2nd order. Then, the surface roughnesses were calculated from the topographies. Surface roughness of the layers was evaluated both in terms of the root mean square (RMS) average of height deviation taken from the mean image data plane (R_q), and the arithmetic average of the absolute values of the surface height deviations measured from the mean plane (R_a). In R_a and R_q equations, Z(x) is the function that describes the surface profile analyzed in terms of height (Z) and position (x) of the sample over the evaluation length "L". Thus, R_a is the arithmetic mean of the absolute values of the height of the surface profile Z(x). The RMS roughness of a surface is similar to the roughness average, with the only difference being the mean squared absolute values of surface roughness profile (De Oliveira et al., 2012).

$$R_q = \sqrt{\frac{1}{L}\int_0^L |Z^2(x)|\,dx} \tag{2}$$

$$R_a = \frac{1}{L}\int_0^L |Z(x)|\,dx \tag{3}$$

For surface roughness measurements, at least 3 different areas of each sample were scanned and the results were evaluated as the arithmetic mean of these scans.

The thickness measurements of the layers were performed only in air imaging. Firstly, the sample surface was scratched slightly (without damaging the substrate) with sterile blades wrapped with parafilm, and then, the scanning was performed. The layer

thickness was calculated from the depth of the scratch (obtained from the height profile f aline crossing the scratcho). The thickness measurements were repeated at least 2 times from at least 5 different parts of the stratch, and the results were calculated as the arithmetic average of these measurements. In order to observe the differences in the thicknesses of coatings prepared with drying and without drying, the scans were taken of both types of samples for both Lysozyme-Gum arabic and Lysozyme-Iota carrageenan LbL coatings.

2.2.7. Characterization of the LbL Coatings by Scanning Electron Microscopy (SEM)

Scanning Electron Microscopy (SEM) (FEI Quanta 250 FEG, USA) was used for characterization of the surface morphologies. In SEM analysis, corona treated PP films were used as substrates. All samples were completely dried in a desiccator containing silicon beadsprior to analysis. After drying, LbL films were coated with gold (0.05nm) in the presence of argon gas using a K550 X sputter coater (Quorum Technologies, London). Coating the film surface with gold was necessary to give electrical conductive properties to the nanolayer coatings. Samples were treated with an acceleration voltage of 3 kV and in 10 μm to 100 μm working distances. At least 2 samples were scaned for each of the 5th and 10th layer of the LbL coatings.

2.2.8. Oxygen Transmission Rate (OTR) Measurements

Oxygen transmission rates (OTR) of the LbL coated PP film samples were determined using the gas permeation instrument, (PBI Dansensor Lyssy, L-100-5000 Manometric Gas permeability Tester, Denmark) according to the ASTM D1434-82 standard. In the differential pressure method (manometric method), permeation across a film is driven by a difference in absolute pressure across the film. The sample is placed in a chamber connected to a vacuum pump. The pressure difference across the sample is created by maintaining the test gas at atmospheric pressure in the upper chamber, while vacuum is applied in the lower measuring chamber. As the gas permeates through the sample, the pressure in the lower measuring chamber increases. By measuring the change in pressure over time and finding the slope of the change once it becomes linear, the

oxygen transmission rate across the film can be determined. The measurements were carried out at constant temperature (23 °C) and relative humidity (0% RH) conditions with 5-10 cm^3/min gas flow on samples composed of 10 layers prepared with drying and without drying step. In order to make reliable comparisons with the literature data, which is usually given in terms of permeabilities, the following relation was used:

$$Permeability = \frac{OTR}{\Delta P} * L_{film} \quad (4)$$

where, ΔP is the pressure difference across the film, and L_{film} is the thickness of the tested film.

2.2.9. Water Vapor Transmission Rate (WVTR) Measurements

Mocon Permatran-W model 3/33 water vapor permeation measurement system was used in order to measure the water vapor transmission rates of the LbL coated PP films. All WVTR tests were conducted at 37.8 ºC and 90% RH according to the ASTM F1249 standard.

The device is composed of test cells, which are divided into two chambers seperated by the sample material. The inner chamber is filled with nitrogen and the outer chamber with water vapor. The test film was placed between the two cells where the uncoated PP surface of the film was in the water vapor rich side. Carrier gas, nitrogen, was passed through ultra pure water to adjust the RH and was allowed to flow into the test cell. While the water vapor diffused through the test film, it was carried by nitrogen to the detector. Nitrogen flow rate was set to 100 cm^3/min. The data were recorded as water vapor transmission rate (WVTR). For both Lysozyme-Gum arabic and Lysozyme-Iota carrageenan LbL coatings, 10 layered samples were prepared with and without drying step. At least two different samples for each formulation were tested and their average was reported.

In order to make reliable comparisons with the literature data, which is usually given in terms of permeabilities, the following relation was used:

$$Permeability = \frac{WVTR}{S(R_1 - R_2)} * L_{film} \quad (5)$$

where, R_1 is relative humidity at the source expressed as a fraction (R_1 = 0.9 for 90% RH

chamber), R_2 is relative humidity of the vapor sink expressed as a fraction ($R_2 = 0$ for the 0% RH chamber (dry side)), S is the vapor pressure of water at the test temperature and L_{film} is the thickness of the tested film.

2.2.10. Statistical Analysis

All experiments were carried out in at least 2 replicates and for each replicate at least 2 measurements were performed. Statistical analysis of the datas is performed by using MINITAB® release 17 (Minitab Inc., State College, Pa., U.S.A.) The results were measured as arithmetic mean of the obtained datas and they were shown with their standard deviation. All results were controlled by one-way analysis of variance (ANOVA), and significant differences ($p < 0.05$) were determined by Tukey test.

CHAPTER 3

RESULTS AND DISCUSSION

3.1. Preliminary Results

As preliminary analysis, the zeta potential of polyelectrolyte solutions at various pH values were performed in order to determine the appropriate LbL assembly conditions for each polyelectrolyte solution and the multilayer growth follow-up wavelength(s) used in UV-Vis spectroscopy experiments were determined.

3.1.1. Zeta Potential Measurements of Lysozyme, Gum Arabic and Iota Carrageenan

The formation of multilayer coatings/films by LbL assembly is based on the sequential adsorption of oppositely charged polyelectrolytes on a substrate which posses a net surface charge. Since the adsorption is the result of electrostatical interactions (mainly), the surface charge density of each polyelectrolytes in the dilute solution is important. The electrical charge of the polyelectrolytes provide crucial information on how these polyelectrolytes will behave during the process of polyelectrolyte multilayer construction. However, the main factor that determines the behavior of polyelectrolytes in polar solutions is their zeta potential (effective surface charge) values. When a particle is suspended in liquid, it is surrounded by an ionic shell composed of two regions; an inner region called the Stern layer where the ions are strongly bound and an outer diffuse region where they are less firmly attached as shown in Figure 3.1. When the particle moves, ions within a certain boundary in the diffuse layer move with it, but any ions beyond the boundary do not move with the particle. This boundary is called the surface of hydrodynamic shear or the slipping plane. The potential on this surface is called the zeta potential and it reflects the effective surface charge of the particle. Generally, when all the particles have a large positive or negative zeta potential (where the positivity and negativity is greater or lower than +30mV and −30mV), they repel each other and the

dispersion is stable. On the other hand, when the particles have low zeta potential values, the repulsive forces may not sufficient to prevent the particles from the aggregating (Wongsagonsup et al., 2005). The most important factor affecting the zeta potential value of the weak polyelectrolyte molecules in a solution is the pH of the solution, because the pH of the medium determines how much of the ionizable groups on the polyelectrolyte are ionized. In addition to the solution pH, concentration and type of polyelectrolytes, ionic strength, the dielectric constant and temperature of the medium affect zeta potential. Some authors state that the effect of pH is much stronger than that of ionic strength and other factors on an electrostatic self-assembly process of a weak polyelectrolytes (Choi and Rubner 2005; Fu et al., 2005). Therefore, in this study, pH was selected as the only factor for zeta potential measurements.

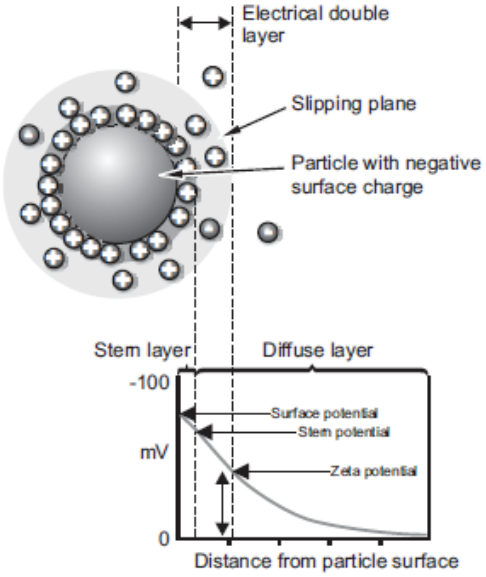

Figure 3.1. Zeta Potential of a particle with negative surface charge (Source: Nanotechnology in Soil Science, 2015).

The zeta potential of lysozyme and gum arabic particles in dilute solutions of 0.2 % (w/v) at 3 different pH values (3,5,7), and iota carrageenan particles in solutions of 0.2 % (w/v) at 3 different pH values (6,7,8) were determined as described in Section 2.2.2. The results of the measurements with standard deviations are given in Table 3.1. As expected, the zeta potential of gum arabic shows a decreasing trend (increasing in magnitude) with an increase in the solution pH. This is because pKa of gum arabic is 2.0 due to the presence of glucuronic acids in its structure (Gulao Eda et al., 2016). Carboxylate polysaccharides like gum arabic get deprotonated (become anionic) at a pH range higher than their pKa. The more the solution pH is away from the pKa, the more

the polyelectrolytes are deprotonated, resulting in decreasing zeta potential (increasing in magnitude) with pH. Porto et al. (2014) reported that the arabic gum possessed negative electrical charge within the whole range of pH evaluated (from 2 to 8) and the corresponding zeta potential ranged from -2.7 (pH 2) to -28.6 mV (pH 6) at 0.2% (w/v) concentration (Porto et al., 2014).

The pH-dependent zeta potential results of lysozyme solutions are evaluated with their standard deviations. As expected, there is increase in zeta potential with decrease in pH of the lysozyme solution. This is because the pI of lysozyme is ~ 11. Therefore, as the pH of the medium is reduced below 11, the net positive charge of the protein becomes prominent (K and Bandyopadhyay, 2012). The results are consistent with the literature. For instance, Medeiros et al. (2012) reported that a zeta potential value of +25.67±2.27 mV was found for 0.2% (w/v) lysozyme at pH 3.8. In another study, they reported a value of +29.27±3.18 mV for 0.2 % (w/v) lysozyme at pH 3.8 (Medeiros et al., 2013).

Since the pKa value of the anionic sulfate groups on iota carrageenan is around 2, the zeta potential decreases (increases in magnitude) with pH above this value as seen in Table 3.1. The results confirm to those of similar studies in the literature. Medeiros et al. (2012), determined that a kappa-carrageenan solution (0.2 % (w/v)) at pH 7 exhibited a zeta-potential of −60.53 ± 0.15 mV. Carneiro-da-Cunha et al. (2011) reported zeta potential values of -39.6 mV and -56.8 mV for 0.2 % (w/v) solutions of kappa carrageenan at pH 5 and pH 7, respectively.

Table 3.1. Zeta potential of Gum arabic, Lysozyme and Iota carrageenan solutions at different pH values.

pH	**Zeta Pot. (mV) ± SD**
Gum arabic pH-3	-8.667 ± 1.902[a]
Gum arabic pH-5	-23.173 ± 5.579[b]
Gum arabic pH-7	-39.141 ± 3.184[c]
Lysozyme pH-3	46.770 ± 3.180[a]
Lysozyme pH-5	31.457 ± 0.608[b]
Lysozyme pH-7	7.182 ± 1.091[c]
Iota carrageenan pH-6	-44.420 ± 2.940[a]
Iota carrageenan pH-7	-46.540 ± 8.220[a]
Iota carrageenan pH-8	-54.750 ± 8.750[a]

3.1.2. Determination of the Multilayer Growth Follow-Up Wavelength Used in UV-Vis Spectroscopy Experiments

Before monitoring layer-by-layer assembly in UV-Vis spectroscopy experiments, it is necessary to determine the wavelength at which each type of polyelectrolyte exhibits highest absorbance in the UV range**.** For that purpose, dilute solutions (0.01-0.2 % w/v) of lysozyme, gum arabic and iota carrageenan were prepared separately and analyzed with UV-Vis spectroscopy at wavelengths in the range of 190-400 nm. The absorption spectra of each type of polyelectrolyte are shown in Figure 3.2. As expected, a characteristic peak of absorption for lysozyme was obtained at 280 nm, which is the excitation wavelength of proteins due to their content of tyrosine (Tyr), tryptophan (Trp), and phenylalanine (Phe) amino acids. For gum arabic, there is a slight peak at 280 nm due to its small protein content (~2 % (w/w)). On the other hand, a characteristic peak was not obtained for iota carrageenan. Neither gum arabic nor iota carrageenan comprise a characteristic chromophore that absorbs energy within the visible range. Yet, all the polyelectrolytes exhibit the highest absorbance values in the range 190-195 nm. According to these results, it was decided to monitor the multilayer formation by following the absorption at two wavelengths; i.e., 280 nm to monitor the amount of protein adsorption, and 195 nm to monitor the total adsorbed mass.

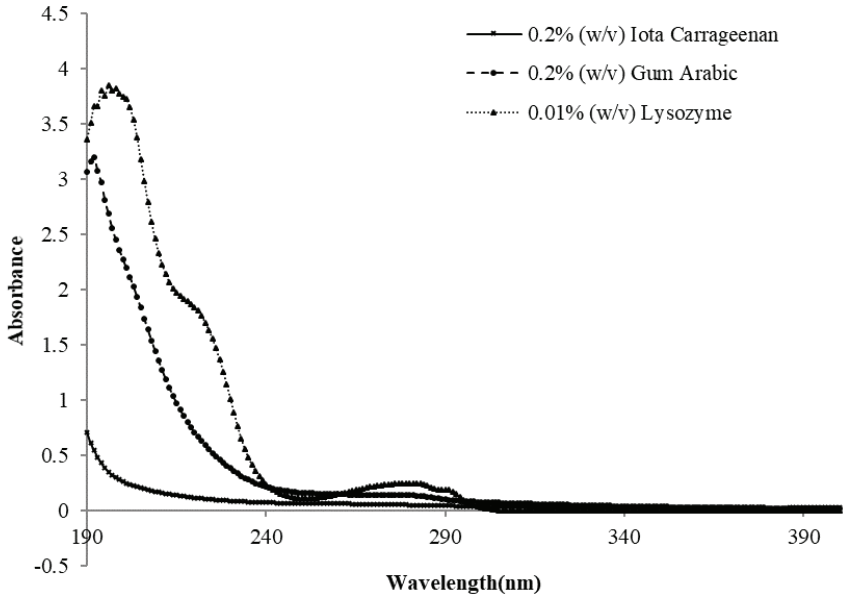

Figure 3.2. UV-Vis absorption spectra of 0.01-0.2 % (w/v) lysozyme, gum arabic and iota carrageenan solutions within the wavelength range of 190-400nm.

3.2. LbL coatings Fabricated from Lysozyme and Gum Arabic

The LbL coatings fabricated from lysozyme and gum arabic were characterized by using UV-Vis spectroscopy, surface plasmon resonance (SPR) analysis, atomic force microscopy (AFM) and scanning electron microscopy (SEM). However, oxygen and water vapor transmission rate of the coatings were measured in order to determine film properties.

3.2.1. UV-Visible Spectroscopy Results

The formation of LbL coatings from lysozyme and gum arabic was carried out by dipping method and followed by UV-Visible spectroscopy. The effects of solution pH, the adsorption (dipping) time of polyelectrolytes, number of layers and exclusion of intermediate drying steps on multilayer formation were examined. In order to observe the effect of solution pH, the pH combinations of pH 3 & 3, pH 5 & 5, pH 3.8 & 5.3 and pH 7 & 7 were chosen considering the pI of Lysozyme (~ 11) and pKa of Gum arabic (~ 2). The effect of adsorption time was examined through two different dipping times; 10 min and 20 min. Additionally, two different adsorption time combinations (1st layer for 30 min and the remaining layers for 5 min; all lysozyme layers for 20 min and all gum arabic layers for 5 min) were tested for the reasons explained below in Section 3.2.1.2. LbL coating formation using the selected pH combinations and dipping times were monitored up to 10 layers.

3.2.1.1. Effect of Solution pH

It is well known that the solution pH influences the degree of ionization of weak polyelectrolytes, which changes their effective surface charge density. Thus it affects the propagation of the LbL assembly process (Shiratori and Rubner, 2000). The deposition of the LbL coating (ten successive lysozyme (Lyso) and gum arabic (Gum) layers) on the quartz slides was followed by UV–vis spectroscopy at 195 nm after each deposition step at 4 different pH combinations (Lyso pH 3 & Gum pH 3, Lyso pH 5 & Gum pH 5, Lyso pH 3.8 & Gum H 5.3 and Lyso pH 7 & Gum pH 7). In these experiments, 20 min was

selected as the adsorption time, because the highest amounts of deposition were obtained with it (see Figure 3.4).

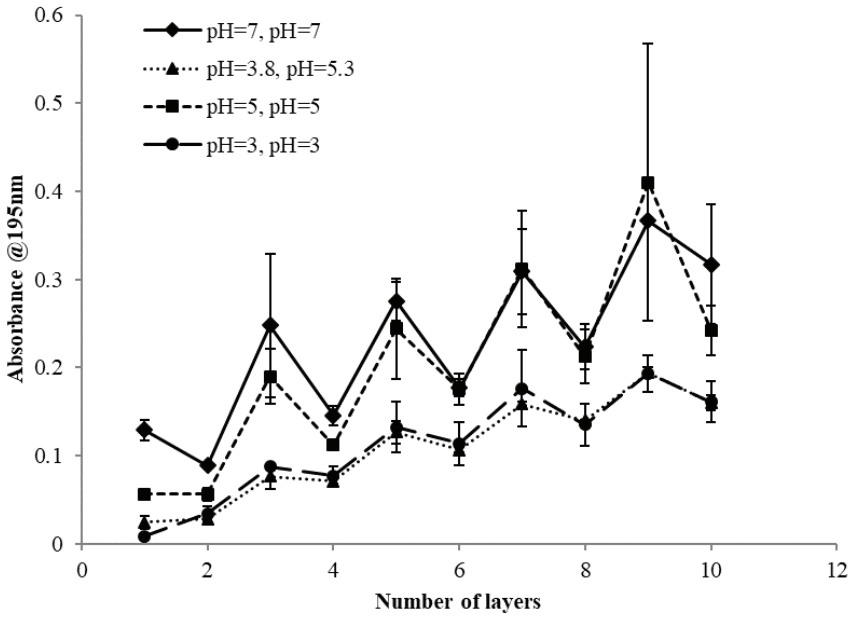

Figure 3.3. Monitoring the effect of solution pH on Lysozyme-Gum Arabic multilayer formation by UV-Vis spectroscopy. (The absorbances at 195 nm was monitored. Adsorption time was 20 minute. Error bars represent the standard deviations).

Figure 3.3 shows that the film growth behavior was similar in all pH combinations, showing a zig-zag trend. It is observed that the absorbance increases with each LZ deposition step and decreases partially at each GA adsorption step (except the 2nd layers for low pH conditions). This behavior suggests that some of the pre-adsorbed LZ comes of upon the adsorption of GA, probably due to formation of a soluble complex between LZ and GA. The figure also shows that the most succesful LbL deposition was obtained with the pH 7 & 7 combination. Lyso pH 3 & Gum pH 3, and Lyso pH 3.8 & Gum pH 5.3 combinations gave similar results with each other. Although Lyso pH 7 & Gum pH 7, and Lyso pH 5 & Gum pH 5 combinations exhibit similar zig-zag trends, there is higher absorbance (thus, more deposited mass) at especially the 1st layer of Lyso pH 7 & Gum pH 7 combination. This must be due to the increasing effective (negative) charge density at the quartz surface with increasing pH, which is the consequence of higher numbers of ionized surface silanol groups at higher pH (Behrens and Grier, 2001). One should keep in mind that it is not only the polyelectrolytes of which the degree of ionization is affected by the solution pH. The surface charge density of the quartz (silica) substrate is also influenced by the solution pH and ionic strength. It is known that the

ionization of surface silanol groups is too low at very acidic conditions, and the degree of ionization increases with pH. Therefore, the reason that the highest amount of lysozyme adsorption was obtained at pH 7 at the first layer despite of the lowest zeta potential of the polyelectrolyte must be that the surface of the quartz subtrate had much more negatively charged sites to bind a larger number of lysozyme molecules compared to the cases of lower pH. This result also suggests that the achievement of a good surface coverage in the first deposition step is very important for a more succesfull propagation of the LbL process.

3.2.1.2. Effect of Adsorption Time

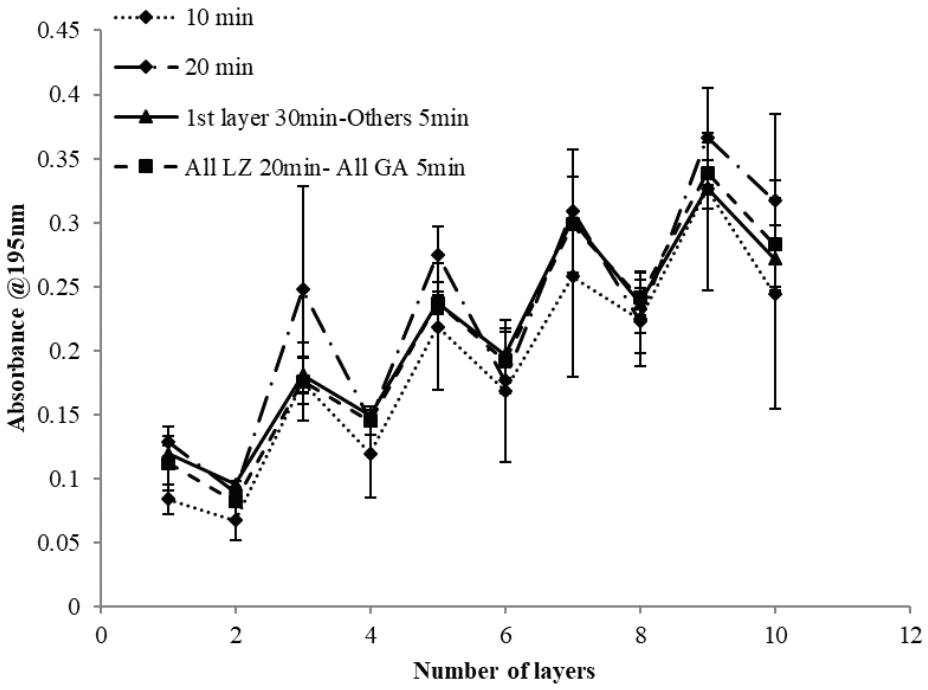

Figure 3.4. Monitoring the effect of adsorption time on Lysozyme-Gum Arabic multilayer deposition at pH 7&7 combination by UV-Vis spectroscopy. (The absorbances at 195 nm was monitored. Error bars represent the standard deviations).

One of the factors that determine the success of the layered deposition and the properties of LbL film is the adsorption time of polyelectrolytes to the substrates. In general, the longer adsorption time gives more successful LbL formation. The reason might be that the polymer chains have enough time to relax and reconstruct on the surface as well as inside the multilayers for long deposition times, while, they have limited time

to settle down on the surface for short deposition times (Yu et al., 2017). Adsorption time typically ranges from 5 to 20 minutes since the equilibration time at which the substrate surface is saturated with the adsorbed polyelectrolyte is usually considered to be 10-20 minutes.

The effect of adsorption time on LbL film formation was investigated by UV-Visible spectroscopy for the pH combination of Lyso pH 7 & Gum pH 7. Firstly, 10 min and 20 min adsorption times were experimented. As Figure 3.4 shows, the lowest absorbance values were obtained with 10 min adsorption time at each deposition step. Therefore, it is clear that 10 min was not sufficient to achieve surface saturation of the polyelectrolytes. On the other hand, 20 min adsorption time gave the largest amounts of deposition, especially at LZ deposition steps. In order to check if surface saturation was achieved at the first layer with 20 min, the 1st LZ adsorption step was repeated trying a longer (30 min) adsorption time. When the measured absorbance values were considered (Figure 3.4), it was concluded that 20 min adsorption time was sufficient for surface saturation.

As stated before, the zig-zag trend in the absorbance vs number of layers graphs indicates that some of the pre-adsorbed LZ comes off from the surface probably due to formation of soluble complexes between LZ and GA (and their release from the coating-water interface). In order to test if shortening the adsorption times for the GA deposition steps would somehow restrain the release/loss of soluble LZ-GA complexes from the coatings, and thus result in larger amounts of deposited mass at the end of the process, 5 min adsorption times were experimented for GA deposition (both keeping the LZ deposition time at 20 min and restricting it to 5 min). The results (Figure 3.4) suggest that surface saturation is also critically important during the GA adsorption steps, and 5 min is definitely not sufficient. This is inferred from the observations that the amount of LZ deposition at the subsequent steps, whether it was for 20 min or 5 min, did not differ, while significantly larger amounts of LZ deposition was obtained for the case where 20 min was adopted in the deposition of both types of polyelectrolytes. The total amount of adsorbed mass at the end of 10^{th} deposition step was also the highest (as the absorbance was highest). These results also support the findings of Alotaibi et al. (2018), who determined that the substrate should be immersed in each polyelectrolyte solution for more than 12 min for an optimal LbL deposition (Alotaibi et al., 2018).

3.2.1.3. Effect of Number of Layers

The previous UV-Vis spectroscopy results at pH 7&7 combination and 20 min adsorption time shows that the absorbance values at 195 nm increase linearly with the deposition of each bilayer indicating a successful propagation of the LbL coating formation. This is also proved by the *in situ* SPR experiments of which the results are given in Section 3.2.2.

3.2.1.4. Effect of Intermediate Drying Step

Another factor that can have important effects on the buildup and the structure of polyelectrolyte multilayers (PEMs) is the intermediate drying process. The effects of intermediate drying step on PEM formation from LZ and GA were explored at the pH combination pH 7&7, and at 20 minute adsorption time. Some samples were air-dried by leaving them at room temperature after each layer deposition step for a few minutes (dried samples) while others were not (wet samples). In order to see effect of drying step, drying was applied only after the 1st, 5th and 10th deposition steps. Firstly, samples were dried at room temperature, and then, nitrogen flow was applied gently to the surface to be sure they were fully dried.

Figure 3.5. shows that dried LbL films had higher absorbance values relative to wet LbL films, which suggests that more lysozyme and gum arabic deposition were obtained with the application of intermediate drying. 1st layer (Lysozyme) gives almost the same absorbance with the last layer 10th layer (Gum arabic) at non-dried LbL film. Therefore, the drying step is necessary for enough re-adsorption (Chen et al., 2001). And it also shows that drying is crucial for long adsorption time. Furthermore, these results indicate that drying process leads to more adsorption sites to become available for the adsorption of the next polyelectrolyte. In the study of Raposo et al. (1997), similar results were attained from LbL deposition of poly(o-methoxyaniline) (POMA) and POMA/poly(vinylsulfonic acid sodium salt) (PVS) on glass substrates.

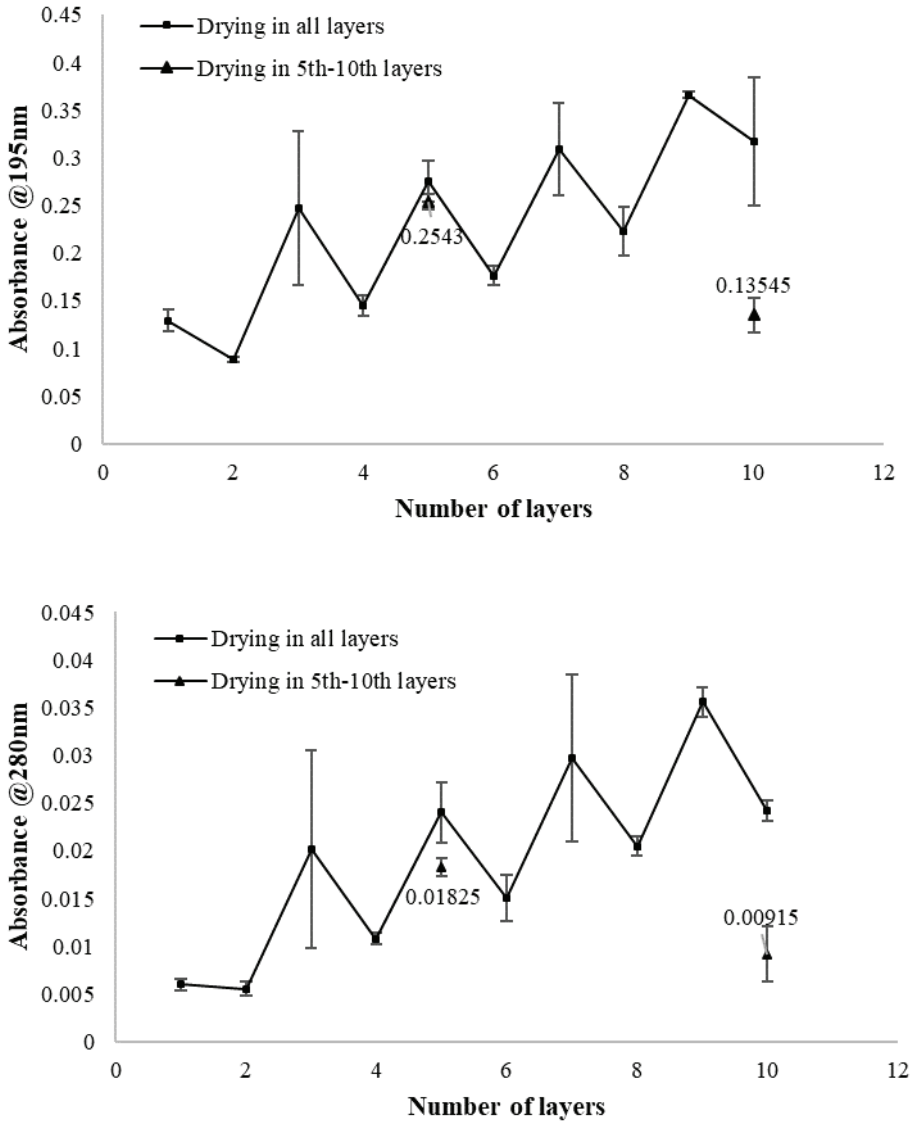

Figure 3.5. Monitoring the effect of drying step on Lysozyme-Gum Arabic multilayer deposition at pH 7&7 combination by UV-Vis spectroscopy. (The absorbances at 195 nm and 280 nm were monitored. Error bars represent the standard deviations).

3.2.2. Surface Plasmon Resonance (SPR) Results

In this section, SPR experiments were performed in scanning mode. Thus, the shift in SPR angle due to the deposition of polyelectrolytes occurring at the metal dielectric interface can be observed as a function of time. Figure 3.6. shows the formation of LZ-GA LbL coatings at pH 7&7 and 10 min adsorption time. The red arrows show the times when the sample (lysozyme or gum arabic) solutions were injected at each deposition step and the blue arrows indicate when the rinse solution was injected. Due to

the limitations in the configuration of the instrument (the necessity to work with a peristaltic pump to ensure flow and limited capacity of the injection loop), the adsorption was performed for up to 10 minutes at each step.

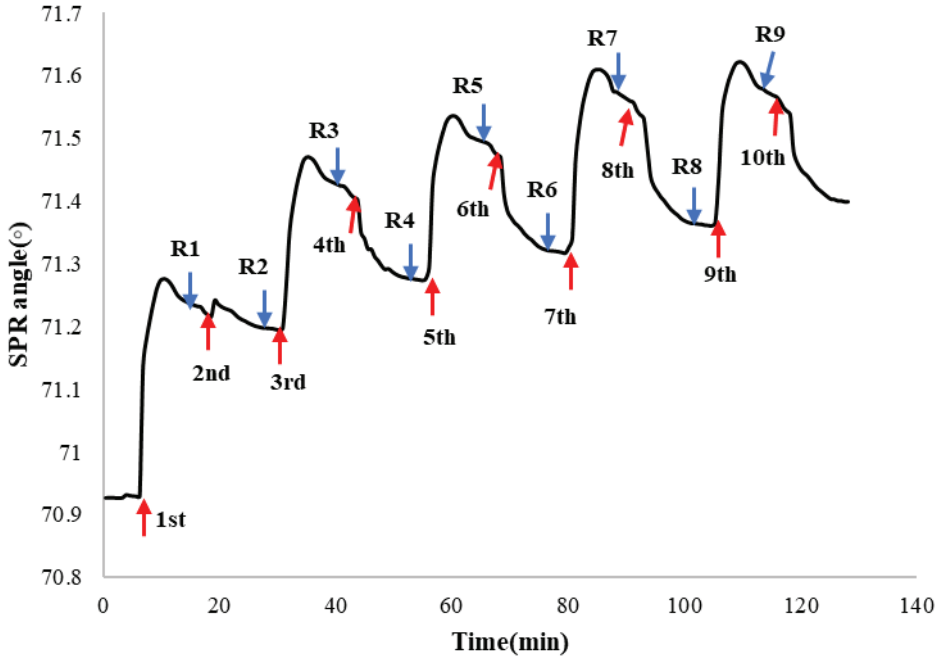

Figure 3.6. Monitoring the change in SPR angle with the deposition of each layer (LZ-GA). (0.2 % (w/v) solutions at pH 7-7 were used. The adsorption time was 10 min. Red arrows show the time at which lysozyme and gum arabic solutions were injected, blue arrows show the time at which rinsing solution was injected).

With the first injection (arrow number 1) (Figure 3.6), it appears that the lysozyme adsorption on the sensor began to take place rapidly, and over time excess lysozyme molecules which were weakly bound to the surface began to be released from the surface along with the flow. There was also a decrease in the SPR angle by the injection of the rinsing solution. In the second step, by the injection of gum arabic solution slight increase was observed in the SPR angle and weakly bound gum arabic molecules were released from the surface with flow. Moreover, there was a decrease in the signal when the second rinsing step was applied. For the rest of the layers (3rd-LZ, 4th-GA, 5th-LZ, 6th-GA, 7th-LZ, 8th-GA, 9th-LZ and 10th-GA layers), similar SPR angle change trend observed: as lysozyme solution was injected, there was sharp increase in the signal. This was followed by desorption of the pre-adsorbed lysozyme from interface with the deposition of gum arabic on it, probably due to formation of soluble complexes between them. The same trend was also obtained in UV-Vis spectroscopy experiments.

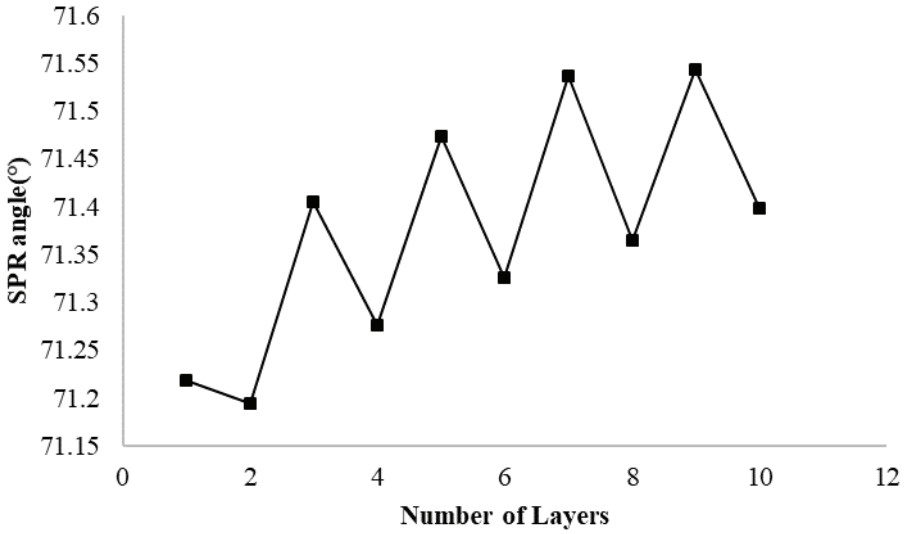

Figure 3.7. Shifts in SPR angle during the adsorption of each layer in LbL assembly of lysozyme and gum arabic (0.2 (w/v) % solutions at pH 7&7, 10 min adsorption time).

3.2.3. Atomic Force Microscopy (AFM) Results

The morphology of film surface was characterized by atomic force microscopy. According to UV-Vis spectroscopy results, the best LZ-GA LbL formation was obtained at pH 7&7 combination and with 20 min adsorption time. These conditions were used for AFM analysis. AFM air scans were performed in dynamic mode using a silicon tip probe (300 kHz resonance frequency, 40 N / m spring constant). AFM imaging in fluid medium was performed '*in situ'* after formation of layers in the flow cell of instrument. Scans were conducted in static mode with a silicon nitrate Scanasyst-fluid (+) probe (resonance frequency 150 kHz, spring constant 0.7 N / m).

Figure 3.8 shows a comparison of three-dimensional AFM images taken under both air and fluid media. The data scales were equalized for each layer to compare air and fluid medium differrences. *In situ* and in-air AFM analysis were applied to 1^{st}-LZ, 2^{nd}-GA, 5^{th}-LZ, 6^{th}-GA, 9^{th}-LZ and 10^{th}-GA layers. According to AFM image results, the surface coverage is increasing with the increase in number of layers. In-air and fluid medium images, first two layers show similar results in topoghraphy and roughness. However, the roughness starts to rise dramatically in *in situ* analysis after 5^{th} layer.

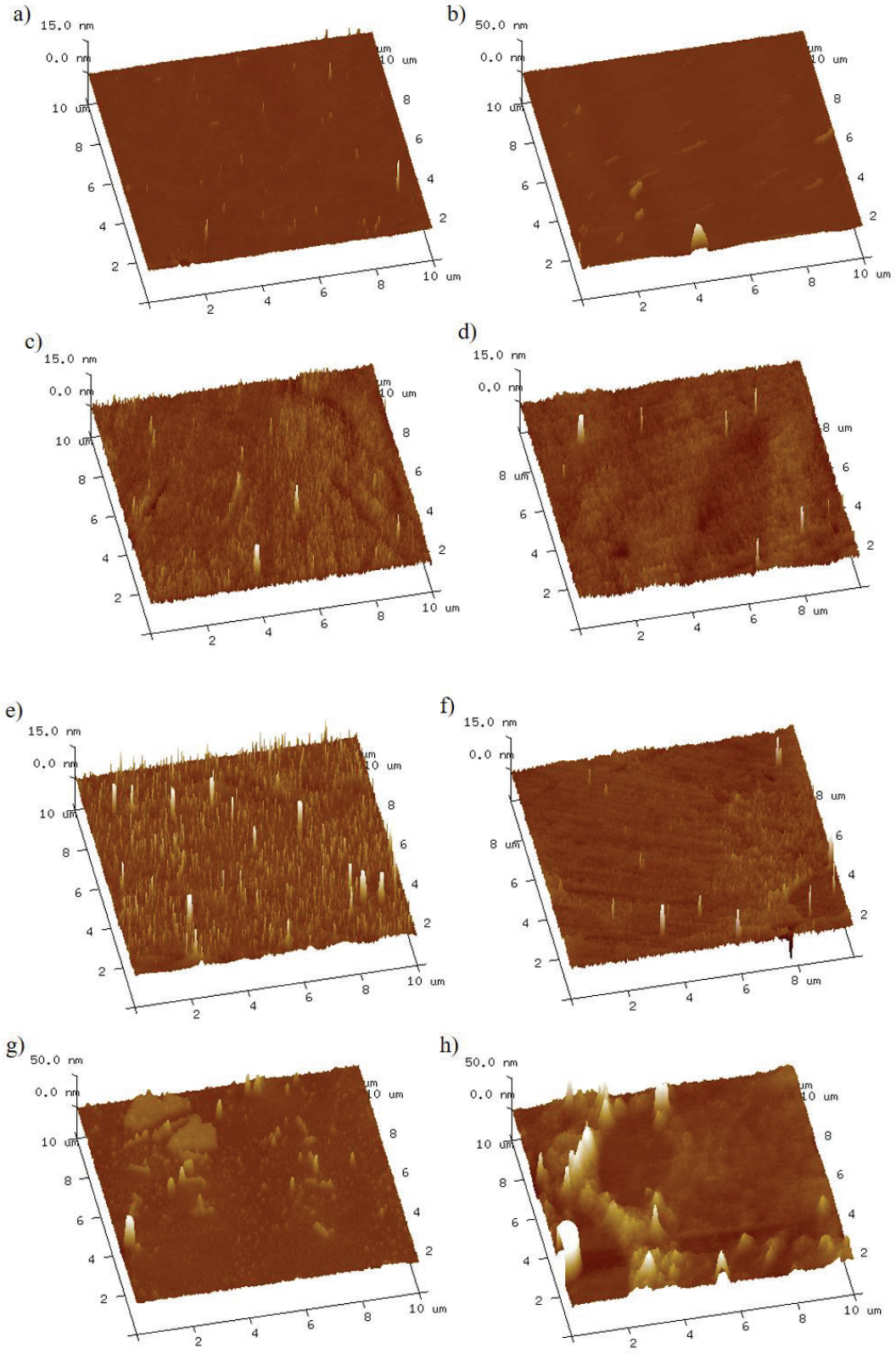

Figure 3.8. AFM images (in air and in fluid) of surface topography of layers obtained by LZ-GA LbL assembly at pH 7&7 combination with 20 min adsorption time. Scan area is 10x10 μm^2. Data scales of the images were equalized. (a) Plain glass-air, (b)Plain glass-fluid, (c) 1st layer (LZ)-air, (d) 1st layer (LZ)-fluid, (e) 2nd layer (GA)-air, (f) 2nd layer (GA)-fluid, (g) 5th layer (LZ)-air, (h) 5th layer (LZ)-fluid

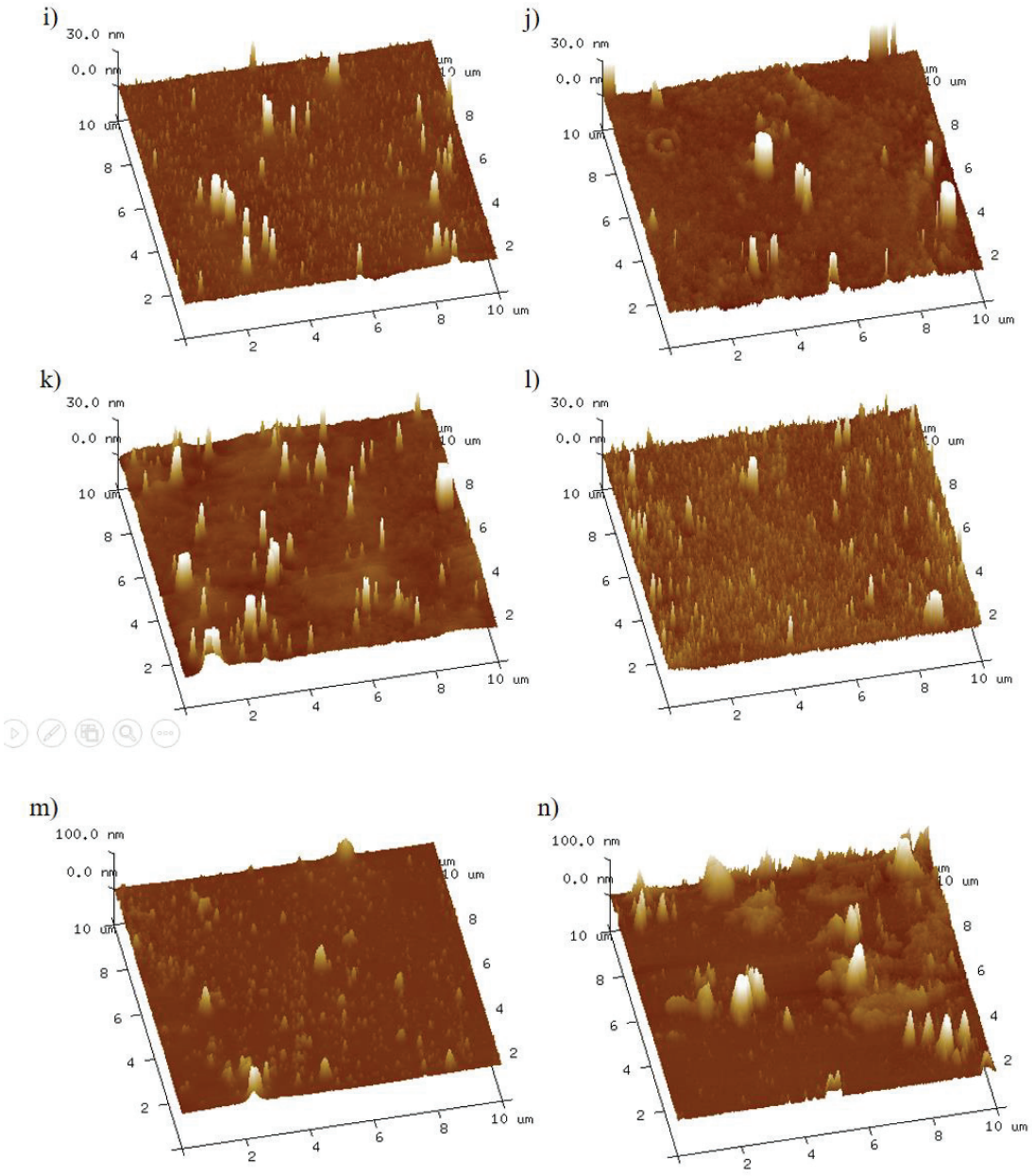

Figure 3.8. AFM images (in air and in fluid) of surface topography of layers obtained by LZ-GA LbL assembly at pH 7&7 combination with 20 min adsorption time. Scan area is 10x10 μm^2. Data scales of the images were equalized. (i) 6^{th} layer (GA)-air, (j) 6^{th} layer (GA)-fluid, (k) 9^{th} layer (LZ)-air, (l) 9^{th} layer (LZ)-fluid, (m)10^{th} layer (GA)-air, (n) 10^{th} layer (GA)-fluid.

Especially, for the last layers, in-air images exhibit more homogenous and smoother surfaces compared to in-fluid images. This might be because of two effects. First, the presence of water during *in situ* imaging might have facilitated the releasing of soluble complexes from the interface. This is because the molecules have higher lateral and vertical mobility within the coatings in the presence of water. This, in return, might

have resulted in less homogenous surfaces, and thus rougher layers. Another reason could be that as the evaporation of water during the dehydration of aggregates might have induced the capillary forces, causing the collapse and fusion of the aggregates, and producing a compact and thin layer (Zhang et al., 2012).

A previous study showed that in *in situ* AFM analysis, skipping the intermediate drying steps in the LbL assembly led to the loose deposition of silicate and TiO_2 nanoparticles and therefore produced highly porous silicate/TiO_2 films with large thicknesses. In contrast, the application of LbL assembly with drying was shown to producethin silicate/TiO_2 films with compact structures (Zhang et al., 2012).

Table 3.2. The surface roughness values of LZ-GA LbL layers in air and fluid medium obtained from 10x10 μm^2 scan areas. Statistically significant differences were tested with ANOVA and significant differences ($P < 0.05$) were determined by Tukey test. Exponential values with different letters were significantly different.

Number of layers	Image Rq(nm)±SD	Image Ra(nm)±SD
Air-1st layer	1.643 ± 1.014^{CD}	0.888 ± 0.334^{cd}
Air-2nd layer	1.255 ± 0.858^{D}	0.549 ± 0.268^{d}
Air-5th layer	3.12 ± 0.558^{CD}	1.496 ± 0.288^{bcd}
Air-6th layer	2.43 ± 0.675^{CD}	1.095 ± 0.077^{cd}
Air-9th layer	3.268 ± 0.913^{CD}	1.443 ± 0.174^{bcd}
Air-10th layer	3.512 ± 2.019^{C}	1.748 ± 1.106^{bc}
Fluid-1st layer	1.388 ± 0.494^{CD}	0.938 ± 0.250^{cd}
Fluid-2nd layer	1.031 ± 0.120^{CD}	0.699 ± 0.029^{cd}
Fluid-5th layer	13.075 ± 1.276^{A}	5.782 ± 0.781^{a}
Fluid-6th layer	8.974 ± 0.516^{B}	2.65 ± 0.531^{b}
Fluid-9th layer	4.07 ± 1.983^{C}	2.087 ± 0.384^{bc}
Fluid-10th layer	13.1 ± 0.0^{AB}	7.34 ± 0.0^{a}

Table 3.2. shows the roughness values obtained from AFM air and fluid medium analysis. The ANOVA results state that there are significant differences in roughness values after the 5^{th} deposition step between air and fluid medium results. When AFM roughness images and Rq-Ra values of the layers are considered together, it can be

understood that the intermediate drying step makes the LbL film flatter, and this means some re-organization of surface charges takes place, and drying blocks the inner and inter layer mobility of molecules which may cause charge saturation at the surface (Chen et al., 2001).

Thickness of the layers were determined by stratch method in air medium. The thicknesses of only the 5^{th}-LZ and 10^{th}-GA layers were measured for coatings prepared both with (dry) and without (wet) intermediate drying steps. The results are given in Table 3.3. According to the results, there is no significant difference in the thicknesses of 10^{th} layer between dried and non-dried samples ($P > 0.05$). However, there is a significant difference in the 5^{th} layers between dried and non-dried samples ($P < 0.05$).

Table 3.3. Changes in thickness of the LZ-GA LbL coatings with respect to number of layers and inclusion of intermediate drying step. Statistically significant differences were tested with ANOVA and significant differences ($P < 0.05$) were determined by the Tukey test. Exponential values with different letters are significantly different.

Samples	Thickness(nm)
5th layer^{dry}	67.875 ± 18.077^{a}
10th layer^{dry}	70.028 ± 40.999^{a}
5th layer^{wet}	28.868 ± 12.108^{b}
10th layer^{wet}	65.47 ± 37.207^{a}

The close images of 1^{st}-LZ and 2^{nd}-GA layers from AFM analysis are shown in Figure 3.10. It shows that adsorption of polyelectrolytes seems to be in the form of aggregates. The first layer LZ has roughness values as Rq: 0.551nm-Ra: 0.308nm, however, 2^{nd} layer GA has roughness values as Rq:2.41 nm - Ra:1.60 nm, indicating that the roughness values increase with adsorption of gum arabic layer.

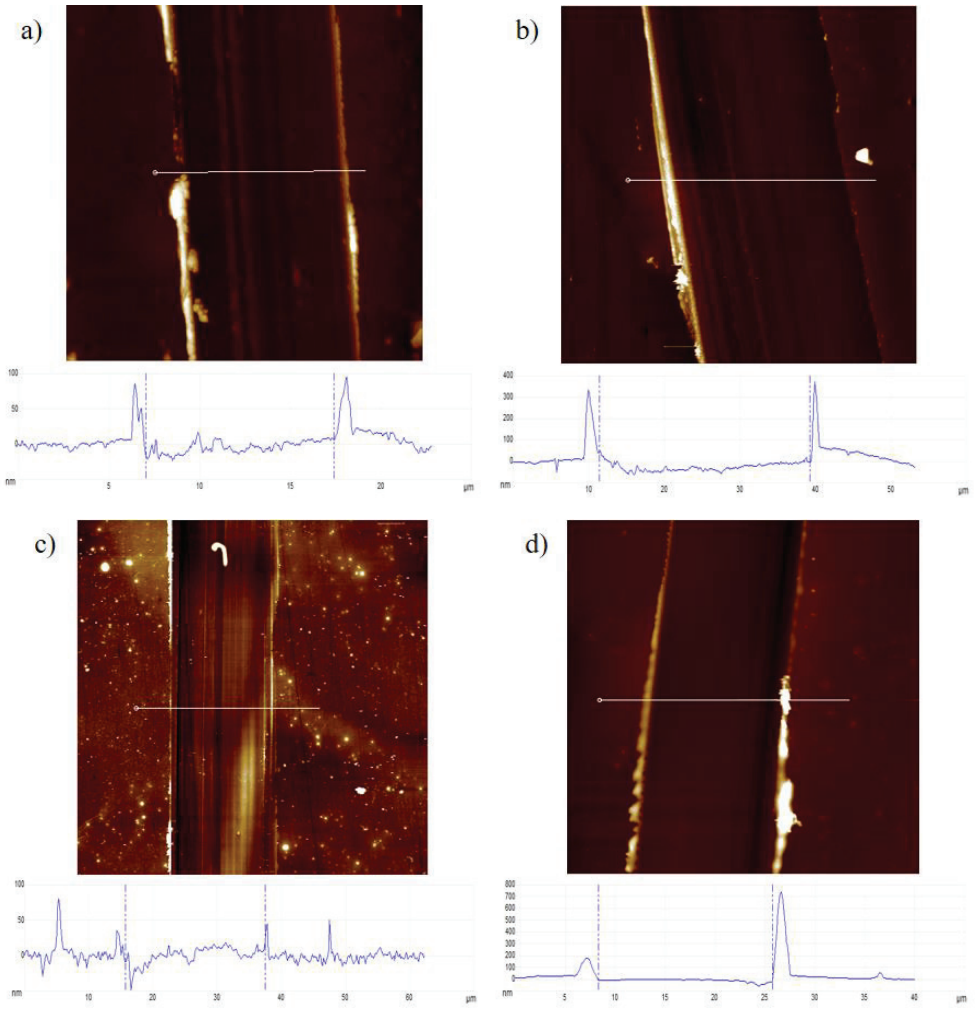

Figure 3.9. Determination of 5th and 10th layer thicknesses for both LZ-GA LbL coatings which are prepared with drying and without drying step using stratch method by scanning atomic force microscopy. The height profiles of the white section lines are given in the bottom of the each image. (a) 5th layer (no drying)-LZ, (b) 5th layer (with drying)-LZ, (c) 10th layer (no drying)-GA, (d) 10th layer (with drying)-GA.

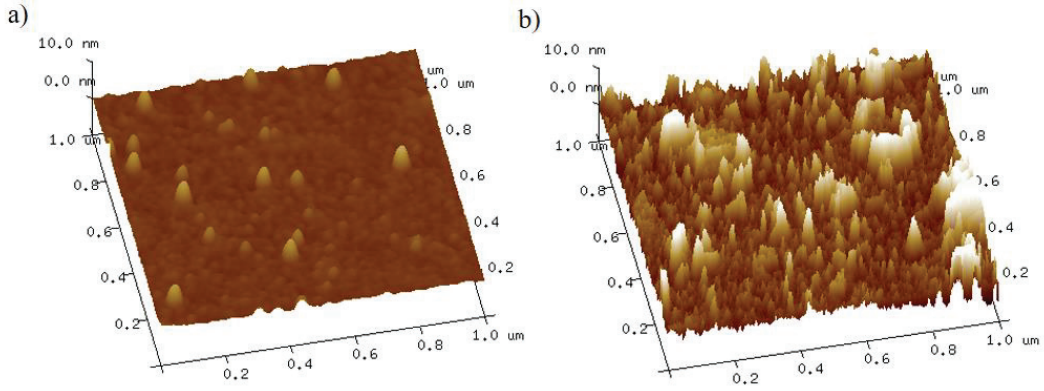

Figure 3.10. AFM images (in air) of surface topography of the (a)1st layer LZ and (b)2nd layer GA obtained by applying intermediate drying step at pH 7&7 combination with 20 min adsorption time. Scan area is 1x1 μm^2.

3.2.4. Scanning Electron Microscopy Results

The surface structure of LZ-GA LbL coatings were analyzed by scanning electron microscopy. The LbL coating samples were prepared at pH 7&7 combination, using 20 min adsorption time with intermediate drying steps. SEM images of the LZ-GA coating on a corona treated polypropylene substrate are shown in Figure 3.11. The images confirm the formation of a LZ-GA LbL coating on the substrate. The images of the 5th-LZ and 10th-GA layers show homogenous multilayer coatings on PP. Furthermore, the surface morphology of the 5th layer and the 10th layer are similar.

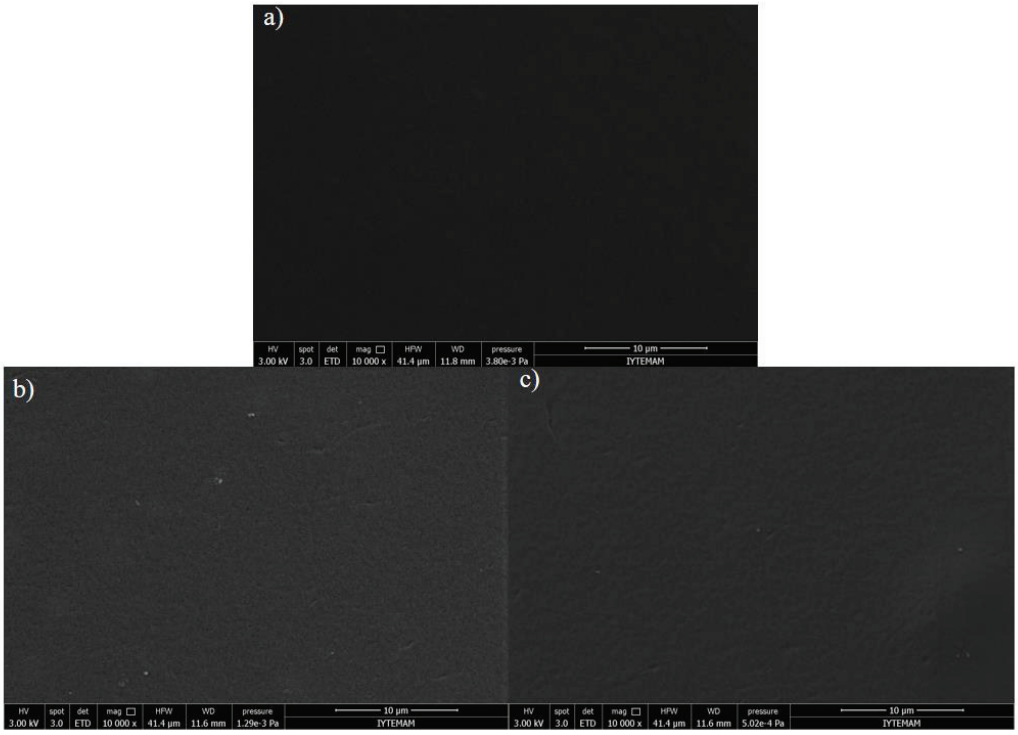

Figure 3.11. Scanning electron microscopy images of surface morphology of a) blank corona treated polypropylene (PP) film surface, b) 5 layers of LZ-GA LbL coating on corona treated PP c) 10 layers of LZ-GA LbL coating on corona treated PP. (Magnification 10,000× ,scale bar 10 μm).

3.2.5. Oxygen Permeability and Water Vapor Permeability Results

Oxygen transmission rate of Lysozyme-Gum arabic coated PP film samples was determined by using gas permeation instrument. The measurements were conducted at constant temperature (23 °C) and relative humidity (0% RH) conditions with 5-10

cm^3/min gas flow. For this experiment, 10 and 20 layered the non-drying LbL, and 10 layered drying LbL PP films were prepared. LZ-GA at pH 7&7 combination and 20 min adsorption time were used.

The OTR of blank PP and multilayer-coated PP film is shown in Table 3.4. In this case, with the deposition of LZ/GA layers, the reported OTR values of the PP film was decreased by 56.8% for 10 layered samples prepared with intermediate drying steps, 26.7% for 10 layered samples prepared without intermediate drying steps, and 27.3% for 20 layered samples prepared without drying steps. Since the 20 layered and 10 layered non-dried LbL coatings gave almost the same OTR values, the results indicate that the exclusion of intermediate drying resultes in lower efficiency in terms of barrier properties. The drying of the materials can modify the structure of the materials as it was observed in AFM and UV-Vis spectroscopy analyses. The exclusion of the intermediate drying steps resulted in inhomogenous film formation on the substrate, which, in return, led to higher OTR values.

Another factor that affects the quality and shelf life of the fresh products is the water vapor permeability of the films. The coatings were also tested for WVTR (Table 3.4). In this case, with the deposition of LZ/GA layers, the reported WVTR values of the PP film was decreased by 32% for 10 layered samples prepared with intermediate drying steps, 15% for 10 layered samples prepared without intermediate drying steps, and 29% for 20 layered samples prepared without drying steps. When 10 layered coatings are compared to each other with respect to the inclusion of drying step, results show that there is difference between PP^{dry}_{10} and PP^{wet}_{10} LbL coatings. Inclusion of drying step lead to decrease of water vapor transmission rate of the PP. The reason for this could be that the drying removes water from the film to make the layers more compact and more difficult to be hydrated, so the film surface still remains hydrophobic (Enescu et al., 2015). Moreover, as it was shown in AFM roughness results, inclusion of drying step leads to homogenous surfaces, which results in improvement in water vapour barrier properties.

Table 3.4. Oxygen and Water vapor transmission results for LbL films obtained by lysozyme and gum arabic at pH 7. Statistically significant differences tested with ANOVA and significant differences ($P < 0.05$) determined by the Tukey test. Exponential values with differennt letters were significantly different.

Samples (LZ-GA)	Oxygen transmission rate (ml/m^2-24hr) ± SD	Water vapour transmission rate ($grams/m^2$-24hr) ± SD
Blank PP	624.78 ± 0.0^{a}	7.193 ± 0.41^{A}
PP_{10}^{wet}	457.68 ± 59.08^{b}	6.022 ± 0.760^{AB}
PP_{20}^{wet}	453.89 ± 0.0^{b}	4.977 ± 0.210^{B}
PP_{10}^{dry}	269.33 ± 10.36^{c}	4.783 ± 0.216^{B}

In order to compare the gas barrier properties of the LbL coatings obtained in this study with those obtained in similar studies from the literature, the gas permeabilities of the individual 10 layered coatings were calculated. The calculation of WVP of the LZ-GA LbL coatings were made according to the ideal laminate theory:

$$\frac{P_L}{\Sigma \ell i} = \frac{WVTR_L}{S(R_1 - R_2)} = \frac{1}{\Sigma(\ell_i / P_i)}$$

where, WVTR : water vapor transmission rate of the LbL coated PP film = 4.783 $g/(m^2.day)$, S_{H2O} (38 °C) = 6626.122 Pa (vapor pressure of H_2O at 38 °C), R_1= 0.9 (relative humidity at the source), R_2= 0 (relative humidity at the sink), ℓ_i = thickness of layer, P_i = permeability of layer, P_L = permeability of the whole film.

The calculation for OP of the LZ-GA LbL coating can be done by following equation which is ideal laminate theory:

$$\frac{P_L}{\Sigma \ell_i} = \frac{1}{\Sigma\left(\ell_i / P_i\right)} = \frac{T_{RL}}{\Delta P}$$

where, ΔP: pressure difference across the film = 5000Pa, T_{RL} : oxygen transmission rate of the LbL coated PP film = 269.33 $mL/(m^2.day)$, ℓi = thickness of layer, P_i = permeability of layer, P_L = permeability of the whole film.

As the standard deviations of the thickness measurements by AFM were high, the permeability calculations were performed considering both the lower and upper limits of the measured thicknesses. Therefore, the calculated values are given as a range in Table

3.5. As it is seen from the table, both the WVP and the OP of the LbL coatings obtained from LZ/GA in this study are 1 to 2 orders of magnitude lower than those of similar films/coatings obtained by others. Therefore, the results suggest that a very promising application of these coatings in combination with MAP for the preservation of fresh/fresh-cut produce.

Table 3.5. Comparison of LZ/GA LbL coatings with other coatings from literature in terms of OP (oxygen permeability) and WVP (water vapor permeability).

Sample	OP (mL/m.Pa.day)	WVP (g/m.Pa.day)	References
Blank PP	2.50×10^{-6}	2.41×10^{-8}	This study
10 layered (LZ-GA) LbL coating (dry)	$(2.75\text{-}10.51) \times 10^{-9}$	$(0.87 - 3.33) \times 10^{-10}$	This study
Starch+nanocellulose dispersed by GA		2.05×10^{-4}	Vigneshwaran et al. 2011
Chi edible coating	4.61×10^{-7}	7.43×10^{-9}	Fajardo et al. 2010
5 layers of k-carra/lys	6.49×10^{-8}	1.12×10^{-8}	Medeiros et al. 2011
5 layers of alg/chi		7.67×10^{-9}	Carneiro-da-Cunha et al. 2010

3.3. LbL coatings Fabricated from Lysozyme and Iota Carrageenan

The characterization of the coatings was performed by using UV-Vis spectroscopy, surface plasmon resonance (SPR) analysis, atomic force microscopy (AFM) and scanning electron microscopy (SEM). However, oxygen and water vapor transmission rate of the coatings were measured in order to determine film properties.

3.3.1. UV-Visible Spectroscopy Results

In this section the LbL coating made from Lysozyme (LZ) and Iota carrageenan (IC) was examined by UV-Vis Spectroscopy. Effects of solution pH, the adsorption(dipping) time, inclusion of drying step were observed by this experiments. In order to observe the effect of pH value of solution, for Lysozyme-Iota carrageenan coating pH 3.8 & 8.4, pH 7 & 7 and pH 8 & 8 combinations are chosen considering pI:11 value of Lysozyme and pKa:2 of Iota carrageenan. In order to investigate the effect of adsorption time on LbL assembly, two dipping time were chosen; 10 min and 20 min. To

investigate the effects of drying after each deposition step on the properties of the LZ-IC LbL coating, LbL samples with and without drying step were prepared.

LbL coating formation were executed by using selected combinations of pH values, and dipping times were followed up to 10 layers.

3.3.1.1. Effect of Solution pH

The formation of LbL coating on the quartz slides support surface was followed by UV–vis spectroscopy analysis at 195 nm of the ten successive lysozyme (LZ) and iota carrageenan (IC) layers at 3 different pH combinations which are lysozyme pH 7 & iota carrageenan pH 7, lysozyme pH 8 & iota carrageenan pH 8 and lysozyme pH 3.8 & iota carrageenan pH 8.4, after each deposition. 20 min adsorption time was selected for this experiment due to the literature (Xu et al., 2015). Figure 3.12 shows that even though pH 7&7 and pH 8&8 combinations gave same absorbance at 1st and 2nd layers, the most succesful pH combination was provided by lysozyme pH 7 & iota carrageenan pH 7. The pH combination of 3.8(LZ) & 8.4(IC) which are natural pH values for both polyelectrolytes gave less absorbance according to Figure 3.12. For pH 3.8&8.4 combination, there is no distinct trend as seen pH combinations of 7&7 and 8&8. The reason for observing less adsorption on natural pH combination of polyelectrolytes which is 3.8&8.4 combination, can be explaned as follows: A LZ/IC layer adsorbed to the substrate with a positive/negative charge density in the acidic/basic aqueous solution causes a sharp drop in degree of ionization(or reversal of the net electrical charge) basic/acidic IC/LZ solution which substrate immersed in the next step. The surface "redundant" charge which is necessary for continuation of LbL deposition cannot be provided.

3.3.1.2. Effect of Adsorption Time

To investigate the effects of deposition time of polyelectrolytes, LZ-IC LbL films with 5 bilayers were fabricated at different deposition time 10 min and 20 min. Figure 3.13 shows that even though both adsorption times give same absorbance at first 2 layers, the samples which are prepared by using 20 min adsorption time give higher absorbance than 10 min adsorption time. Therefore, 20 min adsorption time was chosen for further

experiments due to this results. This situation is also in agreement with the literature that the general assumption in layered deposition studies based on electrostatic interaction is that the longer the duration of the immersion process, the more successful the layered deposition will be and that the longer deposition time allows macromolecules to equilibrate and form a complete monolayer (Yu et al., 2017).

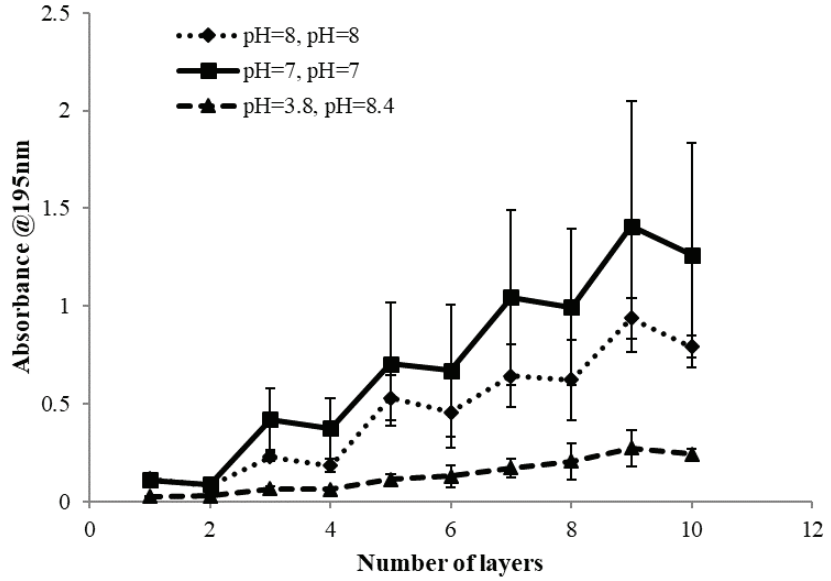

Figure 3.12. Monitoring the effect of solution pH on Lysozyme-Iota carrageenan multilayer formation by UV-Vis spectroscopy. (The absorbances at 195nm was monitored. Adsorption time is 20 minute. Error bars represent the standard deviations.)

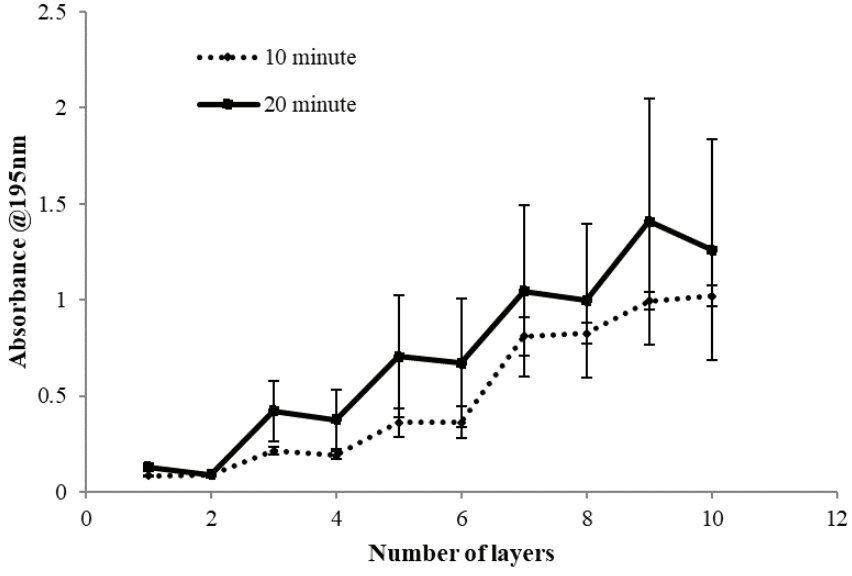

Figure 3.13. Monitoring the effect of adsorption time on Lysozyme-Iota carrageenan multilayer deposition at pH 7&7 combination by UV-Vis spectroscopy. (The absorbances at 195nm was monitored. Error bars represent the standard deviations).

3.3.1.3. Effect of Intermediate Drying Steps

The formation of LbL film formation process depending on intermediate drying step which was produced in combination of lysozyme pH 7 and iota carrageenan pH 7, at 20 minute adsorption time.

To see effect of drying step; drying process was applied only in 1st, 5th and 10th layers. Firstly, samples were dried at room temperature and then nitrogen flow was applied gently to the surface to be sure they are fully dried. From Figure 3.14., it can be seen that more lysozyme and iota carrageenan molecules has been assembled into the dried polyelectrolyte multilayer. The absorbance of a 4-layers film from the normal step (i.e., including a drying step every cycle) is almost equal to a 10 layer film fabricated without drying step. This might because of drying of the materials can make modifications on the structure of the materials which can influence to the dependence of the adsorbed amount with the number of layers, thus, the adsorption of the polyelectrolytes might be blocked. Therefore, the drying step is necessary for enough re-adsorption.

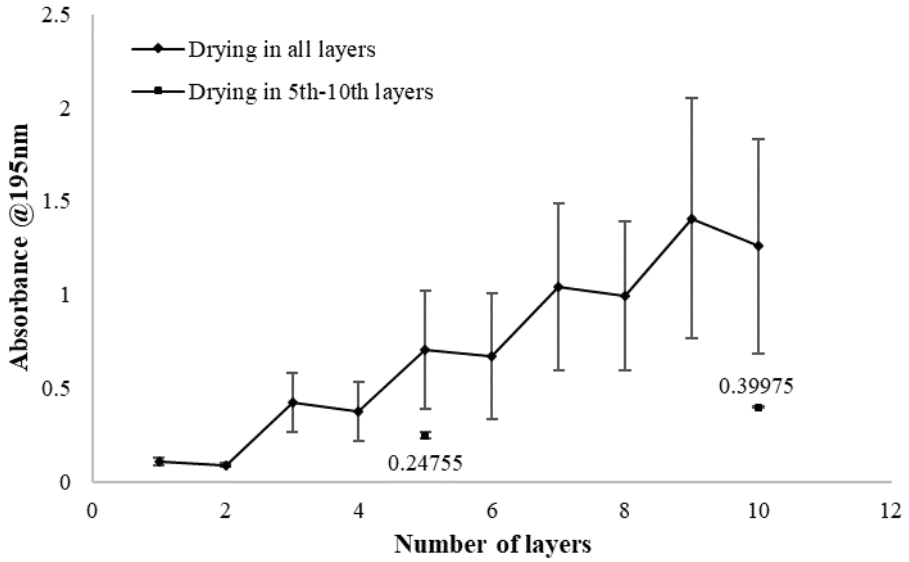

Figure 3.14. Monitoring the effect of drying step on Lysozyme-Iota carrageenan multilayer deposition at pH 7&7 combination and with 20 min adsorption time by UV-Vis spectroscopy. (The absorbances at 195nm was monitored. Error bars represent the standard deviations).

3.3.2. Surface Plasmon Resonance (SPR) Results

SPR experiments were performed in scanning mode. Figure 3.15. shows the formation of Lysozyme -Iota carrageenan LbL coating combination at pH 7-7 and 10 min adsorption time. The red arrows show the times when the sample (lysozyme or iota carrageenan) solutions are injected at each deposition step and the blue arrows indicate when the rinse solution is injected. It can be seen in SPR angle changes, with the first injection (1st layer LZ) that there is pretty fast adsorption of LZ, and after the saturation at the surface, there is release of weakly bound excess amount of LZ before rinsing. And, after injection of IC, a decrease was observed in SPR angle. It might be because of desorption of pre-adsorbed LZ from the interface with the deposition of IC on it, probably due to formation of soluble complexes between them. Untill 8th layer IC, same SPR angle change trend was occured: as LZ was injected, there is sharp increase and with injection of IC there is decrease probably due to soluble complexes between LZ and IC. By applying 8th layer IC to injection loop, it exhibited thorough desorption, the signal decreased to below the starting baseline. Also, this SPR result shows the importance of drying step in this LbL film formation. Same results were also observed in AFM in-situ analysis, after a certain layer deposition, adsorption of the polyelectrolytes was blocked because of releasing of the adsorbed polyelectrolytes from the surface.

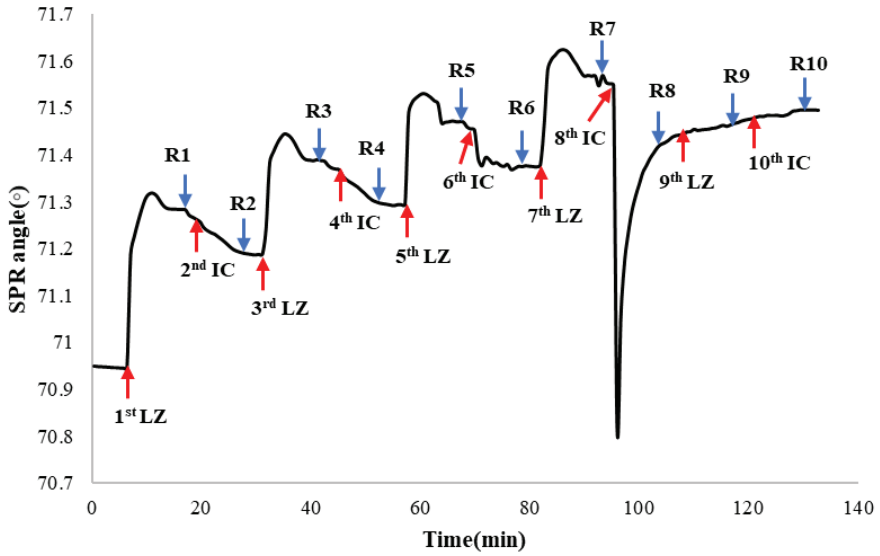

Figure 3.15. Monitoring the change in SPR angle with the deposition of each layer (LZ-IC) (0.2% (w/v) solutions at pH 7-7 were used. The adsorption time was 10 min. Red arrows show the time at which lysozyme and iota carrageenan solutions were injected, blue arrows show the time at which rinsing solution was injected).

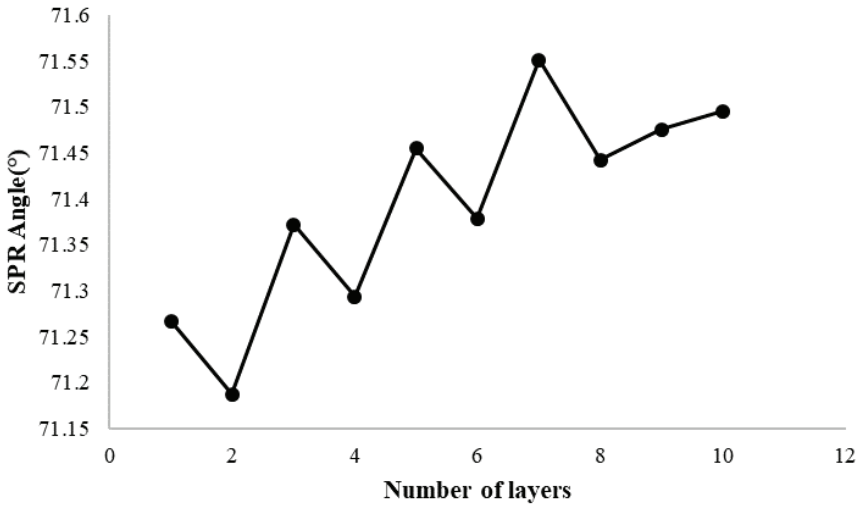

Figure 3.16. Shifts in SPR angle during the adsorption of each layer in LbL assembly of lysozyme and iota carrageenan (0.2 (w/v) % solutions at pH 7&7, 10 min adsorption time).

3.3.3. Atomic Force Microscopy (AFM) Results

AFM was utilized to characterize the morphology of the lysozyme/iota carrageenan multilayer thin films upon solid substrate. From previous results (UV-Vis spectroscopy), it was shown that the appropriate conditions to fabricate LbL coating from lysozyme and iota carrageenan are pH 7&7 combination with 20 min adsorption time. For AFM analysis, this experimental conditions were used for thickness measurements and surface characterization of the coatings. AFM imaging in fluid medium was performed '*in situ*' after formation of layers in the flow cell of instrument. Roughness measurements were applied to 1^{st}, 2^{nd}, 5^{th}, 6^{th}, 9^{th} and 10^{th} layers separately in order to see the effect of layer numbers. Thickness measurements were done to 5^{th} (LZ) and 10^{th} (IC) layers with and without drying step. The roughness was analyzed on at least two independent samples with 3 areas on each (having the number of measurements to be at least 6), but a single image most typical in the range of roughness for each sample is shown in Figure 3.17 and Figure 3.18.

Figure 3.17 shows three-dimensional AFM images of layers obtained in air medium. In order to be able to compare the obtained surface topographies correctly, the data scales of each layer were equalized. The AFM images clearly demonstrate the differences on the surface of uncoated plain glass (a), the LbL film coated with LZ-IC (b), that is, the surface roughness of the uncoated plain glass is much smoother than LbL

coating. When all layers were compared with each other, it can be seen that there is increase in roughness of the layers with the deposition of polyelectrolytes. The AFM images of samples showed peak and valley like structures with the incorporation of lysozyme and iota carrageenan polyelectrolytes and especially after 5th layer the gaps is filled by continuing the add of the polyelectrolytes. So it shows the succes of the layer by layer deposition of LZ-IC.

Figure 3.18. shows comparison of three-dimensional AFM images taken from both air and fluid medium. The data scales were equalized for each layer to compare air and fluid medium diferrences. *In situ* AFM analysis for LZ/IC LbL coating was performed only for 1st(LZ) and 2nd(IC) layers, because in further layers, the coating was adhered on tip of AFM probe and blocked movement of the tip (Figure 3.20.). According to 1st and 2nd layer AFM images, it says that more homogeneous surface structure is observed in liquid medium than air medium. But, the release of the coating from the surface in *in situ* analysis might be because of the desorption from surface during adsorption time (20 min) and it also shows that there is need for drying step for the arrangement of layer by layer assembly on the surface. Also it was observed in SPR analysis that after applying 8th layer to the injection loop, there was sharp drop in SPR angle may be due to desorption of coating from the surface. In each image the round shaped features or semi-spheres can be seen, which might be identified as a roughness protruding from a deposited polyelectrolyte film, pointing to the spatial uniformity of layer by layer films.

The close images of 1st-LZ and 2nd-IC layers from AFM analysis are shown in Figure 3.19. Data scale of images are equilized. It shows that adsorption of polyelectrolytes appears to be in the form of aggregates. The roughness values of 1st layer (LZ) and 2nd layer (IC) are Rq: 0.551-Ra:0.308, Rq:0.463nm-Ra:0.365nm, respectively. The roughness of 1st and 2nd layers are similar with each other. Also, it can be observed that the globular particles of lysozyme on the image of the 1st layer (Su and Li, 2008).

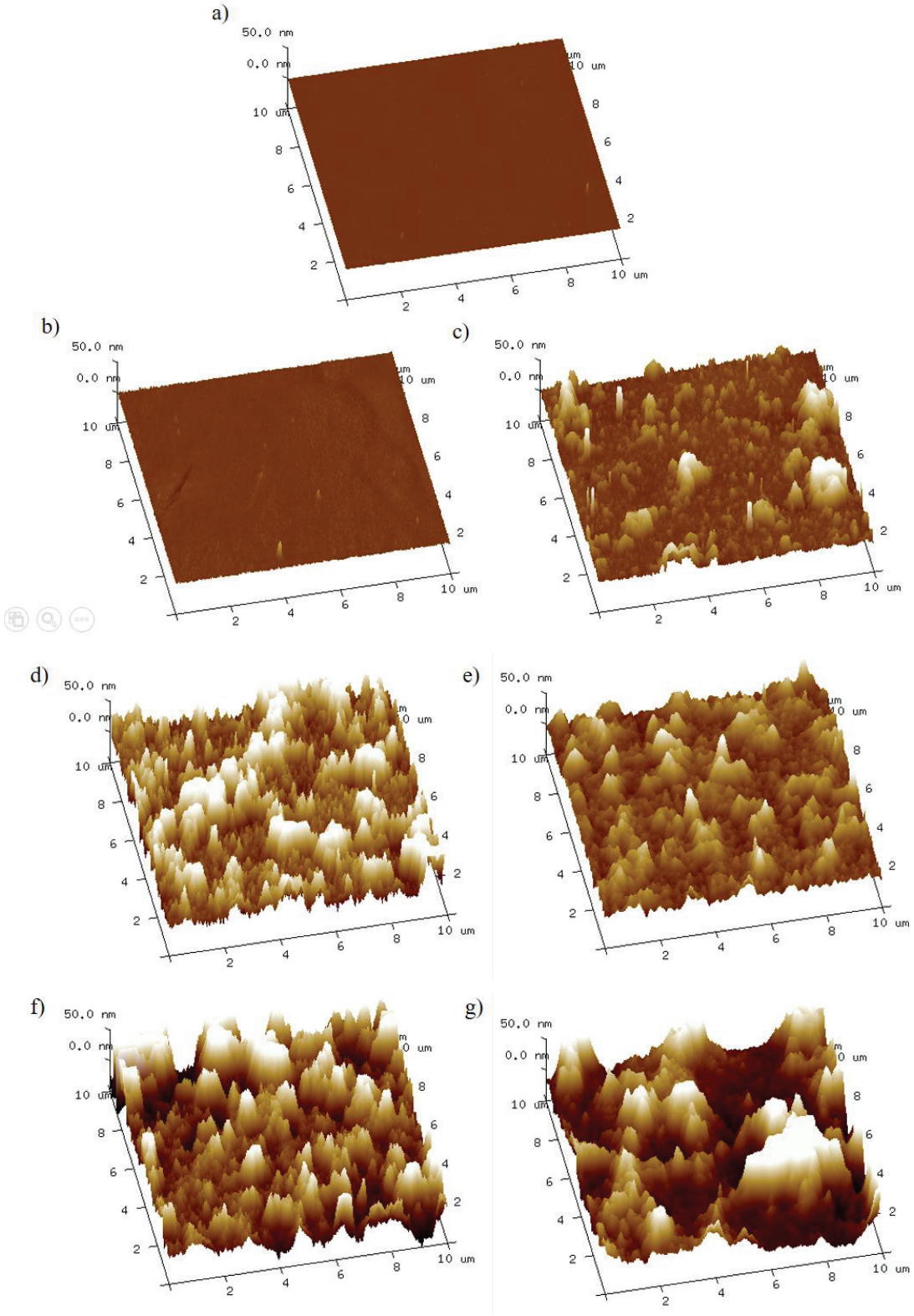

Figure 3.17. AFM images (in-air) of surface topography of the layers obtained with intermediate drying step at pH 7&7 combination of LZ-IC LbL coating with 20 min adsorption time. Scan area is 10x10 μm^2 (a) Plain glass, (b)1st layer LZ, (c)2nd layer IC, (d)5th layer LZ, (e)6th layer IC, (f)9th layer LZ, (g) 10th layer IC.

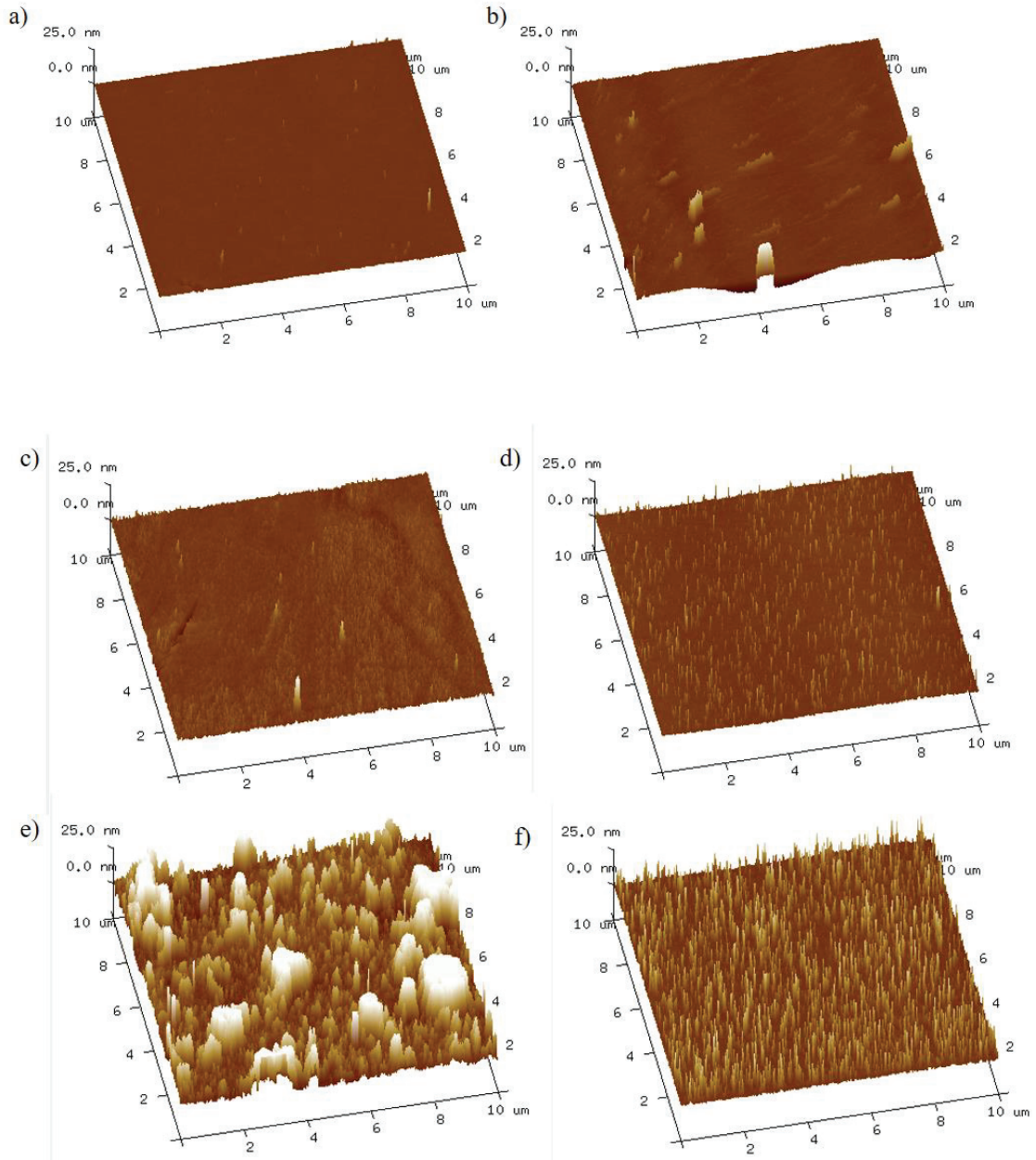

Figure 3.18. AFM images (in-air and in-fluid) of surface topography of the layers obtained by LZ-IC LbL assembly at pH 7&7 combination with 20 min adsorption. Scan area is 10x10 μm^2. Data scales of the images were equalized. (a) Plain glass-air, (b)Plain glass-fluid, (c) 1st layer (LZ)-air, (d) 1st layer (LZ)-fluid, (e) 2nd layer (IC)-air, (f) 2nd layer (IC)-fluid.

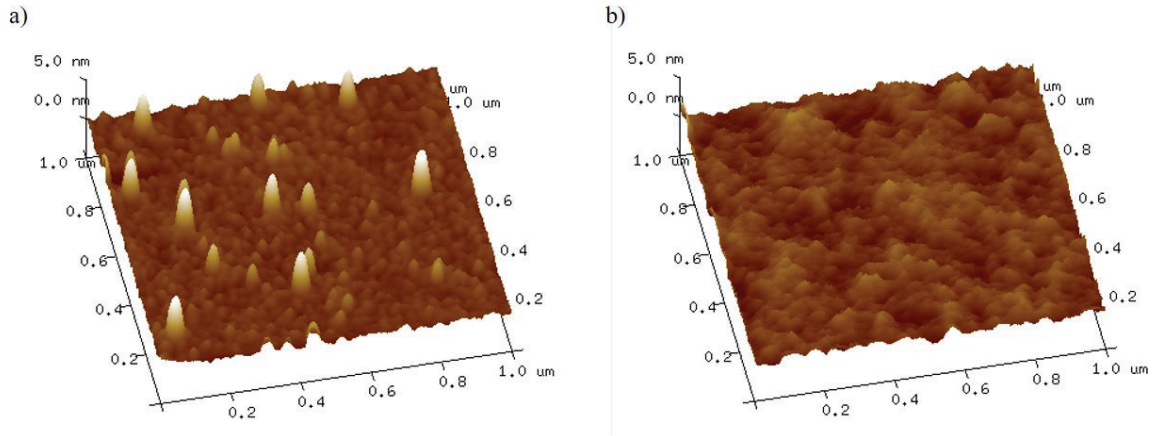

Figure 3.19. AFM images (in-air) of surface topography of the (a)1st layer LZ and (b)2nd layer IC obtained by applying intermediate drying step at pH 7&7 combination with 20 min adsorption time. Scan area is 1x1 μm^2.

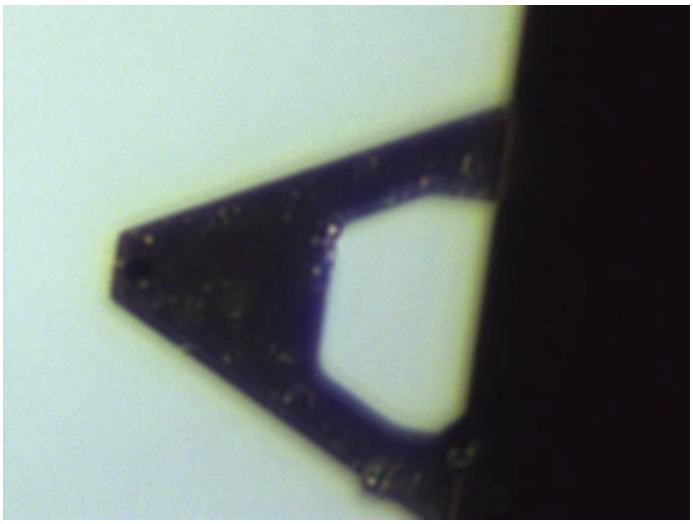

Figure 3.20. AFM tip image from LZ-IC LbL coating *in situ* analysis.

Comparing air and fluid medium AFM analysis in terms of roughness values according to Table 3.6, it shows that even though there is no significant differences from Tukey analysis, air medium gives different surfaces(aggregates) than fluid medium at 1st and 2nd layer of the coating according to roughness images in Figure 3.18. With a number of deposited bilayers, protrudes cover the surface, resulting in the increase in the RMS factor up to 25.26 nm for five bilayers. Despite of high standard deviation values, 1st and 2nd layer thicknesses are statistically different than 10th layer, it also shows that there is differences in morphology and in surface roughness values by changing the number of layers.

Table 3.6. The surface roughness values of LZ-IC LbL layers in air and fluid medium obtained from 10x10 μm^2 scan areas. Statistically significant differences were tested with ANOVA and significant differences ($P < 0.05$) were determined by Tukey test. . Exponential values with different letters are significantly different.

Number of layers	Rq(nm) ± SD	Ra(nm) ± SD
Air - 1st layer	1.64 ± 1.01^{c}	0.88 ± 0.33^{d}
Air - 2nd layer	6.48 ± 4.46^{bc}	3.61 ± 2.85^{cd}
Air -5th layer	18.13 ± 5.14^{ab}	13.0 ± 4.37^{abc}
Air - 6th layer	8.78 ± 6.99^{bc}	6.54 ± 5.31^{bcd}
Air -9th layer	22.48 ± 13.92^{a}	16.01 ± 9.65^{ab}
Air - 10th layer	25.26 ± 9.31^{a}	18.38 ± 7.65^{a}
Fluid -1st layer	1.06 ± 0.12^{c}	0.5 ± 0.04^{d}
Fluid - 2nd layer	2.47 ± 0.24^{bc}	1.31 ± 0.17^{cd}

In order to measure the thickness of the coatings (5^{th}-10^{th} layers, with/without intermediate drying steps), a soft scratch on the sample was made by hand with the help of a parafilm coated razor blade and the stratch images with height profiles of 5^{th}-LZ and 10^{th}-IC layers are shown in Figure 3.21. From stratch images, it can be seen that there is film formation with LZ and IC polyelectrolytes adsorption.

Table 3.7. Changes in thickness of the LZ-IC LbL layers with respect to number of layers and inclusion of intermediate drying step. Statistically significant differences were tested with ANOVA and significant differences ($P < 0.05$) were determined by the Tukey test. Exponential values with different letters are significantly different.

Number of layers	**Thickness(nm)**
5th layer^{dry}	107.72 ± 35.93^{ab}
10th layer^{dry}	127.84 ± 37.89^{a}
5th layer^{wet}	88.95 ± 32.92^{b}
10th layer^{wet}	101.21 ± 62.53^{ab}

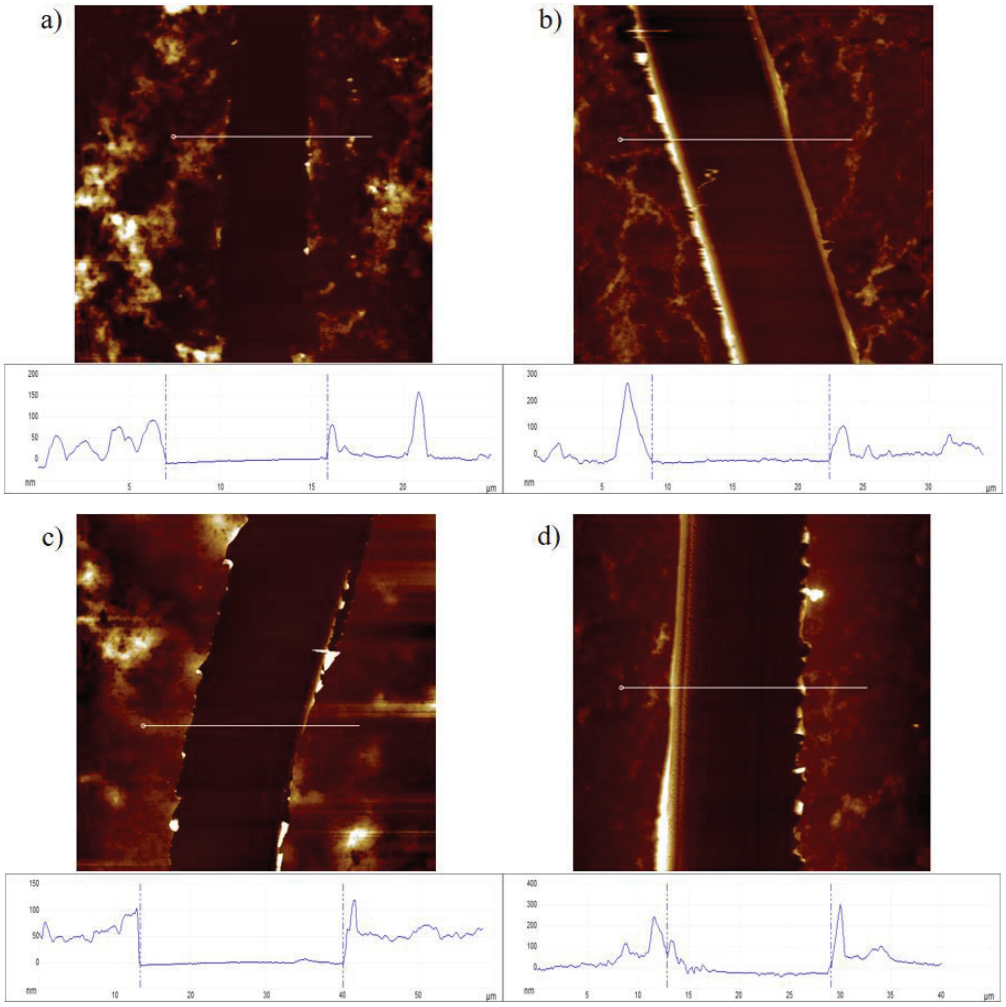

Figure 3.21. Determination of the 5th and 10th layer thicknesses for both LZ-IC LbL coatings which were prepared with drying and without drying step using stratch method by scanning atomic force microscopy. The height profiles of the white section lines are given in the bottom of the each image. (a) 5th layer (no drying)-LZ, (b) 5th layer (with drying)-LZ, (c) 10th layer (no drying)-IC, (d) 10th layer (with drying)-IC.

Comparison of dried and non-dried LbL coating in order film thicknesses are shown in Table 3.7. When we compare dried LbL film and non-dried LbL films seperately in order to number of layers, there is no significant differences between 5th and 10th layers. It might be because of some proteins were peeled out in the bulk polyanion solution. An explain for that: The effect of desorption of the protein may be due to differences in density of the negative charges of dissolved and adsorbed iota carrageenan. Some of the negative charges of adsorbed IC are compensated as a result of electrostatic interactions with positively charged groups of underlying LZ molecules. Higher ionized IC from a bulk solution may compete for positive charges of LZ molecule. Therefore the partial peeling of a LZ from a film into a bulk solution may take place (Kayushina et al., 1996).

When all AFM results are considered, as a result of LZ-IC LbL formation, both planar and cros-layer diffusion cluster structures formed. And because of that there is no significant differences between 5th and 10th layers in order to roughness and thickness measurements.

3.3.4. Scanning Electron Microscopy Results

Figure 3.22 shows corona treated blank PP film, 5 and 10 layers of the two polyelectrolytes, lysozyme and iota carrageenan captured by SEM. From these images it is possible to confirm the formation of the nanolayered coating on the coronated polypropylene surface, corroborating the previous results (AFM, SPR, UV-Vis spectroscopy).

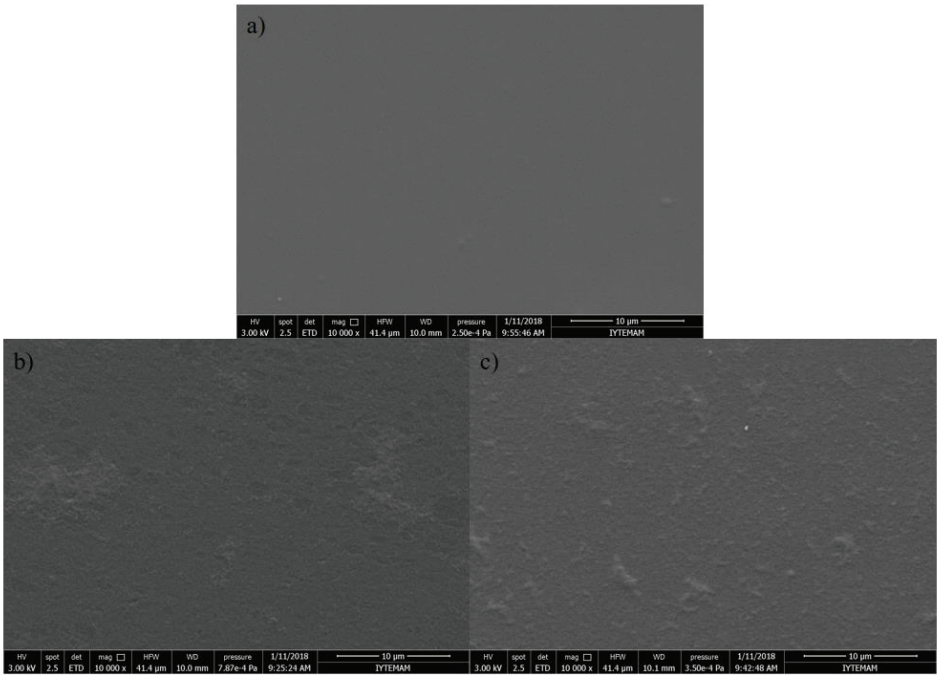

Figure 3.22. Scanning electron microscopy images of surface morphology of a) blank corona treated polypropylene (PP) film surface, b) 5 layers of LZ-IC LbL coating on corona treated PP c) 10 layers of LZ-IC LbL coating on corona treated PP. (Magnification is 10,000×, scale bar is 10 μm).

Comparing the surface of the original coronated PP film (Fig. 3.22a) and the surface of the nanolayered coatings (Fig. 3.22b-c) allows significant differences to be seen. The surface of the nanolayered coating both 5th-LZ and 10th-IC layers exhibits a more pronounced roughness and a higher number of particles, compared with the blank PP surface.

It can be understood from AFM roughness results (for 5th and 10th layers) and SEM results, there are no significant differences in homogeneity of the 5th and 10th layers, however in SEM image shows that there is gaps on the surface of 5th layered PP and, the gaps seems to be filled with applying LbL procedure untill reaching 10th layer. In other words, the lateral growth takes place. The film surface for both 5th and 10th layers were characterized by the presence of small clusters, probably due to formation of polyelectrolyte complexes of LZ/IC onto the surface during the LbL assembly process (Medeiros et al., 2011).

3.3.5. Oxygen Permeability and Water Vapor Permeability Results

Oxygen transmission rate of Lysozyme-Iota carrageenan coated PP film samples was determined by using gas permeation instrument. The measurements were conducted at constant temperature (23 °C) and relative humidity (0% RH) conditions with 5-10 cm^3/min gas flow. For LZ-IC LbL coatings 10 layered samples were prepared with and without drying step. LZ-IC at pH7-7 combination and 20 min adsorption time were used.

The OTR of blank PP and multilayer-coated PP film is shown in Table 3.8. In this case, with the deposition of LZ/IC layers, the reported OTR values of the PP film was decreased by 66.15% for 10-layered samples prepared with intermediate drying steps, and 40.78% for 10-layered samples prepared without intermediate drying steps. The enhanced oxygen barrier property is probably linked to the opposite charge overcompensation during the adsorption step leading to a highly interpenetrating polymeric network, which could reduce free volume for the interfacial polymer (Li et al., 2011; Tzeng et al., 2014). Antonov et al. (2018) showed that not only electrostatic interactions but also non-electrostatic forces such as hydrophobic forces or hydrogen bonds play a significant role in the complexation of kappa carrageenan with lysozyme. Also, polymer chains are confined to a smaller volume through strong interactions (electrostatic attractions and intermolecular H-bonding), which could lead to reduced free volume for the interfacial polymers. Thereby, this situation leads the oxygen molecules to take longer travel through and causes interfacial polymers to have more interactions. This result also shows that exclusion of intermediate drying step resulted in lower efficiency on OTR (40.78%-non dried LbL). Previous results (UV-Vis spectroscopy and AFM) also support this situation.

Wang et al. (2011) showed that drying in between polyelectrolyte deposition steps leads to more coherent polyelectrolyte multilayers with much less surface defects than the ones without drying, and the area fraction of defects decreases with the increase of the deposition cycles.

Table 3.8. Oxygen and water vapor transmission rate results for LbL films obtained by lysozyme and iota carrageenan at pH 7. Statistically significant differences were tested with ANOVA and significant differences ($P < 0.05$) were determined by the Tukey test. Exponential values with differennt letters are significantly different. (Blank PP: uncoated polypropylene, PP_{10}^{dry} : 10 layer LbL coating prepared with drying step, PP_{10}^{wet}: 10 layer LbL coating prepared without drying step)

Samples(LZ-IC)	**Oxygen transmission rate (ml/m^2-24hr)**	**Water vapour transmission rate (grams/m^2-24hours)**
Blank PP	624.78 ± 0.0^{a}	7.193 ± 0.40^{A}
PP_{10}^{dry}	211.515 ± 6.342^{c}	5.130 ± 0.336^{B}
PP_{10}^{wet}	370.005 ± 19.480^{b}	5.194 ± 0.082^{B}

The prepared coatings were tested for WVTR (Table 3.8). Similar to OTR results, the LbL-coated films showed reduction in WVTRs. 28% reduction in the WVTR of the blank PP film was obtained with the deposition of 10-layers of LZ-IC on it with both inclusion and exclusion of intermediate drying steps. The lack of a larger improvement could be due to the hydrophilic nature of I-carrageenan and reduced polymer interaction at the interface due to the plasticizing effect of water, both of which could enhance the water vapor permeability (Svagan et al., 2012; Tecante and Santiago, 2012). The water vapor permeability is strongly governed by the interaction between polymer and water molecules. The reason for decrease in water vapour transmission rate, might be because of the hydrophobic amino acid chains of lysozyme contributing to the decrease of the hydrophilicity of the lysozyme/i-carrageenan nanocoating (Medeiros et al., 2014). There is no significant difference between dried and non-dried LZ-IC LbL coatings in terms of WVTR.

In order to compare the gas barrier properties of the LbL coatings obtained in this study with those obtained in similar studies from the literature, the gas permeabilities of the individual 10 layered LZ/IC coatings were calculated according to the ideal laminate theory as described in Section 3.2.5. As the standard deviations of the thickness

measurements by AFM were high, the permeability calculations were performed considering both the lower and upper limits of the measured thicknesses. Therefore, the calculated values are given as a range in Table 3.9. As it is seen from the table, both the WVP and the OP of the LbL coatings obtained from LZ/IC in this study are 1 to 2 orders of magnitude lower than those of similar films/coatings obtained by others. Therefore, the results suggest that a very promising application of these coatings in combination with MAP for the preservation of fresh/fresh-cut produce.

Table 3.9. Comparison of LZ/IC LbL coatings with other coatings from literature in terms of OP (oxygen permeability) and WVP (water vapor permeability).

Sample	OP(mL/m.Pa.day)	WVP(g/m.Pa.day)	References
Blank PP	$2.50x10^{-6}$	$2.41x10^{-8}$	This study
10 layers of LZ/IC (dry)	$(5.76 -10.62)x10^{-9}$	$(2.7- 4.98)x10^{-10}$	This study
5 layers of k-carra/lys	$6.49x10^{-8}$	$1.12x10^{-8}$	Medeiros et al. 2011
5 layers of k-carra/chi	$2.79x10^{-8}$	$1.73x10^{-8}$	Pinheiro et al. 2012
5 layers of alg/chi		$7.67x10^{-9}$	Carneiro-da-Cunha et al. 2010
Chi edible coating	$4.61x10^{-7}$	$7.43x10^{-9}$	Fajardo et al. 2010
I-carra edible coating	$4.67x10^{-4}$	$2.01x10^{-4}$	Hambleton et al. 2008

CHAPTER 4

CONCLUSIONS

In this study, the effects of solution pH, adsorption time, number of layers, and inclusion of drying in between deposition steps on the LbL assembly and structure of multilayered coatings from lysozyme/gum arabic and lysozyme/iota carrageenan were studied. The multilayer formation was monitored by UV-Vis spectrometer. According to UV-Vis spectrometer results, the optimal solution pH combination and adsorption time were found as pH 7-7 and 20 min, respectively, for both types of coatings. UV-Vis, SPR and AFM results confirmed successful LbL deposition of lysozyme (LZ)/gum arabic (GA) and LZ/iota carrageenan (IC).

For the LZ/GA LbL coating, the same zig-zag trend as in UV-Vis spectrometer results was observed in SPR experiments. The reason is presumed to be the desorption of some of the pre-adsorbed LZ from the interface with the deposition of GA on it, probably due to formation of soluble complexes between them. The roughness (in air and fluid medium) and thickness of the LZ/GA LbL coatings were characterized using AFM. *In situ* AFM analysis showed that non-dried LbL coatings were rougher than dried LbL coatings. UV-Vis spectrometry and AFM results showed that drying step was crucial to obtain more mass deposition and more homogenous LbL coatings especially at long adsorption times. The oxygen transmission rate (OTR) and the water vapor transmission rate (WVTR) of the corona treated PP films were reduced by 57% and 32%, respectively, with the deposition of 5 bilayers of LZ/GA on them. Exclusion of intermediate drying step resulted in lower efficiencies (27% and 15% respectively). These results are in agreement with the literature such that the intermediate drying step can lead to surface modifications, which might alter the adsorbed amount with the number of layers, leading in some cases to the complete hindering of the adsorption, thus stopping the propagation of the assembly process.

For LZ/IC LbL film formation, *in situ* analysis (AFM and SPR), once more proved the necessity of intermediate drying steps for a successful propagation of the deposition. It was observed in AFM analyses that the roughness of the layers increased with the

deposition of each layer. SEM results showed that the gaps in 5th layers were filled and the surface got more homogenous as the LbL assembly was continued up to 10th layer. The resulting multilayer films caused reduction in OTR (up to 66.15%) and WVTR (up to 27%) compared to the blank PP. The samples which were prepared skipping the intermediate drying steps showed lower efficiency in oxygen transmission with 40.7%. No significant differences were found between non-dried LbL and dried LbL coatings in terms WVTR. The lack of a larger improvement could be due to more hydrophilic nature of I-carrageenan and reduced polymer interaction at the interface due to the plasticizing effect of water.

Overall, the LbL coatings obtained in this study possess good gas barrier properties, which is very promising for their use in the preservation of fresh/fresh-cut produce in combination with MAP applications. However, the permeability of the films might change after contacting with food materials. Therefore, these films must be tested on fresh produce to determine their real performance. The potential antimicrobial activity of the coatings (due to lysozyme) should further be investigated. Further characterization methods (i.e. neutron reflectometry) may be helpful to understand the internal organization of the LZ/GA and LZ/IC within the coatings.

REFERENCES

Aharoni, N.; Rodov, V.; Fallik, E.; Porat, R.; Pesis, E.; Lurie, S. In *Controlling humidity improves efficacy of modified atmosphere packaging of fruits and vegetables*, Europe-Asia Symposium on Quality Management in Postharvest Systems-Eurasia 2007 804, 2007; pp 121-128.

Allahvaisi, S., Polypropylene in the industry of food packaging. In *Polypropylene*, InTech: 2012.

Alotaibi, H. F.; Al Thaher, Y.; Perni, S.; Prokopovich, P., Role of processing parameters on surface and wetting properties controlling the behaviour of layer-by-layer coated nanoparticles. *Current Opinion in Colloid & Interface Science* **2018,** *36*, 130-142.

Antonov, Y. A.; Zhuravleva, I. L.; Cardinaels, R.; Moldenaers, P., Macromolecular complexes of lysozyme with kappa carrageenan. *Food Hydrocolloids* **2018,** *74*, 227-238.

Arnon, H.; Granit, R.; Porat, R.; Poverenov, E., Development of polysaccharides-based edible coatings for citrus fruits: A layer-by-layer approach. *Food chemistry* **2015,** *166*, 465-472.

Arnon, H.; Zaitsev, Y.; Porat, R.; Poverenov, E., Effects of carboxymethyl cellulose and chitosan bilayer edible coating on postharvest quality of citrus fruit. *Postharvest Biology and Technology* **2014,** *87*, 21-26.

Barbeyron, T.; Michel, G.; Potin, P.; Henrissat, B.; Kloareg, B., iota-Carrageenases constitute a novel family of glycoside hydrolases, unrelated to that of kappa-carrageenases. *Journal of Biological Chemistry* **2000**.

Behrens, S. H.; Grier, D. G., The charge of glass and silica surfaces. *The Journal of Chemical Physics* **2001,** *115* (14), 6716-6721.

Benkerroum, N., Antimicrobial activity of lysozyme with special relevance to milk. *African Journal of Biotechnology* **2008,** *7* (25).

Bertrand, P.; Jonas, A.; Laschewsky, A.; Legras, R., Ultrathin polymer coatings by complexation of polyelectrolytes at interfaces: suitable materials, structure and properties. *Macromolecular rapid communications* **2000,** *21* (7), 319-348.

Bieker, P.; Schönhoff, M., Linear and exponential growth regimes of multilayers of weak polyelectrolytes in dependence on pH. *Macromolecules* **2010,** *43* (11), 5052-5059.

Bifani, V.; Ramírez, C.; Ihl, M.; Rubilar, M.; García, A.; Zaritzky, N., Effects of murta (Ugni molinae Turcz) extract on gas and water vapor permeability of carboxymethylcellulose-based edible films. *LWT - Food Science and Technology* **2007,** *40* (8), 1473-1481.

Blodgett, K. B.; Langmuir, I., Built-up films of barium stearate and their optical properties. *Physical Review* **1937,** *51* (11), 964.

Bourgoin, A.; Zablackis, E.; Poli, J. B., Characterization of α-carrageenan solution behavior by field-flow fractionation and multiangle light scattering. *Food Hydrocolloids* **2008,** *22* (8), 1607-1611.

Cao, D.; Wu, H.; Li, Q.; Sun, Y.; Liu, T.; Fei, J.; Zhao, Y.; Wu, S.; Hu, X.; Li, N., Expression of recombinant human lysozyme in egg whites of transgenic hens. *PloS one* **2015,** *10* (2), e0118626.

Carneiro-da-Cunha, M. G.; Cerqueira, M. A.; Souza, B. W.; Carvalho, S.; Quintas, M. A.; Teixeira, J. A.; Vicente, A. A., Physical and thermal properties of a chitosan/alginate nanolayered PET film. *Carbohydrate Polymers* **2010,** *82* (1), 153-159.

Carneiro-da-Cunha, M. G.; Cerqueira, M. A.; Souza, B. W. S.; Teixeira, J. A.; Vicente, A. A., Influence of concentration, ionic strength and pH on zeta potential and mean hydrodynamic diameter of edible polysaccharide solutions envisaged for multinanolayered films production. *Carbohydrate Polymers* **2011,** *85* (3), 522-528.

Charles, F.; Guillaume, C.; Gontard, N., Effect of passive and active modified atmosphere packaging on quality changes of fresh endives. *Postharvest biology and Technology* **2008,** *48* (1), 22-29.

Chauhan, P. S.; Saxena, A., Bacterial carrageenases: an overview of production and biotechnological applications. *3 Biotech* **2016,** *6* (2), 146.

Chen, J.; Luo, G.; Cao, W., The study of layer-by-layer ultrathin films by the dynamic contact angle method. *Journal of colloid and interface science* **2001,** *238* (1), 62-69.

Chiarelli, P. A.; Johal, M. S.; Holmes, D. J.; Casson, J. L.; Robinson, J. M.; Wang, H.-L., Polyelectrolyte spin-assembly. *Langmuir: the ACS journal of surfaces and colloids* **2002,** *18* (1), 168-173.

Choi, J.; Rubner, M. F., Influence of the degree of ionization on weak polyelectrolyte multilayer assembly. *Macromolecules* **2005,** *38* (1), 116-124.

De Oliveira, R.; Albuquerque, D.; Cruz, T.; Yamaji, F.; Leite, F., Measurement of the nanoscale roughness by atomic force microscopy: basic principles and applications. In *Atomic force microscopy-imaging, measuring and manipulating surfaces at the atomic scale*, InTech: 2012.

De Souza, N. C.; Silva, J. R.; Pereira-da-Silva, M. A.; Raposo, M.; Faria, R. M.; Giacometti, J. A.; Oliveira, O. N., Dynamic scale theory for characterizing surface morphology of layer-by-layer films of poly (o-methoxyaniline). *Journal of Nanoscience and nanotechnology* **2004,** *4* (5), 548-552.

Decher, G., Fuzzy nanoassemblies: toward layered polymeric multicomposites. *science* **1997,** *277* (5330), 1232-1237.

Decher, G., Layer-by-layer assembly (putting molecules to work). *Multilayer thin films* **2012**, 1-21.

Decher, G.; Schlenoff, J. B., *Multilayer thin films: sequential assembly of nanocomposite materials*. John Wiley & Sons: 2006.

Enescu, D.; Frache, A.; Geobaldo, F., Formation and oxygen diffusion barrier properties of fish gelatin/natural sodium montmorillonite clay self-assembled multilayers onto the biopolyester surface. *RSC Advances* **2015,** *5* (75), 61465-61480.

Evans, M.; Ratcliffe, I.; Williams, P. A., Emulsion stabilisation using polysaccharide–protein complexes. *Current Opinion in Colloid & Interface Science* **2013,** *18* (4), 272-282.

Fajardo, P.; Martins, J.; Fuciños, C.; Pastrana, L.; Teixeira, J.; Vicente, A., Evaluation of a chitosan-based edible film as carrier of natamycin to improve the storability of Saloio cheese. *Journal of Food Engineering* **2010,** *101* (4), 349-356.

Fonseca, S. C.; Oliveira, F. A.; Brecht, J. K., Modelling respiration rate of fresh fruits and vegetables for modified atmosphere packages: a review. *Journal of food engineering* **2002,** *52* (2), 99-119.

Fu, J.; Ji, J.; Yuan, W.; Shen, J., Construction of anti-adhesive and antibacterial multilayer films via layer-by-layer assembly of heparin and chitosan. *Biomaterials* **2005,** *26* (33), 6684-6692.

Gezgin, Z.; Lee, T.; Huang, Q., Nanoscale properties of biopolymer multilayers. *Food Hydrocolloids* **2017,** *63*, 209-218.

Gulao Eda, S.; de Souza, C. J.; Andrade, C. T.; Garcia-Rojas, E. E., Complex coacervates obtained from peptide leucine and gum arabic: formation and characterization. *Food chemistry* **2016,** *194*, 680-6.

Halthur, T. J.; Claesson, P. M.; Elofsson, U. M., Stability of polypeptide multilayers as studied by in situ ellipsometry: effects of drying and post-buildup changes in temperature and pH. *Journal of the American Chemical Society* **2004,** *126* (51), 17009-17015.

Hambleton, A.; Debeaufort, F.; Beney, L.; Karbowiak, T.; Voilley, A., Protection of active aroma compound against moisture and oxygen by encapsulation in biopolymeric emulsion-based edible films. *Biomacromolecules* **2008,** *9* (3), 1058-1063.

Hashemi, M. M.; Aminlari, M.; Moosavinasab, M., Preparation of and studies on the functional properties and bactericidal activity of the lysozyme–xanthan gum conjugate. *LWT-Food Science and Technology* **2014,** *57* (2), 594-602.

Iler, R., Multilayers of colloidal particles. *Journal of colloid and interface science* **1966,** *21* (6), 569-594.

Jiang, C.; Markutsya, S.; Pikus, Y.; Tsukruk, V. V., Freely suspended nanocomposite membranes as highly sensitive sensors. *Nature materials* **2004,** *3* (10), 721.

Jourdain, L.; Leser, M. E.; Schmitt, C.; Michel, M.; Dickinson, E., Stability of emulsions containing sodium caseinate and dextran sulfate: relationship to complexation in solution. *Food Hydrocolloids* **2008,** *22* (4), 647-659.

Ghosh, A. K.; Bandyopadhyay, P., Polysaccharide-protein interactions and their relevance in food colloids. In *The complex world of polysaccharides*, InTech: 2012.

Kadefi, A. A., Prevention of ripening in fruits by use of controlled atmospheres. *Prevention* **1980**, 51-54.

Kader, A. A.; Zagory, D.; Kerbel, E. L.; Wang, C. Y., Modified atmosphere packaging of fruits and vegetables. *Critical Reviews in Food Science & Nutrition* **1989,** *28* (1), 1-30.

Kayushina, R.; Lvov, Y.; Stepina, N.; Belyaev, V.; Khurgin, Y., Construction and X-ray reflectivity study of self-assembled lysozyme/polyion multilayers. *Thin Solid Films* **1996,** *284*, 246-248.

Kharlampieva, E.; Kozlovskaya, V.; Sukhishvili, S. A., Layer-by-layer hydrogen-bonded polymer films: from fundamentals to applications. *Advanced Materials* **2009,** *21* (30), 3053-3065.

Koutsimanis, G.; Getter, K.; Behe, B.; Harte, J.; Almenar, E., Influences of packaging attributes on consumer purchase decisions for fresh produce. *Appetite* **2012,** *59* (2), 270-280.

Kyriacou, M. C.; Rouphael, Y., Towards a new definition of quality for fresh fruits and vegetables. *Scientia Horticulturae* **2018,** *234*, 463-469.

Li, Y.; Wang, X.; Sun, J., Layer-by-layer assembly for rapid fabrication of thick polymeric films. *Chemical Society Reviews* **2012,** *41* (18), 5998-6009.

Li, Y. C.; Mannen, S.; Morgan, A. B.; Chang, S.; Yang, Y. H.; Condon, B.; Grunlan, J. C., Intumescent All-Polymer Multilayer Nanocoating Capable of Extinguishing Flame on Fabric. *Advanced Materials* **2011,** *23* (34), 3926-3931.

Lin, D.; Zhao, Y., Innovations in the development and application of edible coatings for fresh and minimally processed fruits and vegetables. *Comprehensive Reviews in Food Science and Food Safety* **2007,** *6* (3), 60-75.

Liu, D. S.; Ashcraft, J. N.; Mannarino, M. M.; Silberstein, M. N.; Argun, A. A.; Rutledge, G. C.; Boyce, M. C.; Hammond, P. T., Spray Layer-by-Layer Electrospun Composite Proton Exchange Membranes. *Advanced Functional Materials* **2013,** *23* (24), 3087-3095.

Liu, Y.; Yang, J.; Zhao, Z.; Li, J.; Zhang, R.; Yao, F., Formation and characterization of natural polysaccharide hollow nanocapsules via template layer-by-layer self-assembly. *Journal of colloid and interface science* **2012,** *379* (1), 130-140.

Lourenço, J. M.; Ribeiro, P. A.; do Rego, A. M. B.; Raposo, M., Counterions in layer-by-layer films—Influence of the drying process. *Journal of colloid and interface science* **2007,** *313* (1), 26-33.

Luckarift, H. R.; Dickerson, M. B.; Sandhage, K. H.; Spain, J. C., Rapid, room-temperature synthesis of antibacterial bionanocomposites of lysozyme with amorphous silica or titania. *Small* **2006,** *2* (5), 640-643.

Lvov, Y.; Ariga, K.; Onda, M.; Ichinose, I.; Kunitake, T., A careful examination of the adsorption step in the alternate layer-by-layer assembly of linear polyanion and polycation. *Colloids and Surfaces A: Physicochemical and Engineering Aspects* **1999,** *146* (1-3), 337-346.

Maoz, R.; Netzer, L.; Gun, J.; Sagiv, J., Self-assembling monolayers in the construction of planned supramolecular suctures and as modifiers of surface properties. *Journal de chimie physique* **1988,** *85*, 1059-1065.

Medeiros, B. G. d. S.; Pinheiro, A. C.; Carneiro-da-Cunha, M. G.; Vicente, A. A., Development and characterization of a nanomultilayer coating of pectin and chitosan–Evaluation of its gas barrier properties and application on 'Tommy Atkins' mangoes. *Journal of Food Engineering* **2012,** *110* (3), 457-464.

Medeiros, B. G. d. S.; Pinheiro, A. C.; Teixeira, J. A.; Vicente, A. A.; Carneiro-da-Cunha, M. G., Polysaccharide/Protein Nanomultilayer Coatings: Construction, Characterization and Evaluation of Their Effect on 'Rocha' Pear (Pyrus communis L.) Shelf-Life. *Food and Bioprocess Technology* **2011,** *5* (6), 2435-2445.

Medeiros, B. G. d. S.; Souza, M. P.; Pinheiro, A. C.; Bourbon, A. I.; Cerqueira, M. A.; Vicente, A. A.; Carneiro-da-Cunha, M. G., Physical characterisation of an alginate/lysozyme nano-laminate coating and its evaluation on 'Coalho'cheese shelf life. *Food and Bioprocess Technology* **2014,** *7* (4), 1088-1098.

Meng, X.; Zhang, M.; Adhikari, B., Extending shelf-life of fresh-cut green peppers using pressurized argon treatment. *Postharvest Biology and Technology* **2012,** *71*, 13-20.

Mermut, O.; Barrett, C. J., Effects of charge density and counterions on the assembly of polyelectrolyte multilayers. *The Journal of Physical Chemistry B* **2003,** *107* (11), 2525-2530.

Mine, Y.; Ma, F.; Lauriau, S., Antimicrobial peptides released by enzymatic hydrolysis of hen egg white lysozyme. *Journal of Agricultural and Food Chemistry* **2004,** *52* (5), 1088-1094.

Mohammadi, M.; Salehi, A.; Branch, R. J.; Cygan, L. J.; Besirli, C. G.; Larson, R. G., Growth Kinetics in Layer-by-Layer Assemblies of Organic Nanoparticles and Polyelectrolytes. *ChemPhysChem* **2017,** *18* (1), 128-141.

Nepal, D.; Balasubramanian, S.; Simonian, A. L.; Davis, V. A., Strong antimicrobial coatings: single-walled carbon nanotubes armored with biopolymers. *Nano letters* **2008,** *8* (7), 1896-1901.

Pinheiro, A. C.; Bourbon, A. I.; Medeiros, B. G. d. S.; da Silva, L. H.; da Silva, M. C.; Carneiro-da-Cunha, M. G.; Coimbra, M. A.; Vicente, A. A., Interactions

between κ-carrageenan and chitosan in nanolayered coatings—Structural and transport properties. *Carbohydrate Polymers* **2012,** *87* (2), 1081-1090.

Porto, B. C.; Augusto, P. E. D.; Cristianini, M., A Comparative Study Between Technological Properties of Cashew Tree Gum and Arabic Gum. *Journal of Polymers and the Environment* **2014,** *23* (3), 392-399.

Priya, A. J.; Vijayalakshmi, S.; Raichur, A. M., Enhanced survival of probiotic Lactobacillus acidophilus by encapsulation with nanostructured polyelectrolyte layers through layer-by-layer approach. *Journal of agricultural and food chemistry* **2011,** *59* (21), 11838-11845.

Radeva, T.; Kamburova, K.; Petkanchin, I., Formation of polyelectrolyte multilayers from polysaccharides at low ionic strength. *Journal of colloid and interface science* **2006,** *298* (1), 59-65.

Raposo, M.; Pontes, R.; Mattoso, L.; Oliveira, O., Kinetics of adsorption of poly (o-methoxyaniline) self-assembled films. *Macromolecules* **1997,** *30* (20), 6095-6101.

Richardson, J. J.; Björnmalm, M.; Caruso, F., Technology-driven layer-by-layer assembly of nanofilms. *Science* **2015,** *348* (6233), aaa2491.

Sandhya, Modified atmosphere packaging of fresh produce: Current status and future needs. *LWT - Food Science and Technology* **2010,** *43* (3), 381-392.

Ščetar, M.; Kurek, M.; Galić, K., Trends in fruit and vegetable packaging–a review. *Hrvatski časopis za prehrambenu tehnologiju, biotehnologiju i nutricionizam* **2010,** *5* (3-4), 69-86.

Schlenoff, J. B.; Dubas, S. T.; Farhat, T., Sprayed polyelectrolyte multilayers. *Langmuir : the ACS journal of surfaces and colloids* **2000,** *16* (26), 9968-9969.

Souza, M. P.; Vaz, A. F.; Cerqueira, M. A.; Texeira, J. A.; Vicente, A. A.; Carneiro-da-Cunha, M. G., Effect of an edible nanomultilayer coating by electrostatic self-assembly on the shelf life of fresh-cut mangoes. *Food and bioprocess technology* **2015,** *8* (3), 647-654.

Su, Y.-l.; Li, C., Stable multilayer thin films composed of gold nanoparticles and lysozyme. *Applied Surface Science* **2008,** *254* (7), 2003-2008.

Svagan, A. J.; Åkesson, A.; Cárdenas, M.; Bulut, S.; Knudsen, J. C.; Risbo, J.; Plackett, D., Transparent films based on PLA and montmorillonite with tunable oxygen barrier properties. *Biomacromolecules* **2012,** *13* (2), 397-405.

Távora, L.; Raghavan, G.; Orsat, V., Storage of cranberries in plastic packaging. *Journal of Food Technology* **2004,** *2* (1), 28-34.

Tecante, A.; Santiago, M. d. C. N., Solution properties of κ-carrageenan and its interaction with other polysaccharides in aqueous media. In *Rheology*, InTech: 2012.

Tsukruk, V.; Bliznyuk, V.; Visser, D.; Campbell, A.; Bunning, T.; Adams, W., Electrostatic deposition of polyionic monolayers on charged surfaces. *Macromolecules* **1997,** *30* (21), 6615-6625.

Tzeng, P.; Maupin, C. R.; Grunlan, J. C., Influence of polymer interdiffusion and clay concentration on gas barrier of polyelectrolyte/clay nanobrick wall quadlayer assemblies. *Journal of Membrane Science* **2014,** *452*, 46-53.

van de Velde, F.; de Ruiter, G., Biopolymers Online 2005. *Piculell in Food Polysaccharides and Their Applications, 2nd ed.(Eds.: AM Stephen, GO Phillips, PA Williams)*.

van de Velde, F.; Lourenço, N. D.; Pinheiro, H. M.; Bakker, M., Carrageenan: A food-grade and biocompatible support for immobilisation techniques. *Advanced Synthesis & Catalysis* **2002,** *344* (8), 815-835.

Van Duffel, B.; Schoonheydt, R. A.; Grim, C. P.; De Schryver, F. C., Multilayered clay films: atomic force microscopy study and modeling. *Langmuir : the ACS journal of surfaces and colloids* **1999,** *15* (22), 7520-7529.

Vargas, M.; Albors, A.; Chiralt, A.; González-Martínez, C., Quality of cold-stored strawberries as affected by chitosan–oleic acid edible coatings. *Postharvest biology and technology* **2006,** *41* (2), 164-171.

Vigneshwaran, N.; Ammayappan, L.; Huang, Q., Effect of Gum arabic on distribution behavior of nanocellulose fillers in starch film. *Applied Nanoscience* **2011,** *1* (3), 137-142.

Wang, L.; Wang, L.; Su, Z., Surface defects in polyelectrolyte multilayers: Effects of drying and deposition cycle. *Soft Matter* **2011,** *7* (10), 4851.

Williams, P.; Phillips, G.; Randall, R., Structure–function relationships of gum arabic. *Gums and stabilisers for the food industry* **1990,** *5*, 25-36.

Wongsagonsup, R.; Shobsngob, S.; Oonkhanond, B.; Varavinit, S., Zeta Potential and Pasting Properties of Phosphorylated or Crosslinked Rice Starches. **2005,** *57* (1), 32-37.

Wu, T.; Jiang, Q.; Wu, D.; Hu, Y.; Chen, S.; Ding, T.; Ye, X.; Liu, D.; Chen, J., What is new in lysozyme research and its application in food industry-A review. *Food chemistry* **2018**.

Xiang, F.; Tzeng, P.; Sawyer, J. S.; Regev, O.; Grunlan, J. C., Improving the gas barrier property of clay–polymer multilayer thin films using shorter deposition times. *ACS applied materials & interfaces* **2013,** *6* (9), 6040-6048.

Xu, J.; Yang, L.; Hu, X.; Xu, S.; Wang, J.; Feng, S., The effect of polysaccharide types on adsorption properties of LbL assembled multilayer films. *Soft matter* **2015,** *11* (9), 1794-1799.

Yan, J.; Luo, Z.; Ban, Z.; Lu, H.; Li, D.; Yang, D.; Aghdam, M. S.; Li, L., The effect of the layer-by-layer (LBL) edible coating on strawberry quality and metabolites during storage. *Postharvest Biology and Technology* **2019,** *147*, 29-38.

Yoo, D.; Shiratori, S. S.; Rubner, M. F., Controlling bilayer composition and surface wettability of sequentially adsorbed multilayers of weak polyelectrolytes. *Macromolecules* **1998,** *31* (13), 4309-4318.

Yu, J.; Meharg, B. M.; Lee, I., Adsorption and interlayer diffusion controlled growth and unique surface patterned growth of polyelectrolyte multilayers. *Polymer* **2017,** *109*, 297-306.

Zacharia, N. S.; Modestino, M.; Hammond, P. T., Factors influencing the interdiffusion of weak polycations in multilayers. *Macromolecules* **2007,** *40* (26), 9523-9528.

Zagory, D.; Kader, A. A., Modified atmosphere packaging of fresh produce. *Food Technol* **1988,** *42* (9), 70-77.

Zhang, L.; Liu, H.; Zhao, E.; Qiu, L.; Sun, J.; Shen, J., Drying and nondrying layer-by-layer assembly for the fabrication of sodium silicate/TiO_2 nanoparticle composite films. *Langmuir : the ACS journal of surfaces and colloids* **2012,** *28* (3), 1816-1823.

Zhang, L.; Sun, J., Layer-by-layer deposition of polyelectrolyte complexes for the fabrication of foam coatings with high loading capacity. *Chemical Communications* **2009,** (26), 3901-3903.

Zhang, L.; Sun, J., Layer-by-layer codeposition of polyelectrolyte complexes and free polyelectrolytes for the fabrication of polymeric coatings. *Macromolecules* **2010,** *43* (5), 2413-2420.

Zhang, X.; Chen, H.; Zhang, H., Layer-by-layer assembly: from conventional to unconventional methods. *Chemical Communications* **2007,** (14), 1395-1405.

Zhao, C.; Zhao, Q.; Zhang, Y.; Zhou, M. In *The Effect of Gum Arabic on the Dispersion of Cement Pastes*, Proceedings of the 11th International Congress for Applied Mineralogy (ICAM), Springer: 2015; 483-494.

APPENDIX A

ANOVA TABLES

Table A.1. Analyses of Variance table for zeta potential of 0.2% lysozyme(LZ) at different pH values(3, 5, 7).

Source	DF	Adj SS	Adj MS	F-Value	P-Value
LZ	2	4781,93	2390,97	615,93	0,000
Error	15	58,23	3,88		
Total	17	4840,16			

S = 1,97024 R-sq = 98,80% R-sq(adj)= 98,64%

Table A.2. Grouping information for zeta potential of 0.2% lysozyme(LZ) at different pH values(3,5,7) using the Tukey method and 95% confidence.

LZ	N	Mean	Grouping
pH3	6	46,77	A
pH5	6	31,457	B
pH7	6	7,182	C

Table A.3. Analyses of Variance table for zeta potential of 0.2% gum arabic(GA) at different pH values(3, 5, 7).

Source	DF	Adj SS	Adj MS	F-Value	P-Value
GA	2	2788,3	1394,16	93,17	0,000
Error	15	224,5	14,96		
Total	17	3012,8			

S = 3,86828 R-sq = 92,55% R-sq(adj)= 91,56%

Table A.4. Grouping information for zeta potential of 0.2% gum arabic(GA) at different pH values(3,5,7) using the Tukey method and 95% confidence.

GA	N	Mean	Grouping
pH3	6	-8,667	A
pH5	6	-23,17	B
pH7	6	-39,14	C

Table A.5. Analyses of Variance table for zeta potential of 0.2% iota carrageenan (IC) at different pH values(6, 7, 8).

Source	DF	Adj SS	Adj MS	F-Value	P-Value
IC	2	357,8	178,91	3,51	0,056
Error	15	763,6	50,90		
Total	17	1121,4			

S = 7,13476 R-sq = 31,91% R-sq(adj)= 22,83%

Table A.6. Grouping information for zeta potential of 0.2% iota carrageenan(IC) at different pH values(6,7,8) using the Tukey method and 95% confidence.

IC	N	Mean	Grouping
pH6	6	-44,42	A
pH7	6	-46,54	A
pH8	6	-54,75	A

Table A.7. Analyses of Variance table of air vs fluid medium for roughness (Rq (nm)) of multilayered film formation obtained by 0.2% lysozyme and 0.2% gum arabic at pH 7.

Source	DF	Adj SS	Adj MS	F-Value	P-Value
Layer number	11	635,14	57,740	46,27	0,000
Error	40	49,92	1,248		
Total	51	685,06			

S = 1,11715 R-sq = 92,71% R-sq(adj)= 90,71%

Table A.8. Grouping information of air vs fluid medium for roughness(Rq (nm)) of multilayered film formation obtained by 0.2% lysozyme and 0.2% gum arabic at pH 7 using the Tukey method and 95% confidence.

Layer number	N	Mean	Grouping
Fluid-10	1	13,10	A B
Fluid-5	4	13,075	A
Fluid-6	3	8,973	B
Fluid-9	3	4,07	C
Air-10	6	3,512	C
Air-9	6	3,268	C D
Air-5	5	3,120	C D
Air-6	6	2,430	C D
Air-1	5	1,644	C D
Fluid-1	4	1,389	C D
Air-2	6	1,255	D
Fluid-2	3	1,0313	C D

Table A.9. Analyses of Variance table of air vs fluid medium for roughness(Ra (nm)) of multilayered film formation obtained by 0.2% lysozyme and 0.2% gum arabic at pH 7.

Source	DF	Adj SS	Adj MS	F-Value	P-Value
Layer number	11	120,82	10,9840	42,58	0,000
Error	40	10,32	0,2580		
Total	51	131,14			

S = 0,507926 R-sq = 92,13% R-sq(adj)= 89,97%

Table A.10. Grouping information of air vs fluid medium for roughness(Ra (nm)) of multilayered film formation obtained by 0.2% lysozyme and 0.2% gum arabic at pH 7 using the Tukey method and 95% confidence.

Layer number	N	Mean	Grouping
Fluid-10	1	7,340	A
Fluid-5	4	5,782	A
Fluid-6	3	2,650	B
Fluid-9	3	2,087	B C
Air-10	6	1,748	B C
Air-5	5	1,496	B C D
Air-9	6	1,4433	B C D
Air-6	6	1,0950	C D
Fluid-1	4	0,938	C D
Air-1	5	0,889	C D
Fluid-2	3	0,6997	C D
Air-2	6	0,549	D

Table A.11. Analyses of Variance table of inclusion or exclusion of intermediate drying step for thickness of multilayered film formation obtained by 0.2% lysozyme and 0.2% gum arabic at pH 7.

Source	DF	Adj SS	Adj MS	F-Value	P-Value
Number of layers	3	20886	6961,9	8,21	0,000
Error	68	57646	847,7		
Total	71	78532			

S = 29,1158 R-sq = 26,60% R-sq(adj)= 23,36%

Table A.12. Grouping information of inclusion or exclusion of intermediate drying step for thickness of multilayered film formation obtained by 0.2% lysozyme and 0.2% gum arabic at pH 7 using the Tukey method and 95% confidence (52: 5th layer- with drying step, 51: 5th layer- without drying step, 102: 10th layer- with drying step, 101: 10th layer- without drying step).

Number of layers	N	Mean	Grouping
102	18	70,0	A
52	24	67,88	A
101	12	65,5	A
51	18	28,87	B

Table A.13. Analyses of Variance table of inclusion or exclusion of intermediate drying step for oxygen transmission rate of multilayered film formation obtained by 0.2% lysozyme and 0.2% gum arabic at pH 7.

Source	DF	Adj SS	Adj MS	F-Value	P-Value
LZ/GA	3	126512	42170,5	46,89	0,001
Error	4	3598	899,4		
Total	7	130109			

S = 29,9907 R-sq = 97,23% R-sq(adj) = 95,16%

Table A.14. Grouping information of inclusion or exclusion of intermediate drying step for oxygen transmission rate of multilayered film formation obtained by 0.2% lysozyme and 0.2% gum arabic at pH 7 using the Tukey method and 95% confidence (0: Blank PP, 101: 10th layer- without drying step, 102: 10th layer- with drying step, 201:20th layer-without drying step).

LZ/GA	N	Mean	Grouping
0	2	624,8	A
101	2	457,7	B
201	2	453,9	B
102	2	269,33	C

Table A.15. Analyses of Variance table of inclusion or exclusion of intermediate drying step for water vapour transmission rate of multilayered film formation obtained by 0.2% lysozyme and 0.2% gum arabic at pH 7.

Source	DF	Adj SS	Adj MS	F-Value	P-Value
Samples LZ/GA	3	7,3756	2,4585	11,74	0,019
Error	4	0,8373	0,2093		
Total	7	8,2130			

S = 0,457527 R-sq = 89,80% R-sq(adj) = 82,16%

Table A.16. Grouping information of inclusion or exclusion of intermediate drying step for water vapour transmission rate of multilayered film formation obtained by 0.2% lysozyme and 0.2% gum arabic at pH 7 using the Tukey method and 95% confidence (0:Blank PP, 101: 10th layer- without drying step, 102: 10th layer- with drying step, 201:20th layer-without drying step).

LZ/GA	N	Mean	Grouping
0	2	7,193	A
101	2	6,022	A B
201	2	4,977	B
102	2	4,783	B

Table A.17. Analyses of Variance table of air vs fluid medium for roughness (Rq (nm)) of multilayered film formation obtained by 0.2% lysozyme and 0.2% iota carrageenan at pH 7.

Source	DF	Adj SS	Adj MS	F-Value	P-Value
Number of layers	7	3389	484,15	8,62	0,000
Error	35	1967	56,19		
Total	42	5356			

S = 7,49597 R-sq = 63,28% R-sq(adj) = 55,94%

Table A.18. Grouping information of air vs fluid medium for roughness (Rq (nm)) of multilayered film formation obtained by 0.2% lysozyme and 0.2% iota carrageenan at pH 7 using the Tukey method and 95% confidence.

Number of layers	N	Mean	Grouping
Air-10	6	25,27	A
Air-9	6	22,48	A
Air-5	8	18,14	A B
Air-6	7	8,79	B C
Air-2	5	6,49	B C
Fluid-2	3	2,477	B C
Air-1	5	1,644	C
Fluid-1	3	1,0687	C

Table A.19. Analyses of Variance table of air vs fluid medium for roughness (Ra (nm)) of multilayered film formation obtained by 0.2% lysozyme and 0.2% iota carrageenan at pH 7.

Source	DF	Adj SS	Adj MS	F-Value	P-Value
Number of layers	7	1861	265,84	8,50	0,000
Error	35	1095	31,28		
Total	42	2956			

S = 5,59253 R-sq = 62,96% R-sq(adj) = 55,55%

Table A.20. Grouping information of air vs fluid medium for roughness (Ra (nm)) of multilayered film formation obtained by 0.2% lysozyme and 0.2% iota carrageenan at pH 7 using the Tukey method and 95% confidence.

Number of layers	N	Mean	Grouping
Air-10	6	18,38	A
Air-9	6	16,01	A B
Air-5	8	13,00	A B C
Air-6	7	6,54	B C D
Air-2	5	3,61	C D
Fluid-2	3	1,3133	C D
Air-1	5	0,889	D
Fluid-1	3	0,5087	D

Table A.21. Analyses of Variance table of inclusion or exclusion of intermediate drying step for thickness of multilayered film formation obtained by 0.2% lysozyme and 0.2% iota carrageenan at pH 7.

Source	DF	Adj SS	Adj MS	F-Value	P-Value
Number of layers	3	17871	5957	3,34	0,023
Error	83	148049	1784		
Total	86	165920			

S = 42,2342 R-sq = 10,77% R-sq(adj) = 7,55%

Table A.22. Grouping information of inclusion or exclusion of intermediate drying step for thickness of multilayered film formation obtained by 0.2% lysozyme and 0.2% iota carrageenan at pH 7 using the Tukey method and 95% confidence (52: 5th layer- with drying step, 51: 5th layer- without drying step, 102: 10th layer- with drying step, 101: 10th layer- without drying step).

Number of layers	N	Mean	Grouping
102	17	127,85	A
52	19	107,73	A B
101	16	101,2	A B
51	35	88,96	B

Table A.23. Analyses of Variance table of inclusion or exclusion of intermediate drying step for oxygen transmission rate of multilayered film formation obtained by 0.2% lysozyme and 0.2% iota carrageenan at pH 7.

Source	DF	Adj SS	Adj MS	F-Value	P-Value
Samples LZ/IC	2	173878	86939,1	621,39	0,000
Error	3	420	139,9		
Total	5	174298			

S = 11,8284 R-sq = 99,76% R-sq(adj) = 99,60%

Table A.24. Grouping information of inclusion or exclusion of intermediate drying step for oxygen transmission rate of multilayered film formation obtained by 0.2% lysozyme and 0.2% iota carrageenan at pH 7 using the Tukey method and 95% confidence (0: Blank PP, 101: 10th layer- without drying step, 102: 10th layer- with drying step).

Samples

LZ/IC	N	Mean	Grouping
0	2	624,8	A
101	2	370,0	B
102	2	211,51	C

Table A.25. Analyses of Variance table of inclusion or exclusion of intermediate drying step for water vapour transmission rate of multilayered film formation obtained by 0.2% lysozyme and 0.2% iota carrageenan at pH 7.

Source	DF	Adj SS	Adj MS	F-Value	P-Value
Samples LZ/IC	2	5,5005	2,75023	28,58	0,011
Error	3	0,2887	0,09623		
Total	5	5,7891			

S = 0,310203 R-sq = 95,01% R-sq(adj) = 91,69%

Table A.26. Grouping information of inclusion or exclusion of intermediate drying step for water vapour transmission rate of multilayered film formation obtained by 0.2% lysozyme and 0.2% iota carrageenan at pH 7 using the Tukey method and 95% confidence (0: Blank PP, 101: 10th layer- without drying step, 102: 10th layer- with drying step).

Samples

LZ/IC	N	Mean	Grouping
0	2	7,193	A
101	2	5,1939	B
102	2	5,130	B